

**Program on Technology Innovation:
Effect of Negligible Inelastic Behavior on
High Frequency Response**

1012967

Program on Technology Innovation: Effect of Negligible Inelastic Behavior on High Frequency Response

1012967

Technical Update, December 2005

EPRI Project Managers
R. Kassawara
L. Sandell

Cosponsor
U.S. Department of Energy
Office of Nuclear Energy Sciences & Technology
19901 Germantown Road, NE-20
Germantown, MD 20874-1290

Project Manager
B.P. Singh

DISCLAIMER OF WARRANTIES AND LIMITATION OF LIABILITIES

THIS DOCUMENT WAS PREPARED BY THE ORGANIZATION(S) NAMED BELOW AS AN ACCOUNT OF WORK SPONSORED OR COSPONSORED BY THE ELECTRIC POWER RESEARCH INSTITUTE, INC. (EPRI). NEITHER EPRI, ANY MEMBER OF EPRI, ANY COSPONSOR, THE ORGANIZATION(S) BELOW, NOR ANY PERSON ACTING ON BEHALF OF ANY OF THEM:

(A) MAKES ANY WARRANTY OR REPRESENTATION WHATSOEVER, EXPRESS OR IMPLIED, (I) WITH RESPECT TO THE USE OF ANY INFORMATION, APPARATUS, METHOD, PROCESS, OR SIMILAR ITEM DISCLOSED IN THIS DOCUMENT, INCLUDING MERCHANTABILITY AND FITNESS FOR A PARTICULAR PURPOSE, OR (II) THAT SUCH USE DOES NOT INFRINGE ON OR INTERFERE WITH PRIVATELY OWNED RIGHTS, INCLUDING ANY PARTY'S INTELLECTUAL PROPERTY, OR (III) THAT THIS DOCUMENT IS SUITABLE TO ANY PARTICULAR USER'S CIRCUMSTANCE; OR

(B) ASSUMES RESPONSIBILITY FOR ANY DAMAGES OR OTHER LIABILITY WHATSOEVER (INCLUDING ANY CONSEQUENTIAL DAMAGES, EVEN IF EPRI OR ANY EPRI REPRESENTATIVE HAS BEEN ADVISED OF THE POSSIBILITY OF SUCH DAMAGES) RESULTING FROM YOUR SELECTION OR USE OF THIS DOCUMENT OR ANY INFORMATION, APPARATUS, METHOD, PROCESS, OR SIMILAR ITEM DISCLOSED IN THIS DOCUMENT.

ORGANIZATION(S) THAT PREPARED THIS DOCUMENT

ARES Corporation, Inc.

This is an EPRI Technical Update report. A Technical Update report is intended as an informal report of continuing research, a meeting, or a topical study. It is not a final EPRI technical report.

NOTE

For further information about EPRI, call the EPRI Customer Assistance Center at 800.313.3774 or e-mail askepri@epri.com.

Electric Power Research Institute and EPRI are registered service marks of the Electric Power Research Institute, Inc.

Copyright © 2005 Electric Power Research Institute, Inc. All rights reserved.

CITATIONS

This document was prepared by

ARES Corporation, Inc.
5 Hutton Centre Drive
Suite 610
Santa Ana, CA 92707

Principal Investigators
K. Merz
G. Hardy

This document describes research sponsored by the Electric Power Research Institute (EPRI) and the U.S. Department of Energy under Award No. (DE-FC07-04ID14533). Any opinions, findings, and conclusions or recommendations expressed in this material are those of the author(s) and do not necessarily reflect the views of the Department of Energy.

This publication is a corporate document that should be cited in the literature in the following manner:

Program on Technology Innovation: Effect of Negligible Inelastic Behavior on High Frequency Response. EPRI, Palo Alto, CA, and U.S. Department of Energy, Germantown, MD: 2005. 1012967.

ACKNOWLEDGEMENTS

EPRI wishes to acknowledge the members of the Technical Review and Advisory Group for their support of this research project:

Robert Kennedy (Chair)	RPK Structural Consulting
Orhan Gurbuz	Consultant
Don Moore	Southern Nuclear
Carl Stepp	Earthquake Hazards Solutions

ABSTRACT

This report presents the results of a project conducted for the Electric Power Research Institute (EPRI) to investigate the effect of negligible inelastic behavior associated with high-frequency ground motions on nuclear power plant (NPP) components. This project has been labeled “Task S2.2” within the EPRI/DOE New Plant Seismic Issues Resolution Program. The study was performed to further develop a rational procedure for treating response spectra rich in high-frequency energy for use in seismic design of NPPs. Due to the small displacements associated with high frequency acceleration levels, the seismic margin of a typical NPP component with even a limited amount of inelastic deformation capability is much greater in the high frequency portion of the response spectrum than it is in the low frequency portion of the response spectrum. Response modification factors are developed to modify the high frequency portion of elastic response spectra which conservatively account for the additional NPP component capacity inherent to the limited non-linear behavior associated with high frequency input.

Several previous EPRI research efforts have demonstrated that high frequency ground motion (with frequency content on the order of 10 Hz and greater) are not damaging to structures, systems and components, even those that possess only a limited amount of inelastic deformation capability. The effect of material inelastic behavior on high frequency response of structures and in-structure mounted equipment has been ignored in the design of nuclear power plants. One prior study (EPRI TR-102470) considered the analytical basis for demonstrating that equipment with even limited inelastic deformation capability can sustain high frequency input motion and not exceed a negligible deformation limit. Herein, the term negligible refers to any of several non-linear mechanisms with very small deformation capacity that can affect the high frequency response of a component but which have a negligible effect on the low frequency response. The limiting case that was considered in TR-102470 was a typical item of power plant equipment, such as a control cabinet, that would be controlled by weld anchorage capacity when subjected to seismic input. Conservative models were used to determine the effect of negligible inelastic response on high frequency elastic response spectra amplitudes. These models correspond to an electrical cabinet that is anchored at its base by a minimum fillet weld loaded in the transverse direction. Based upon inelastic response simulations, a simplified computational procedure was developed and applied to the elastic response spectral ordinate at a given frequency. The amplification of the building is included in this simplified procedure in the form of an input scale factor applied to the elastic response input level. The guidance developed in TR-102470 is applicable only for strain-based response behavior and does not address the functional response behavior of active components (e.g., relay chatter).

The procedures developed in this study facilitate a more consistent margin between the failure level and the design capacity across all dynamic frequencies. In general, equipment anchorage components have non-linear limit state resistance behavior, which may be characterized by a negligible level of inelastic deformation. This behavior results in the additional attenuation of the seismic response of equipment in the high frequency range. This report provides a more detailed review of key assumptions used within the prior EPRI TR-102470 study, presents a more direct development of the basis of the reduction procedure, and presents examples of the inelastic correction procedure applied to a greater variety of elastic spectral shapes with differing frequency content. Response modification factors in the range of 0.85 to 0.75 are demonstrated

for a typical CEUS SSE shape for a rock site. In addition, this study presents seismic qualification options for potentially high frequency-sensitive devices, such as electrical relays and contactors.

CONTENTS

1 INTRODUCTION	1-1
Contents of the Report	1-2
2 BACKGROUND.....	2-1
3 NON-LINEAR ANCHORAGE BEHAVIOR.....	3-1
Background.....	3-1
Fillet Weld Load-Deformation Behavior	3-3
Cyclic Response Effects	3-5
4 EVALUATION MODELS	4-1
Background.....	4-1
Shear Resistance Model.....	4-2
Input Scaling Approach.....	4-6
Spectral De-amplification Approach.....	4-7
Overturning Resistance Model.....	4-8
Non-Linear Response Correlation.....	4-13
5 HIGH FREQUENCY STRUCTURAL RESPONSE BEHAVIOR.....	5-1
Response of Building Mounted Components.....	5-1
Base Input Response Spectra	5-2
Structure Response	5-2
In-Structure Response Spectra.....	5-3
Amplification of Building Mounted Components.....	5-3
Modeling of Structures for Response Determination	5-5
Structure Amplification Study.....	5-9
Flexure Beam.....	5-10
Shear Beam	5-11
Timoshenko Beam	5-13
Selection of Time-History Motions for Amplification Study.....	5-15
Amplification Study Procedure	5-16
Amplification Study Results.....	5-23
6 APPLIED RESPONSE MODIFICATION PROCEDURE	6-1
Seismic Margin Factor	6-1
Response Modification Procedure	6-1
Application of Response Modification Procedure.....	6-2
Application of Modified Design Spectrum	6-4
7 LIMITING AND FUNCTIONAL FAILURE MODES	7-1
Limit State Behavior.....	7-1
Functional Failure Modes.....	7-2

8 SUMMARY AND CONCLUSIONS 8-1
Anchorage Component Limit State Behavior 8-1
Evaluation Models..... 8-2
Amplification of Structures 8-3
Application of Response Modification Procedure..... 8-4
Limiting and Functional Failure Modes 8-5
Recommendations 8-5

9 REFERENCES 9-1

APPENDIX A – AMPLIFICATION STUDY RESULTS A-1

LIST OF FIGURES

Figure 2-1 Example Modified Response Spectra for UHS Shape Anchored to 0.3 g PGA (Reed et al, 1993)	2-2
Figure 3-1 Load-Deformation Characteristics of Concrete Expansion Anchors in Tension	3-2
Figure 3-2 Load-Deformation Characteristics of Connections in Shear	3-2
Figure 3-3 Normalized Load-Deformation of Fillet Weld in Transverse Shear	3-5
Figure 4-1 Transverse Loading of Weld Support Attachment	4-2
Figure 4-2 Basic Shear Resistance Model	4-3
Figure 4-3 Quarter Cycle Series Resistance Function	4-3
Figure 4-4 Cyclic Hysteretic Behavior	4-4
Figure 4-5 Response Spectra for Model Base Input Motion	4-5
Figure 4-6 Spectral Scaling Approach	4-7
Figure 4-7 Spectral De-amplification Approach	4-8
Figure 4-8 Loading of Weld Support Attachment Caused by Overturning	4-9
Figure 4-9 Basic Overturning Resistance Functions	4-9
Figure 4-10 Deformation Kinematics and Force Mechanics	4-10
Figure 4-11 Horizontal Rotational Resistance Function	4-11
Figure 4-12 Basic Overturning Resistance Model	4-11
Figure 4-13 Quarter Cycle Series Resistance Function	4-12
Figure 4-14 Cyclic Hysteretic Behavior	4-12
Figure 5-1 Response of Structure Mounted Oscillator	5-1
Figure 5-2 Example Representative Plant Structure	5-6
Figure 5-3 Finite Element Idealization of Representative Nuclear Structure	5-7
Figure 5-4 Distribution of GammaPhi ($\Gamma_{\phi}[x]$) for Flexure Beam as a Function of Beam Position	5-11
Figure 5-5 Distribution of GammaPhi ($\Gamma_{\phi}[x]$) for Shear Beam as a Function of Beam Position	5-13
Figure 5-6 Distribution of GammaPhi ($\Gamma_{\phi}[x]$) for Timoshenko Beam as a Function of Beam Position	5-15
Figure 5-7 Time History 1: Compatible European Hard Rock Design Motion	5-17
Figure 5-8 Response Spectrum for Time History 1	5-17
Figure 5-9 Time History 2: Example CEUS Rock Design Motion	5-18

Figure 5-10 Response Spectrum for Time History 2.....	5-18
Figure 5-11 Time History 3: ENA Rock Motion, 1982 New Brunswick, CA Mitchell Lake Road Component 28 (3/12/82)	5-19
Figure 5-12 Response Spectrum for Time History 3.....	5-19
Figure 5-13 Example Spectral Amplification for Timoshenko Beam with $f_1 = 5$ Hz, Time History Input 2 (Example CEUS Rock Design Motion).....	5-22
Figure 5-14 Maximum Amplification for Timoshenko Beam with $f_1 = 5$ Hz, Time History Input 2 ($0.2 \leq x/L \leq 0.9$)	5-22
Figure 5-15 Comparison of $f_1 = 3$ Hz Beam Response	5-23
Figure 5-16 Comparison of $f_1 = 5$ Hz Beam Response	5-24
Figure 5-17 Comparison of $f_1 = 7$ Hz Beam Response	5-24
Figure 5-18 Comparison of $f_1 = 9$ Hz Beam Response	5-25
Figure 5-19 Comparison of $f_1 = 6.05$ Hz Timoshenko Beam Response.....	5-25
Figure 6-1 Example CEUS Site Design Spectrum.....	6-9
Figure 6-2 Ground Motions Considered.....	6-9
Figure 6-3 CEUS Rock Site Spectra (5% Spectrum Normalized to $1.5 \times 0.75g$ at 10Hz).....	6-10
Figure 6-4 CEUS Rock Site Modified Spectra (Unreduced Spectrum Normalized to $1.5 \times 0.75g$ at 10 Hz).....	6-10
Figure 6-5 CEUS Rock Site Spectra (5% Spectrum Normalized to $1.0 \times 0.75g$ at 10 Hz).....	6-11
Figure 6-6 CEUS Rock Site Modified Spectra (Unreduced Spectrum Normalized to $1.0 \times 0.75g$ at 10 Hz).....	6-11
Figure 6-7 CEUS Rock Site Spectra (5% Spectrum Normalized to $0.67 \times 0.75g$ at 10 Hz).....	6-12
Figure 6-8 CEUS Rock Site Modified Spectra (Unreduced Spectrum Normalized to $0.67 \times 0.75g$ at 10 Hz).....	6-12
Figure 6-9 CEUS Soil Site Spectra (5% Spectrum Normalized to $1.5 \times 0.75g$ at 10 Hz).....	6-13
Figure 6-10 CEUS Soil Site Modified Spectra (Unreduced Spectrum Normalized to $1.5 \times 0.75g$ at 10 Hz).....	6-13
Figure 6-11 CEUS Soil Site Spectra (5% Spectrum Normalized to $1.0 \times 0.75g$ at 10 Hz).....	6-14
Figure 6-12 CEUS Soil Site Modified Spectra (Unreduced Spectrum Normalized to $1.0 \times 0.75g$ at 10 Hz).....	6-14
Figure 6-13 CEUS Soil Site Spectra (5% Normalized to $0.67 \times 0.75g$ at 10 Hz)	6-15
Figure 6-14 CEUS Soil Site Modified Spectra (Unreduced Spectrum Normalized to $0.67 \times 0.75g$ at 10 Hz).....	6-15

Figure 6-15 European Horizontal Hard Rock Spectra (5% Horizontal Spectrum Normalized to 1.5 x 0.75g at 10 Hz).....	6-16
Figure 6-16 European Horizontal Hard Rock Modified Spectra (Unreduced Horizontal Spectrum Normalized to 1.5 x 0.75g at 10 Hz).....	6-16
Figure 6-17 European Horizontal Hard Rock Spectra (5% Horizontal Spectrum Normalized to 1.0 x 0.75g at 10 Hz).....	6-17
Figure 6-18 European Horizontal Hard Rock Modified Spectra (Unreduced Horizontal Spectrum Normalized to 1.0 x 0.75g at 10 Hz).....	6-17
Figure 6-19 European Horizontal Hard Rock Spectra (5% Horizontal Spectrum Normalized to 0.67 x 0.75g at 10 Hz).....	6-18
Figure 6-20 European Horizontal Hard Rock Modified Spectra (Unreduced Horizontal Spectrum Normalized to 0.67 x 0.75g at 10 Hz).....	6-18
Figure 6-21 Development of Free-Field CEUS Rock Site Design Spectrum (Unreduced Spectrum Normalized to 0.931g at 10 Hz).....	6-19
Figure 6-22 Development of 150 ft. Square Foundation on CEUS Rock Site (Incoherence Reduced Spectrum Normalized to 0.74g at 10 Hz).....	6-19
Figure 7-1 Comparison of Reduced CEUS Rock Site Spectra with Example Certified Plant Design Spectra.....	7-3
Figure A-1 Comparison of Spectral Amplification for Flexure Beam with $f_1 = 3$ Hz Fundamental Frequency with Time History 1 Input Motion.....	A-3
Figure A-2 Comparison of Spectral Amplification for Flexure Beam with $f_1 = 3$ Hz Fundamental Frequency with Time History 2 Input Motion.....	A-3
Figure A-3 Comparison of Spectral Amplification for Flexure Beam with $f_1 = 3$ Hz Fundamental Frequency with Time History 3 Input Motion.....	A-4
Figure A-4 Comparison of Spectral Amplification for Flexure Beam with $f_1 = 5$ Hz Fundamental Frequency with Time History 1 Input Motion.....	A-4
Figure A-5 Comparison of Spectral Amplification for Flexure Beam with $f_1 = 5$ Hz Fundamental Frequency with Time History 2 Input Motion.....	A-5
Figure A-6 Comparison of Spectral Amplification for Flexure Beam with $f_1 = 5$ Hz Fundamental Frequency with Time History 3 Input Motion.....	A-5
Figure A-7 Comparison of Spectral Amplification for Flexure Beam with $f_1 = 7$ Hz Fundamental Frequency with Time History 1 Input Motion.....	A-6
Figure A-8 Comparison of Spectral Amplification for Flexure Beam with $f_1 = 7$ Hz Fundamental Frequency with Time History 2 Input Motion.....	A-6

Figure A-9 Comparison of Spectral Amplification for Flexure Beam with $f_1 = 7$ Hz Fundamental Frequency with Time History 3 Input Motion	A-7
Figure A-10 Comparison of Spectral Amplification for Flexure Beam with $f_1 = 9$ Hz Fundamental Frequency with Time History 1 Input Motion	A-7
Figure A-11 Comparison of Spectral Amplification for Flexure Beam with $f_1 = 9$ Hz Fundamental Frequency with Time History 2 Input Motion	A-8
Figure A-12 Comparison of Spectral Amplification for Flexure Beam with $f_1 = 9$ Hz Fundamental Frequency with Time History 3 Input Motion	A-8
Figure A-13 Comparison of Spectral Amplification for Shear Beam with $f_1 = 3$ Hz Fundamental Frequency with Time History 1 Input Motion	A-9
Figure A-14 Comparison of Spectral Amplification for Shear Beam with $f_1 = 3$ Hz Fundamental Frequency with Time History 2 Input Motion	A-9
Figure A-15 Comparison of Spectral Amplification for Shear Beam with $f_1 = 3$ Hz Fundamental Frequency with Time History 3 Input Motion	A-10
Figure A-16 Comparison of Spectral Amplification for Shear Beam with $f_1 = 5$ Hz Fundamental Frequency with Time History 1 Input Motion	A-10
Figure A-17 Comparison of Spectral Amplification for Shear Beam with $f_1 = 5$ Hz Fundamental Frequency with Time History 2 Input Motion	A-11
Figure A-18 Comparison of Spectral Amplification for Shear Beam with $f_1 = 5$ Hz Fundamental Frequency with Time History 3 Input Motion	A-11
Figure A-19 Comparison of Spectral Amplification for Shear Beam with $f_1 = 7$ Hz Fundamental Frequency with Time History 1 Input Motion	A-12
Figure A-20 Comparison of Spectral Amplification for Shear Beam with $f_1 = 7$ Hz Fundamental Frequency with Time History 2 Input Motion	A-12
Figure A-21 Comparison of Spectral Amplification for Shear Beam with $f_1 = 7$ Hz Fundamental Frequency with Time History 3 Input Motion	A-13
Figure A-22 Comparison of Spectral Amplification for Shear Beam with $f_1 = 9$ Hz Fundamental Frequency with Time History 1 Input Motion	A-13
Figure A-23 Comparison of Spectral Amplification for Shear Beam with $f_1 = 9$ Hz Fundamental Frequency with Time History 2 Input Motion	A-14
Figure A-24 Comparison of Spectral Amplification for Shear Beam with $f_1 = 9$ Hz Fundamental Frequency with Time History 3 Input Motion	A-14
Figure A-25 Comparison of Spectral Amplification for Timoshenko Beam with $f_1 = 3$ Hz Fundamental Frequency with Time History 1 Input Motion	A-15

Figure A-26 Comparison of Spectral Amplification for Timoshenko Beam with $f_1 = 3$ Hz	
Fundamental Frequency with Time History 2 Input Motion	A-15
Figure A-27 Comparison of Spectral Amplification for Timoshenko Beam with $f_1 = 3$ Hz	
Fundamental Frequency with Time History 3 Input Motion	A-16
Figure A-28 Comparison of Spectral Amplification for Timoshenko Beam with $f_1 = 5$ Hz	
Fundamental Frequency with Time History 1 Input Motion	A-16
Figure A-29 Comparison of Spectral Amplification for Timoshenko Beam with $f_1 = 5$ Hz	
Fundamental Frequency with Time History 2 Input Motion	A-17
Figure A-30 Comparison of Spectral Amplification for Timoshenko Beam with $f_1 = 5$ Hz	
Fundamental Frequency with Time History 3 Input Motion	A-17
Figure A-31 Comparison of Spectral Amplification for Timoshenko Beam with $f_1 = 7$ Hz	
Fundamental Frequency with Time History 1 Input Motion	A-18
Figure A-32 Comparison of Spectral Amplification for Timoshenko Beam with $f_1 = 7$ Hz	
Fundamental Frequency with Time History 2 Input Motion	A-18
Figure A-33 Comparison of Spectral Amplification for Timoshenko Beam with $f_1 = 7$ Hz	
Fundamental Frequency with Time History 3 Input Motion	A-19
Figure A-34 Comparison of Spectral Amplification for Timoshenko Beam with $f_1 = 9$ Hz	
Fundamental Frequency with Time History 1 Input Motion	A-19
Figure A-35 Comparison of Spectral Amplification for Timoshenko Beam with $f_1 = 9$ Hz	
Fundamental Frequency with Time History 2 Input Motion	A-20
Figure A-36 Comparison of Spectral Amplification for Timoshenko Beam with $f_1 = 9$ Hz	
Fundamental Frequency with Time History 3 Input Motion	A-20
Figure A-37 Comparison of Spectral Amplification for Timoshenko Beam with $f_1 = 6.05$ Hz	
Fundamental Frequency with Time History 1 Input Motion	A-21
Figure A-38 Comparison of Spectral Amplification for Timoshenko Beam with $f_1 = 6.05$ Hz	
Fundamental Frequency with Time History 2 Input Motion	A-21
Figure A-39 Comparison of Spectral Amplification for Timoshenko Beam with $f_1 = 6.05$ Hz	
Fundamental Frequency with Time History 3 Input Motion	A-22

LIST OF TABLES

Table 4-1 Time History Records Used for Response Correlation Analysis (Reed et al, 1993)	4-16
Table 5-1 Comparison of GammaPhi ($\Gamma_{\phi_i}[x]$) Computed for Two Alternate Model Discretizations	5-8
Table 5-2 Modal Parameters for Flexure Beam	5-11
Table 5-3 Modal Parameters for Shear Beam	5-12
Table 5-4 Modal Parameters for Timoshenko Beam	5-14
Table 5-5 Beam Frequencies Selected for Amplification Study	5-20
Table 6-1 Modified Spectrum Calculation Procedure	6-6
Table 6-2 Example Calculation of Modified Spectrum at 25 Hz.....	6-7
Table 6-3 Full Reduction of Example Design Spectrum	6-8

1

INTRODUCTION

Task S2.2 of the EPRI/DOE New Plant Seismic Issues Resolution Program has been conducted with results presented herein. The objective of this task is to further expand on the results presented in EPRI Report TR-102470 (Reed et al, 1993). This prior study developed an analytical basis for incorporating the effects of inelastic deformation of equipment anchorages on high frequency response of building mounted equipment.

The work conducted under the current study can logically be divided into the following sub-tasks:

Review of anchorage component limit state behavior

The limit state behavior of different types of anchorage components needs to be compared to the behavior of a transverse loaded fillet weld in order to justify the selection of the fillet weld as an analysis surrogate. The design margin, actual ultimate deformation, and low-cycle fatigue strength of fillet welds needs to be quantified.

Development of evaluation models

The SDOF models need to be directly developed to identify any additional simplification of the governing equations. The response correlation of the equivalent linear response models developed in the prior study need reassessment.

Quantify the expected amplification of structures in the high frequency range

The prior study included only a limited effort to estimate an appropriate amplification factor to be used to simulate the response of structure-mounted equipment. An amplification study needs to be implemented to quantify the amplification (in terms of spectral ratios) expected at various positions within a structure. The assertion that current modeling procedures for structures do not produce accurate high frequency response needs demonstration.

Application of response modification procedure

The scaling factor for both amplification and margin effects needs to be defined. The spectral modification procedure needs to be fully described to allow a user to generate a spreadsheet application that accomplishes the elastic spectra modification. Several example cases need to be prepared to demonstrate the effect of frequency content and spectral amplitude on the degree of response modification.

Review of limiting and functional failure modes

It needs to be emphasized that the fillet weld is chosen as a surrogate low bound case and results in a conservative estimate of the effects of any of several non-linear mechanisms with very small deformation capacity. Also, it must be pointed out that the numerical inelastic response is accomplished for the limit state. At the design strength, the actual deformation due to the seismic demand is an order of magnitude less than the maximum limiting deformation. The options available for the case where the high frequency response modification of a site specific design spectrum has frequency regions that exceed the certified qualification level of functional components need to be identified.

Contents of the Report

The results of all work accomplished to modify the high frequency segment of a design spectrum by considering the limited non-linear response of component anchorages is presented in this report. Chapter 2 provides introductory and background material from the prior study. A review of limit state behavior of equipment anchorage components is provided in Chapter 3. The case of a fillet weld with transverse loading is focused on as the limiting case. The development of the equations for equivalent linear models which provide the response of equipment with anchorage non-linearity are presented in Chapter 4. Chapter 5 presents a structure amplification study using simple uniform cantilever beam models of three types—flexure, shear, and Timoshenko. The amplification factors for each case considered are presented in Appendix A. A detailed description of the computational procedure used to accomplish the modification of high frequency response is presented in Chapter 6 along with several example cases showing the reduced response levels achieved. A review of the bounding limit state behavior of equipment and structures is described in Chapter 7 along with a discussion of some possible options for cases where functional requirements, e.g., no relay chatter, must account for the high frequency portion of the input motion that exceed qualification levels of the certified design of equipment for new plants, without consideration of response modification due to limited inelastic behavior. Chapter 8 provides a summary of major study observations, conclusions, and recommendations.

2

BACKGROUND

Several EPRI studies have dealt with the issue of the damage effectiveness of high frequency earthquake ground motion:

- EPRI NP-5930, “A Criterion for Determining Exceedance of the Operating Basis Earthquake”, (Reed et al, 1988).
- NP-7498, “Industry Approach to Seismic Severe Accident Policy Implementation”, (Reed et al, Nov.1991)

In general, these studies discuss the damage thresholds to structures and equipment as determined by high frequency events such as blasting, shock testing, and operational vibration. Then they compare these thresholds to typical seismic spectra levels with focus on the greater than 10 Hz frequency range.

Another study, intended for use in seismic margin studies, EPRI TR-102470, “Analysis of High-Frequency Seismic Events”, (Reed et al, 1993) investigated an analytical basis for modification of high frequency response of equipment up in a building by considering the effects of inelastic deformation of equipment anchorages. One premise of the study was that equipment has additional capacity above the yield level to absorb the small displacement response associated with high-frequency earthquake ground motion. As an example, consider the response displacement associated with the spectral acceleration level of 0.5 g. Using the relationship, $SD = SA/(2\pi f)^2$, the displacement of a 5 Hz system responding at SA = 0.5 g is SD = 0.20 inch while the displacement of a 25 Hz system responding at SA = 0.5 g is SD <0.01 inch. In terms of the behavior of structures and components, a deformation of 0.01 inch or less can be considered as negligible. All connections encountered at nuclear power plants can tolerate inelastic deformations of this order. The study concluded that a minimum 3/16 inch fillet weld loaded in transverse shear represented the limiting case of negligible distortion with a yield displacement on the order of 0.001 inch and the displacement at weld failure taken as 0.01 inch. The study then developed an analysis procedure to reduce the high frequency response of the equipment by accounting for negligible inelastic deformation in the equipment anchorage. The transverse loaded minimum fillet weld was used to represent the least inelastic deformation capacity of nuclear plant anchorages since this would provide an indication of the smallest modification of equipment response. It was recognized that this reduced response would not apply to active equipment that require qualification due to functional requirements, e.g., no relay chatter.

Another premise of TR-102470 was that the ground motion spectrum can be modified and can then be used to generate floor spectra that implicitly include the inelastic response modification of the structure mounted equipment. The effect of amplified building response was included in the analysis procedure as an amplification factor applied to the ground motion. Figure 2-1 shows the example modified response spectra considered in the previous EPRI study.

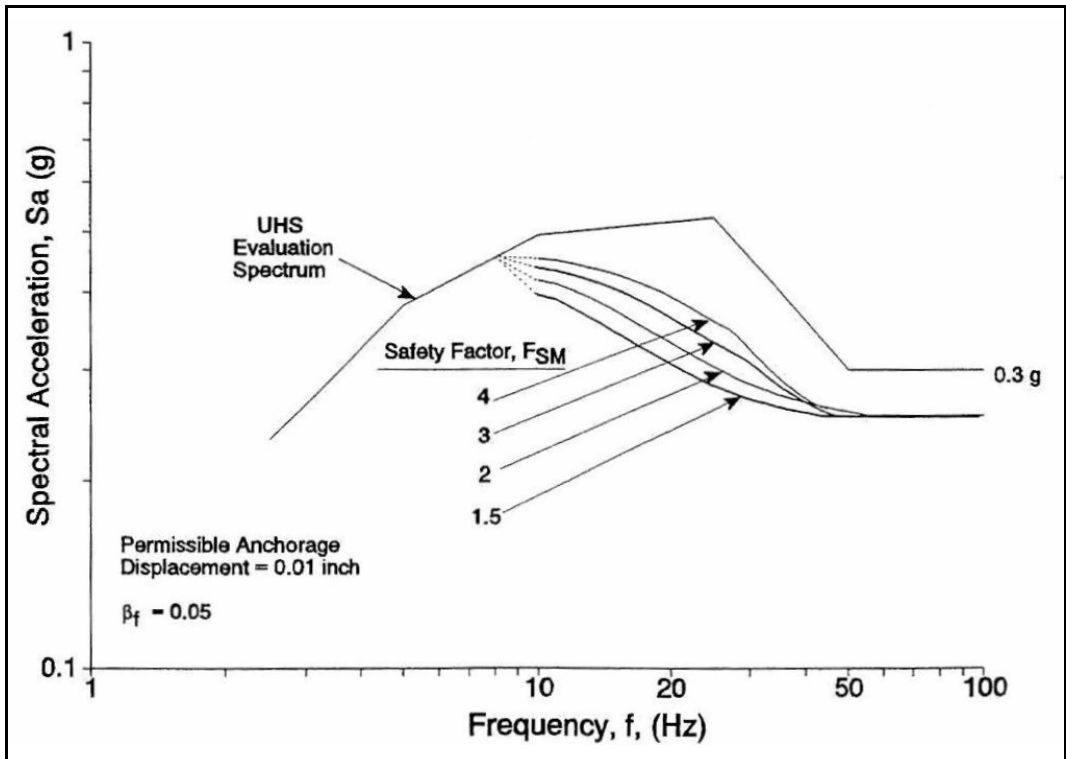


Figure 2-1
Example Modified Response Spectra for UHS Shape Anchored to 0.3 g PGA
(Reed et al, 1993)

The goals of the current report are to provide a more rigorous justification of the key assumptions used in the prior EPRI study, present a more direct development of the basis of the response modification procedure, and present examples of the modification procedure applied to a greater variety of spectral ground motion shapes with differing frequency content.

3

NON-LINEAR ANCHORAGE BEHAVIOR

Background

Anchorage components for equipment are normally designed for code based design strength that equals or exceeds the demand due to seismic forces generated by the equipment response. The deformation of anchorage components is considered to be negligibly small such that the equipment response to low frequency input motion is not appreciably affected by the deformation characteristics of the anchorage. For high frequency input motion, however, the small deformation of the anchorage component can be of the same order as the deformation associated with the input motion. In this case, the small deformation characteristics of the components in the anchorage load path can act to modify the response of the equipment.

The anchorage load path of equipment may include those intermediate elements that transfer base shear and overturning loads to the anchorage component directly attaching the equipment to the structure. Thus, there are a variety of different types of connections (concrete anchors, bolts and welds) that can contribute to the overall deformation behavior of the load path even if a single element is over-strength. Any of these elements, individually or collectively, can provide deformation capacity corresponding to the seismic load. In general, however, the behavior of the anchorage load path will be governed by the anchorage component with the lowest strength.

Figure 3-1 shows a typical load-deformation curve obtained from static pullout tests on post-installed concrete expansion anchors (Fischer, 2005). Tests which load expansion anchors in shear only, indicate that the resulting load-deformation characteristics are more variable, but the shear load-deformation curves show similar values of total deformation (Klingner et al, 1998). Often the eccentricity of the shear load with the concrete surface allows increased deformation due the flexure of the bolt and increased bearing of the bolt within the hole against the surrounding concrete. Dynamic reverse-cycle tests on expansion anchors also indicate that additional deformation can occur.

Figure 3-2 compares the typical load-deformation curves obtained from static tests on bolts and rivets in steel joints subjected to shear loads (Kulak, 1987) with load-deformation curves of static tests on fillet welds. Again the results are variable, depending upon gaps and slip characteristics of the faying surfaces. The determination of the slip coefficient for a given surface condition is normally defined based on the load required to obtain a slip of 0.02 inch. This provides a general estimation of the minimum level of limit state deformation expected for bolted joints loaded in shear.

Fillet welds are also used as load carrying elements in structural connections. They are often used to attach the base frames of plant equipment to steel embedments placed within concrete floor slabs or walls. The design assumption in such cases is that anchorage fillet welds are loaded in pure shear. Such welds would be sized for adequate design strength but the deformation

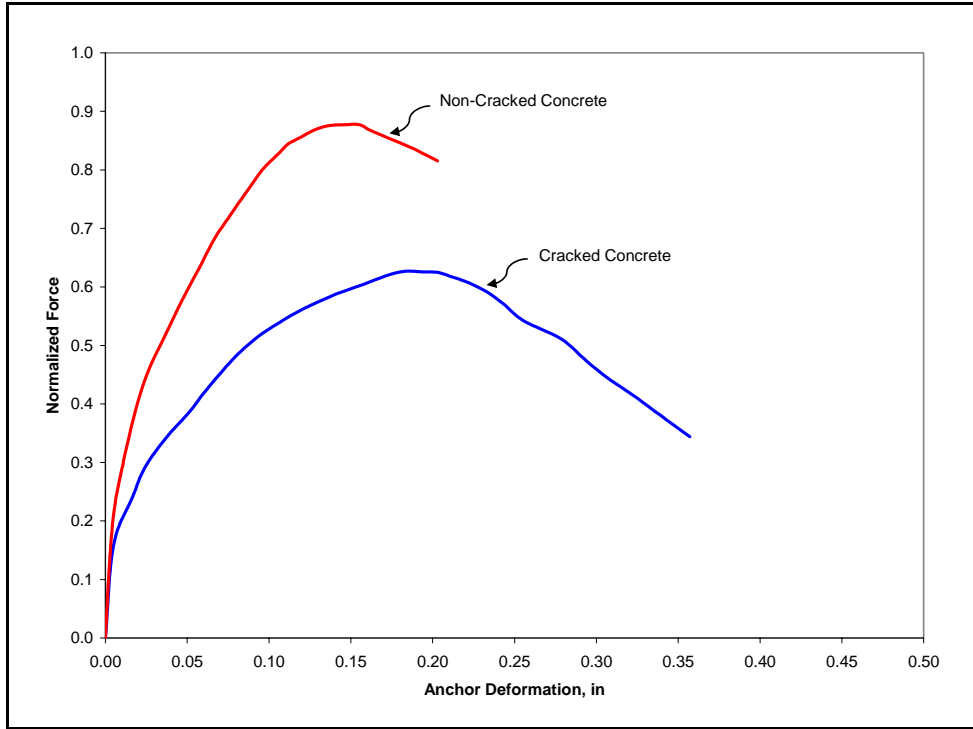


Figure 3-1
Load-Deformation Characteristics of Concrete Expansion Anchors in Tension

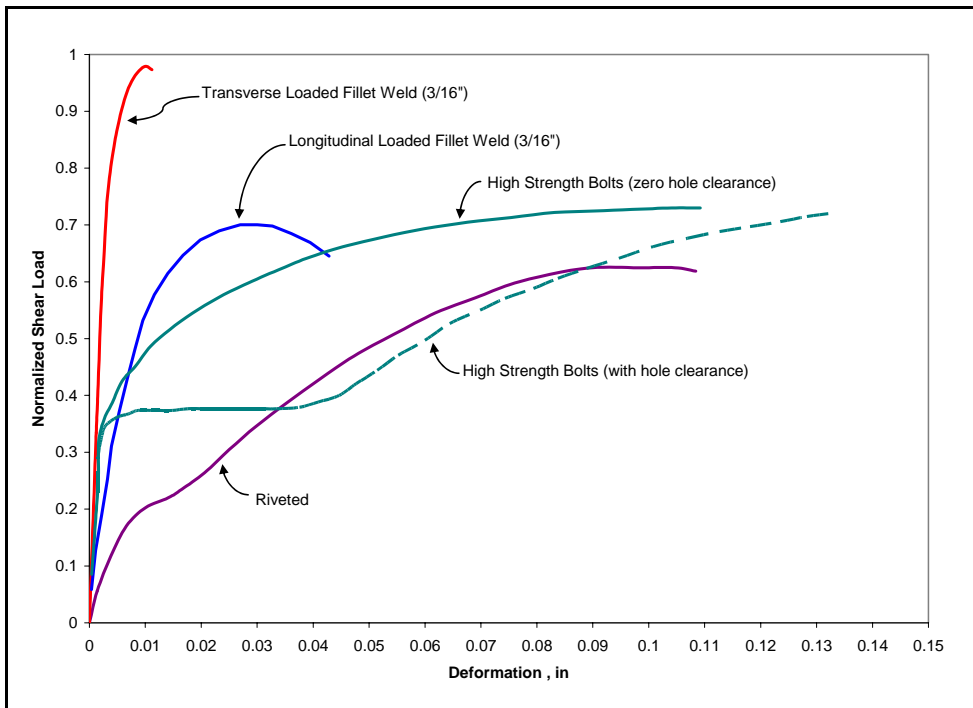


Figure 3-2
Load-Deformation Characteristics of Connections in Shear

capacity of anchorage fillet welds would normally not be a design consideration. Figure 3-2 shows example limit state load-deformation curves for fillet welds loaded in shear which were derived from extensive test data (Lesik and Kennedy, 1988, 1990). As can be noted from Figure 3-2, there is considerable difference between the limit state load-deformation behavior predicted for a minimum 3/16 inch fillet weld (leg size) loaded in transverse shear (loading transverse to the longitudinal axis of the weld), and the same weld loaded in longitudinal shear (loading along the longitudinal axis of the weld). The actual test data indicates that a transversely loaded fillet weld has approximately 40% greater load capacity compared to a longitudinally loaded weld, but approximately 1/3 of the deformation capacity of a longitudinally loaded weld. Thus, a minimum 3/16 inch fillet weld loaded in transverse shear is identified as the anchorage component that has the least deformation capacity (on the order of 0.010 inch). This test based result was used by Reed et al (1993) to conduct a study which demonstrated the effect of small non-linear anchorage deformation on equipment response to high frequency input motion. The logic of this study choice was based on the observation that the fundamental effect of non-linear behavior is to allow additional energy dissipation which effectively modifies and reduces the equipment response. If this effect is determined for the least deformation case, then any consideration of increased deformation capacity of other types of anchorage components would have an even greater modification of equipment response. It should also be noted that electrical cabinets are commonly attached to concrete embedments using minimum 3/16 inch welds since the cabinet base frames have thickness of that order.

Fillet Weld Load-Deformation Behavior

Using test data from a number of investigators, Lesik and Kennedy (1990) developed empirical load-deformation relationships that relate code-based factored resistance of fillet welds, as a function of the direction of loading (0° - 90° , where 0° represents the case of longitudinal loading), to minimum observed test deformation. The relationships recommended by Lesik and Kennedy (1990) were incorporated in the Load and Resistance Factor Design (LRFD) steel design code issued by the American Institute of Steel Construction (Iwankiw, 1997). In the current AISC Specification for Structural Steel Buildings (AISC, 2005), both the LRFD and Allowable Stress Design (ASD) requirements are combined into a single document. For fillet welds in shear, the nominal strength is given by, $R_n = F_w A_w$, where A_w is effective weld throat area. F_w is given by:

$$F_w = 0.6 F_{EXX} [1.0 + 0.5(\sin \theta)^{1.5}] \quad \text{(Equation 3-1)}$$

where F_{EXX} is the weld electrode classification strength in units of ksi and θ is the angle of loading measured from the weld longitudinal axis in degrees. The LRFD design strength is given by, ϕR_n , where ϕ is the resistance factor taken as $\phi = 0.75$ in the case of fillet welds. Eq. 3-1 is the same effective stress relationship proposed by Lesik and Kennedy (1990). When the load-deformation relation of the of the weld is required, the nominal strength is factored by the function, $f(p) = [p(1.9-0.9p)]^{0.3}$, where $p = (\delta/t)/(\delta_m/t)$. In this expression, δ , is the deformation of the weld, t is the fillet weld leg size, and δ_m is the deformation at maximum load given by, $\delta_m/t = 0.209(\theta + 2)^{-0.32}$. These are also the same relationships proposed by Lesik and Kennedy (1990) except that the function $f(p)$ has been simplified.

According to the AISC Specification the LRFD design strength for a transversely loaded ($\theta = 90^\circ$) fillet weld is given by:

$$\phi R_{Tn} = 0.75 (0.6) (1.5) F_{EXX} A_w = 0.675 F_{EXX} A_w \quad \text{(Equation 3-2)}$$

Lesik and Kennedy (1990) developed their strength relationship based on test data obtained with tension loaded specimens. They noted that different strength values are obtained if compression loaded test specimens are used. Using the actual average test longitudinal strength (R_L) to normalize the strength results for tested transverse loaded specimens (R_T), Lesik and Kennedy (1990) obtained the ratio mean $R_T/R_L = 1.431$ for the tension induced shear specimen data set used to develop the load-deformation relation. Based on an available compression induced shear test data set, Lesik and Kennedy (1990) obtained the mean ratio $R_{Tc}/R_{Lc} = 1.185$. Since typical equipment anchorages will undergo both tension and compression induced shear in the base fillet welds during reverse cycle loading, it would appear reasonable to consider that the mean ratio, $R_T/R_L = \frac{1}{2}(1.431 + 1.185) = 1.308$ as a more representative indication of transverse weld strength. Lesik and Kennedy (1990) indicate that the mean longitudinal test strength can be taken as $R_L = 0.749 (1.123) F_{EXX} A_w = 0.841 F_{EXX} A_w$. Thus, the mean transverse weld strength for both tension and compression induced shear may be expressed as $R_T = 1.308 (0.841) F_{EXX} A_w = 1.100 F_{EXX} A_w$. The margin, represented by the ratio of mean test strength to design strength is then

$$R_T/(\phi R_{Tn}) = 1.100/0.675 = 1.63 \quad \text{(Equation 3-3)}$$

therefore, the margin for mean capacity/design strength for a fillet weld load in transverse shear can be conservatively taken as a value of 1.6.

The load-deformation relationship for a fillet weld in transverse shear was developed in terms of the mean strength level as $R = R_T f(p)$. For $\theta = 90^\circ$, the deformation ratio at maximum load is $\delta_m/t = 0.04917$. In addition, Lesik and Kennedy (1990) defined the limiting deformation at rupture as $\delta_u/t = 1.087(\theta + 6)^{-0.65}$. For $\theta = 90^\circ$, the deformation ratio at rupture is $\delta_u/t = 0.05594$. Given these two values, a normalized transverse force deflection curve, $R/R_T = f(\delta/t)$ can be plotted as indicated in Figure 3-3. This represents the expected limit state behavior of fillet welds loaded in transverse shear. This relationship indicates that the ultimate deformation is governed only by the fillet weld leg size. Thus, the length of a weld does not influence the ultimate deformation. A fillet weld that is twice as long will have twice the force capacity but it will have the same deformation as a weld that is half its length. Lesik and Kennedy (1990) also defined an initial linear portion of the load-deflection relationship as, $f(p) = 8.234 p$, $0 < p \leq 0.0325$. For the transverse weld, $R/R_T = (8.234/\delta_m/t) \delta/t = 167.46 \delta/t$, for $\delta/t \leq 0.001598$. An equivalent bilinear resistance function can be defined as indicated in Figure 3-3 which has the same area under the load-deflection curve as the normalized transverse fillet weld load-deformation relationship. Note that the linear portion of the load-deflection relationship is extended to define an effective yield level deformation for the equivalent resistance function. The yield level of the equivalent elasto-plastic function is $R_y/R_T \approx 0.89$ and the corresponding yield deformation is $\delta_y/t = 0.005315$.

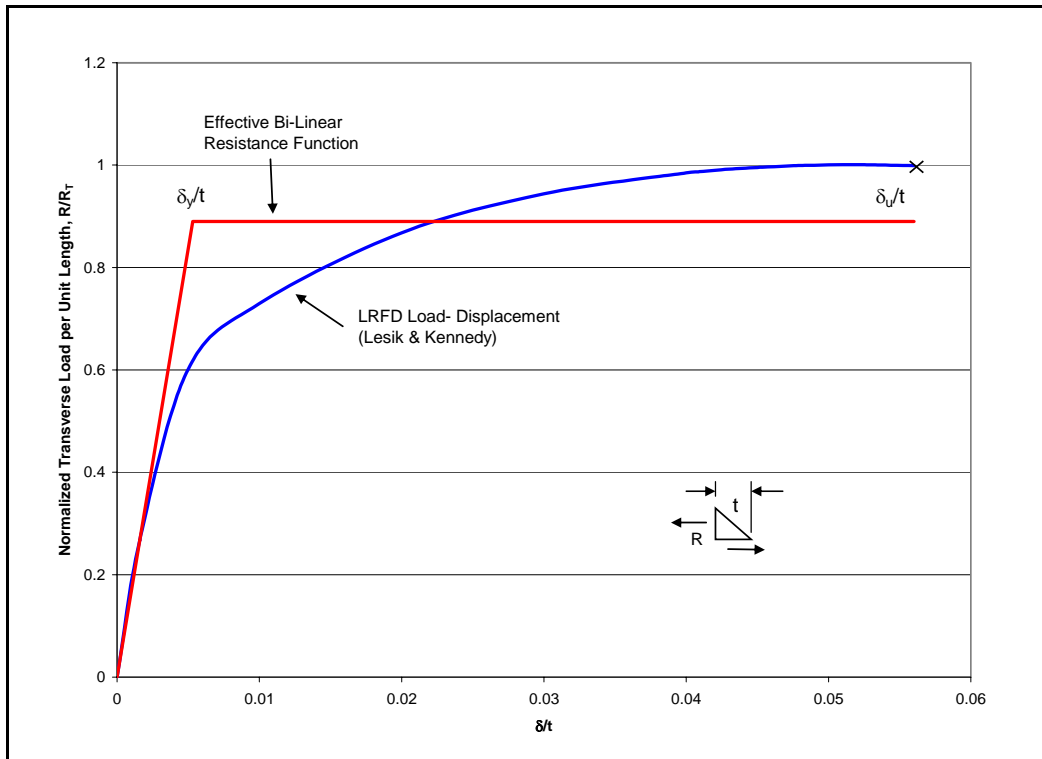


Figure 3-3
Normalized Load-Deformation of Fillet Weld in Transverse Shear

If $t = 3/16$ inch, then $\delta_y = 0.001$ inch and $\delta_u = 0.0105$ inch which provides a maximum deformation ratio of $\mu = \delta_u/\delta_y = 10.5$. If the electrode strength is conservatively chosen as $F_{EXX} = 60$ ksi, and if the effective weld throat area is taken as, $A_w = 0.707 t l$, where l is the weld length, then $R_y/l = 0.89 (1.1) F_{EXX} A_w = 7.8$ kip/inch. The values of $\delta_y = 0.001$ inch and $\delta_u = 0.0105$ are the same values used by Reed et al (1993) for non-linear response studies using the equivalent resistance function. Reed et al (1993) used a slightly more conservative value of $R_y/l = 7.5$ kip/inch to model the effects of a $3/16$ inch minimum fillet weld.

Cyclic Response Effects

Reed, et al (1993) did not address the strength degradation of fillet welds due to reverse cycle loading. The value of δ_u was inferred to be the failure displacement. It was assumed that a weld could sustain several reverse cycles of lesser displacement prior to reaching the failure displacement in the final cycle. The ability of a component to cyclically deform in such a manner is dependent upon a number of factors. The first issue that needs attention is the definition of mean fracture displacement used by Lesik and Kennedy (1990). While the strength levels were determined based on several different data sets generated in different research programs, the load-deformation relationship was determined using test data generated by a single investigator. A subsequent static test program (Bowman and Quinn, 1994) indicated that while transverse fillet weld strength was 1.3 to 1.7 times the longitudinal strength, the ultimate deformation of the transverse specimens (tension induced shear) was significantly greater (by factors of 1.5 to 3.0) than the data set used by Lesik and Kennedy (1990). Since the Lesik and Kennedy (1990) formulas have been included in the AISC Specification, there have been a number of test programs conducted to verify the conservatism of the provisions for fillet weld strength and

deformation capacity. Grondin et al (2002) have shown that the mean fracture displacement ratio was found to exceed $\delta_u/t = 0.114$ and the displacement at maximum load exceeded $\delta_m/t = 0.108$ for a set of 102 tests on transverse loaded fillet welds fabricated with varying different types of weld electrodes. These values are to be compared to the mean values $\delta_u/t = 0.056$ and $\delta_m/t = 0.049$ determined by Lesik and Kennedy (1990) for transverse loaded fillet welds. Callele et al (2005) also indicates, based on review of additional test programs, that the values of fracture displacement given by Lesik and Kennedy (1990) are greatly exceeded. In addition, some tests have shown that, if the attached plate yields, even greater weld displacement at fracture is observed. The summary conclusion of these additional test programs is that the actual weld deformation at fracture is at least a factor of two greater than the values predicted by the Lesik and Kennedy (1990) relationships. Thus, it is concluded that use of the equivalent linear resistance function, shown in Figure 3-3, in the non-linear analyses performed by Reed et al (1993) provide a very conservative measure of equipment response modification if a weld in transverse shear is used as the surrogate anchorage component.

Having established that the measure of deformation capacity used by Reed et al (1993) is much less than the actual estimated failure level, the issue of repeated cycling of a fillet weld under transverse shear loading still needs to be addressed. While the AISC Specification indicates that cyclic fatigue effects in connections need not be considered for cycles less than $N = 20,000$, recent earthquakes have shown that welded steel connections can be susceptible to low-cycle fatigue. In general, the noted low cycle fatigue failures attributed to earthquake cycling were not load carrying fillet welds and the identified concern was often joint configuration design and field weld quality control.

A fillet weld is normally used to join two plates, either as a lap joint or as a T-joint. A fillet weld is associated with two fatigue failure modes. One failure mode is not concerned with the weld itself but rather the failure of the attached plate caused by a crack initiated at the toe of the weld and propagating through the plate. In this case, the toe of the weld is acting as a strain raiser and the material being cycled is within the plate. Most of the fatigue testing performed on fillet weld connections deal with this configuration. It should be noted that for this configuration, the fillet weld can either transfer load (load carrying) or simply attach a non-loaded plate (non-load carrying). The other failure mode is through-the-throat of the weld which is load carrying. The fatigue failure in this case is automatically a fracture mechanics problem since a fillet weld is born with a crack at the root. The surrogate weld anchorage problem, posed as a cabinet frame attached to an embedment plate, is focused on the through-the-throat failure mode.

The subject of low cycle fatigue of welded structural steel connections is an area of active research. Much of the research on load-carrying fillet welds is focused on applications in offshore oil structures, shipbuilding, and bridges. A large portion of this research is concentrated in Europe to support the on-going development of unified European standards and codes. Gurney and MacDonald (1995) have developed a fracture mechanics based approach for the through-the-throat failure mode which validates the approach used in the British Standards and adopted into the draft Eurocodes. The general result is a linear empirical correlation between $\log N$ and $\log S$ where N is the number of cycles and S is a measure of the applied range of stress being cycled. When fatigue data is plotted, the data invariably fits a line (log-log axes) with slope of 3. This value of 3 can actually be traced to the fracture mechanics of the fillet weld configuration. Thus, the fatigue strength of a fillet weld can be expressed as $S^3N = K$ where K is an empirical constant. Currently available data (Fracture Control, 2004) has validated this approach for a

number of different weld types including transverse loaded fillet welds. In general, the available data is focused on the cyclic range of $N=100$ to $N=100,000$ cycles. The few tests that provide data for the range $N<100$ cycles are actually from earthquake research programs on welded steel joints. It appears that this range of ultra-low cycle fatigue is the domain of current seismic research. Ballio and Castiglioni (1995) demonstrate that much of this very low cycle data also approximately fit the $S^3N = K$ relationship if S is re-interpreted as $S^*=E(\Delta\varepsilon)$ where E is the elastic modulus and $\Delta\varepsilon$ is a strain range. If the ratio of strain range to the yield strain is assumed to be equal to the ratio of displacement range to yield displacement, or $\Delta\varepsilon/\varepsilon_y = \Delta\delta/\delta_y$, then $S^*=f_y(\Delta\delta/\delta_y)$ where $f_y = E\varepsilon_y$ is an effective yield stress, $\Delta\delta$ is the range of displacement cycled, and δ_y is the yield displacement. This approach converts the local strain measures to global structural deformations, allowing the overall fatigue evaluation of structural connections using measured test deformations rather than predicting local inelastic strain by analysis. Ferreira et al (1998) apply the method to a series of steel transverse fillet weld cyclic tests (all specimens failed in the weld) with some of the tests having ultra low cycles at failure ($N\sim 30-40$), and find that $\log K = 12.72$ for a effective yield stress of 250 MPa (~ 36 ksi). The slope of the $\log S^* - \log N$ line was 3.09. Displacement ratios up to ± 8 were obtained, however, plate yielding was occurring which may enhance the deformation of the weld. Applying this result to the equivalent idealization used by Reed et al (1993) with an assumed cyclic deformation ratio of ± 10.5 , we estimate S^* as $S^*=250(2)(10.5) = 5250$ MPa. Then, $\log N = 12.72 - 3.09 \log (5250)$, or $N = 17$ full cycles. Recognizing that this estimate of fillet weld cyclic behavior is based on limited test data, it does provide the order of the expected full cycles before fatigue failure. During seismic response, connections are subjected to cyclic loading with peaks of varying fractional amplitude. Various methods for converting fractional peak cycles to equivalent full cycles are used to account for the difference between actual cyclic loading and the full cycle loading used in traditional low-cycle fatigue tests. The equivalent number of full cycles expected during a seismic motion is conservatively estimated to be < 10 . Thus the issue of low cycle fatigue is judged to not be a concern for a transverse loaded fillet weld used as the surrogate anchorage component.

4

EVALUATION MODELS

Background

The consideration of the effects of negligible inelastic deformation on the high frequency response of equipment was the focus of a previous EPRI study (Reed et al, 1989). The study developed two evaluation models to demonstrate the high frequency response behavior of equipment systems mounted within a plant structure. As a first order approximation, it was assumed that the non-linear behavior was concentrated in the anchorage load path with the supporting structure and equipment frame remaining linear. Very general two-degree-of-freedom (2DOF), multi-parameter, systems were derived to allow evaluation of the equipment when subjected to high frequency seismic input motion. One type of model considered the translational response of a squat item of equipment that subjected the support component to horizontal shear forces only. The model considered the partition of the equipment mass between the base and the upper flexible portion of the equipment. Rigid body modes as well as frictional sliding effects were incorporated into the model which was designated as the 'sliding' case. The other type of model considered the translational rotational response of a tall item of equipment that subjected the support component to vertical forces caused by the overturning response of the equipment. This model was very complex with both translational and rotational inertia partitioned between the base and upper flexible portion of the equipment, plus the consideration of gaps allowing free rocking of the equipment. This second model was designated as the 'rocking' model.

A fillet weld, loaded in transverse shear, was then selected as the surrogate anchorage load path component since a minimum size transverse loaded fillet weld would have the least non-linear deformation capacity of all possible anchorage support components considered. Both models, with minimum fillet weld anchorage and selected parameters, were then subjected to non-linear time-history analyses using a set of selected time-history records. Then, an equivalent linear idealization of the response of the models was proposed and additional empirical parameters determined which allowed the response of the models to be estimated using linear response spectra. The study then concluded that the 2DOF models could each be simplified to a single-degree-of-freedom (SDOF) model that then could be used to obtain new design spectra modified to account for non-linear high frequency response de-amplification effects. The previous study fully documented the development of the 2DOF models, the equivalent linearization of each model, and the resulting simplified SDOF model which was then applied to obtain design spectra modified for high frequency non-linear effects. This presentation, however, forces the reader to fully comprehend the complex models and their equivalent linearization before the application of the recommended simplified SDOF models can be understood.

The purpose of the following sections is to present the direct development of the simplified SDOF models and their respective equivalent linearization. It is shown that, in fact, the two models can actually be considered to result in the same equations, resulting in a common equivalent linear response estimation procedure. Since the simplified models do not allow friction sliding or free rocking between gaps, they are denoted in this report as the Shear

Resistance Model and the Overturning Resistance Model to emphasize that only positive anchorage components are considered to be present in the load path.

Shear Resistance Model

The Shear Resistance Model is based on the behavior of a low-aspect ratio equipment item, such that the weld support attachments are subjected to transverse horizontal loading only, as shown in Figure 4-1.

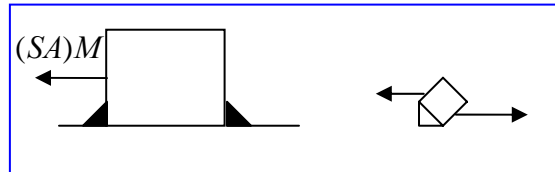


Figure 4-1
Transverse Loading of Weld Support Attachment

The equipment item is characterized as a SDOF system with mass, M , and stiffness K_f , resulting in a fixed-base frequency, f_f , given by:

$$f_f = \frac{1}{2\pi} \sqrt{K_f / M}, \text{ or alternately } K_f = (2\pi f_f)^2 M$$

The weld support component is characterized by a bi-linear resistance function with initial stiffness, K_w , a yield force level, F_y , and an ultimate displacement capacity, δ_u , which is specified by the maximum deformation ratio, $\delta_u / \delta_y = \mu$. The equipment/anchorage system is idealized as series resistance function consisting of a linear equipment resistance and a non-linear weld support attachment resistance as shown in Figure 4-2. It is important to note that the non-linear behavior is confined to the anchorage weld component only. For low frequency systems with substantial elastic response deformation, the presence of a small inelastic deformation in the anchorage component will have a negligible effect on the equipment response.

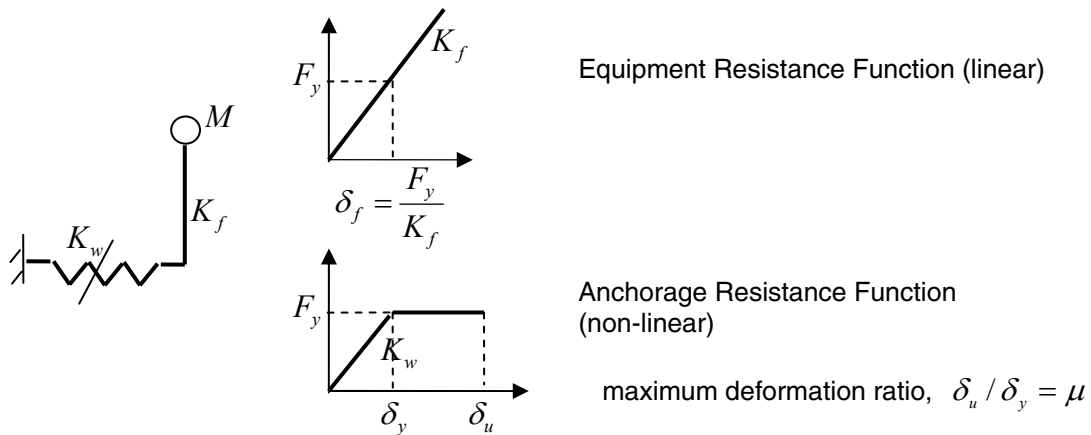


Figure 4-2
Basic Shear Resistance Model

If the series resistance is considered, the combined load-deflection curve defines the quarter cycle resistance function shown in Figure 4-3 results with series stiffness, K^* , defining the yield deformation, δ_y^* , and secant stiffness, K_s , defining the maximum total deformation, δ_u^* . It is important to note that the force level is the same in each resistance component. If the weld stiffness is large compared to the idealized equipment stiffness, then the series stiffness will be approximately equal to the equipment stiffness and the effect on equipment response will be small. If the equipment stiffness is large (i.e., a high frequency item), then the weld stiffness can affect the overall equipment response.

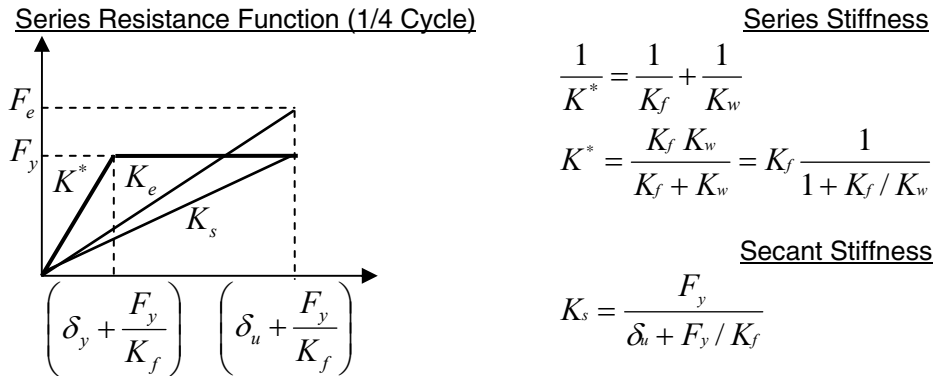


Figure 4-3
Quarter Cycle Series Resistance Function

The quarter cycle resistance function can be used to define the full cycle hysteretic loop shown in Figure 4-4. Investigators (Kennedy, et al, 1984) have shown that an equivalent linear resistance function can be developed which approximates the average reduced stiffness and increased energy dissipation of the non-linear response cycles which occur prior to the peak displacement response. The equivalent system has an effective stiffness, K_e , which is less than the linear

stiffness, K^* , and greater than the minimum secant stiffness, K_s , as shown in Figure 4-3. The energy represented by the area of this loop (or intermediate loop with $\delta_y^* < \delta^* < \delta_u^*$) can be related to the effective damping of the equivalent system.

Full Reverse Cycle Hysteretic Loop

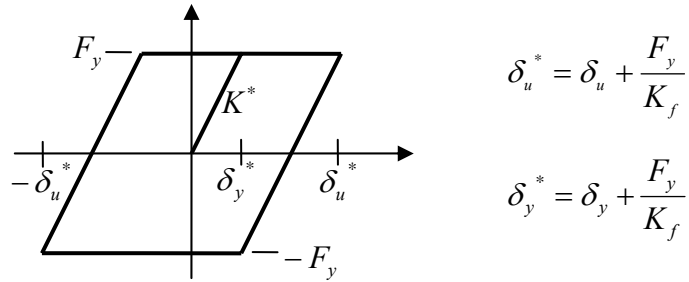


Figure 4-4
Cyclic Hysteretic Behavior

If we define the secant frequency as $f_s = \frac{1}{2\pi} \sqrt{K_s / M}$, then the ratio of secant stiffness to equipment stiffness may be represented as:

$$X = \frac{K_s}{K_f} = \left(\frac{f_s}{f_f} \right)^2 = \frac{F_y}{K_f} \frac{1}{(F_y / K_f + \delta_u)} = \frac{1}{1 + \frac{\delta_u K_f}{F_y}} = \frac{1}{1 + (2\pi f_f)^2 \delta_u \frac{1}{F_y / M}}$$

If we represent the yield force normalized by the equipment mass as the response acceleration causing the initial yield level force, or $SA_y = F_y / M$, then the secant ratio may be expressed as:

$$X = \frac{1}{1 + \frac{(2\pi f_f)^2 \delta_u}{SA_y}} \quad \text{(Equation 4-1)}$$

We now define the effective system frequency, $f_e = \frac{1}{2\pi} \sqrt{\frac{K_e}{M}}$, and let the effective stiffness

ratio be represented as, $X_e = \frac{K_e}{K_f} = \left(\frac{f_e}{f_f} \right)^2$. The prior EPRI study (Reed, et al, 1993)

demonstrated, based on simulation results, that the effective stiffness ratio of an equivalent linear oscillator representing the shear resistance model can be estimated in the form:

$$X_e = 1 - (1 - X)^a \quad \text{(Equation 4-2)}$$

where a is an empirically determined parameter based on statistical regression of the simulation results. The shifted frequency of an equivalent linear oscillator may then be expressed as:

$$f_e = f_f \sqrt{X_e} \quad \text{(Equation 4-3)}$$

Reed et al (1993) also demonstrated that the damping of the equivalent linear oscillator may be estimated in the form:

$$\beta_e = \frac{X}{X_e} [X^{1/2} \beta_f + b \beta_h], \quad \beta_h = \frac{2}{\pi} (1 - X) \left(1 - \frac{1}{\mu} \right) \quad \text{(Equation 4-4)}$$

where b is also an empirically determined parameter based on statistical regression of the simulation results. Given that the parameters a and b are determined, then, if the weld component of the model is proportioned to initiate yielding at a force level corresponding to a given value of yield level acceleration, SA_y , associated with the equipment frequency, f_f , and if the ultimate displacement capacity, δ_u , of the support component is specified by the maximum deformation ratio as, $\delta_u = \mu \delta_y$, the frequency, f_e , and damping, β_e , of the corresponding equivalent linear system is determined by application of eqs. 4-1 through 4-4.

For a given acceleration time-history, representing the horizontal input motion applied at the support anchorage locations, a set of response spectra may be determined. The spectral response of an oscillator with frequency, f_f , and damping, β_f , is denoted as, $SA(f_f, \beta_f)$, and the spectral response of the corresponding equivalent linear oscillator with frequency, f_e , and damping, β_e , is denoted as, $SA(f_e, \beta_e)$, as shown in Figure 4-5. In general, any value of $SA(f_e, \beta_e)$ can be determined from a set of response spectra defined for a range of damping values from, β_f , to a maximum value, $\bar{\beta}_e$.

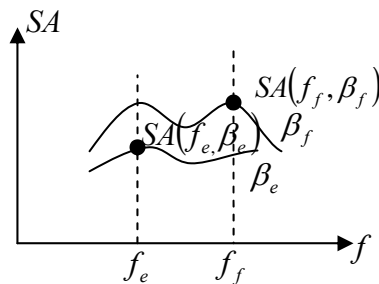


Figure 4-5
Response Spectra for Model Base Input Motion

There are two approaches which can be used to determine the response level associated with the ultimate total displacement capacity, δ_u^* . The first approach considers the yield level of the model to be associated with the spectral level determined by a reference base acceleration time-history motion, or $SA_y = SA(f_f, \beta_f)$. The reference base input time-history motion is then scaled until the total displacement capacity is achieved. This approach is useful for determining parameters a and b of eqs. (4-2) and (4-4) from non-linear time-history simulations. The second approach considers the reference acceleration time-history to remain unscaled, but instead reduces the yield capacity level of the model to a spectral level, $SA_y = SA_e < SA(f_f, \beta_f)$, such that the total displacement capacity is achieved at the spectral acceleration level of the equivalent system, $SA(f_e, \beta_e)$, associated with the spectral acceleration, $SA(f_f, \beta_f)$, which is determined by the reference base acceleration time-history input motion. This approach is useful for the design situation when the reduced yield level is sought which will obtain the total displacement capacity at the design input level. Either approach can be used to determine the input scale factor, F_μ , or the spectral de-amplification factor, $1/F_\mu$, as shown in the following.

Input Scaling Approach

Consider an oscillator which has a yield force level given by the expression $F_y = [SA(f_f, \beta_f)]M$. The response force level of the corresponding effective linear oscillator, is then, $[SA(f_e, \beta_e)]M$. Now consider additional scaling of the equivalent oscillator response to achieve the maximum displacement, $\delta_u^* = (\delta_f + \delta_u)$, or

$$\delta_u^* = (\delta_f + \delta_u) = F_\mu \frac{SA(f_e, \beta_e)}{(2\pi f_e)^2}$$

where F_μ is the non-linear input scale factor, by which the floor input motion must be increased to achieve the maximum displacement, δ_u^* . Note that the pseudo-acceleration approximation, $\frac{SA}{(2\pi f)^2}$, is used to determine the displacement response values.

From Figures 4-2 and 4-3, it may be noted that

$$F_y = K_s \delta_u^* = K_f \delta_f$$

then
$$(\delta_u^*) = \frac{K_f}{K_s} \delta_f = \frac{1}{X} \delta_f$$

but also,
$$\delta_f = \frac{F_y'}{K_f} = \frac{M}{K_f} SA(f_f, \beta_f) = \frac{SA(f_f, \beta_f)}{(2\pi f_f)^2}$$

thus,
$$\delta_u^* = \frac{1}{X} \delta_f = \frac{1}{X} \frac{SA(f_f, \beta_f)}{(2\pi f_f)^2} = F_u \frac{SA(f_e, \beta_e)}{(2\pi f_e)^2}$$

which allows the identification of the input scale factor as

$$F_u = \frac{X_e}{X} \frac{SA(f_f, \beta_f)}{SA(f_e, \beta_e)} \quad \text{(Equation 4-5)}$$

In eq. 4-5, the term, $\left(\frac{X_e}{X}\right)$, represents frequency shift effect and the term, $\left[\frac{SA(f_f, \beta_f)}{SA(f_e, \beta_e)}\right]$, represents the response spectra effect which is dependent on individual spectrum shape and damping. Figure 4-6 shows the scaling approach applied to response spectra.

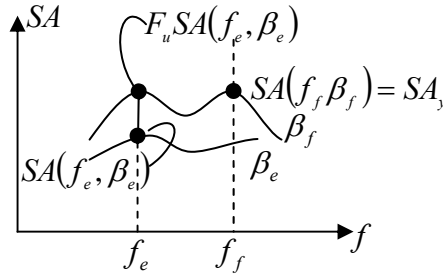


Figure 4-6
Spectral Scaling Approach

Spectral De-amplification Approach

The alternative approach considers reducing the yield level of the

model, $SA_y = SA_e = \frac{SA(f_f, \beta_f)}{F_\mu}$, using a spectral de-amplification factor, $1/F_\mu$. The yield level

acceleration is reduced until the response of the equivalent oscillator achieves the maximum displacement, $\delta_u^* = (\delta_f + \delta_u)$, or

$$\delta_u^* = (\delta_f + \delta_u) = \frac{SA(f_e, \beta_e)}{(2\pi f_e)^2}$$

From 4-3, we note that

$$F_e = K_e \delta_u^* = K_e (\delta_f + \delta_u) = [SA(f_e, \beta_e)] M$$

and
$$F_y = K_s \delta_u^* = K_s (\delta_f + \delta_u)$$

$$\begin{aligned} \text{thus } F_y &= \frac{X}{X_e} F_e = \frac{X}{X_e} [SA(f_e, \beta_e)] M = SA_c M = SA_y M \\ &= \frac{[SA(f_f, \beta_f)] M}{F_\mu} \end{aligned}$$

which allows the identification of the spectral de-amplification factor as

$$1/F_u = \frac{X}{X_e} \frac{SA(f_e, \beta_e)}{SA(f_f, \beta_f)} \quad \text{(Equation 4-6)}$$

Figure 4-7 shows the de-amplification approach applied to response spectra. Comparison of eqs. 4-5 and 4-6 indicate that they are reciprocal relations, thus either approach yields the same maximum total deformation of the shear resistance equipment model.

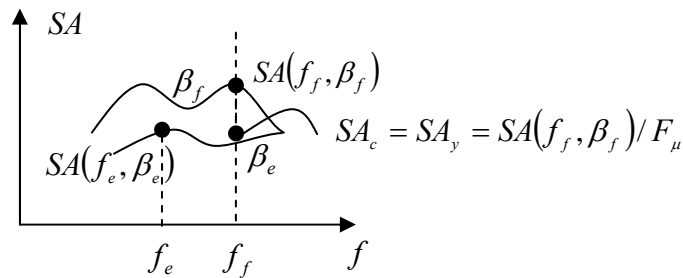


Figure 4-7
Spectral De-amplification Approach

Overturning Resistance Model

The Overturning Resistance Model is based on the behavior of a high-aspect ratio equipment item, such that the weld support attachments are subjected to vertical loading caused by the forces resisting overturning, as shown in Figure 4-8. It is assumed that these overturning forces are large compared to the horizontal transverse shear loading which is also applied to the weld support components.

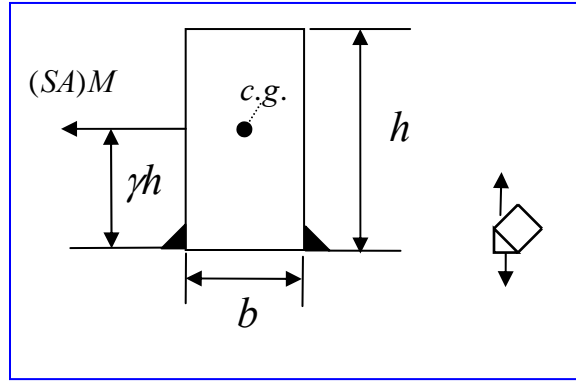


Figure 4-8
Loading of Weld Support Attachment Caused by Overturning

The equipment item is characterized as a SDOF system with mass, M , and stiffness K_f , resulting in a fixed-base frequency, f_f , given by:

$$f_f = \frac{1}{2\pi} \sqrt{K_f / M}, \text{ or alternately } K_f = (2\pi f_f)^2 M$$

The weld support component is characterized by a bi-linear resistance function with initial stiffness, K_w , a yield force level, F_y , and an ultimate displacement capacity, δ_u , which is specified by the maximum deformation ratio, $\delta_u / \delta_y = \mu$. The resistance functions may be idealized as shown in Figure 4-9. Similar to the Shear Resistance Model, the non-linear behavior is confined to the support attachments only.

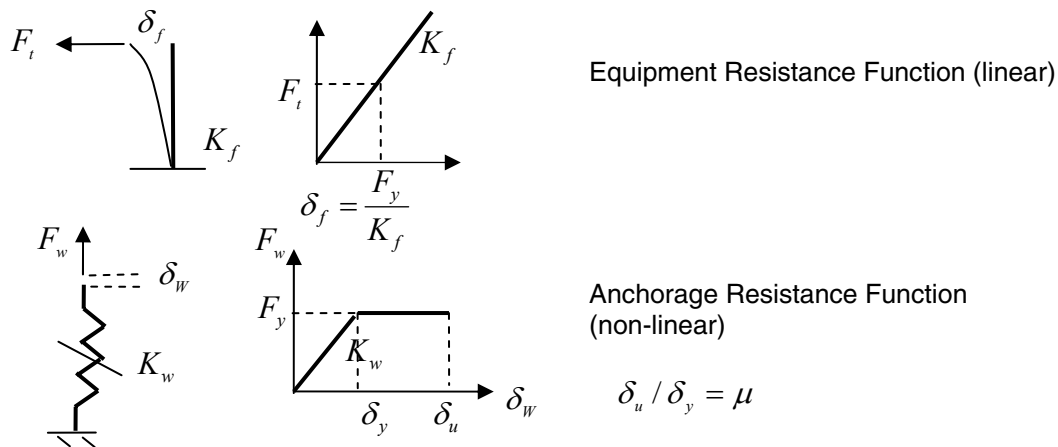
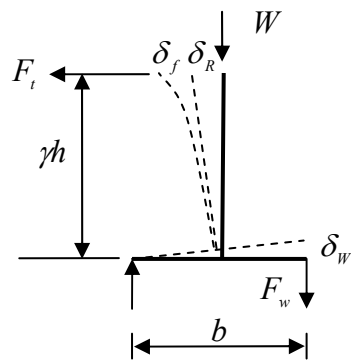


Figure 4-9
Basic Overturning Resistance Functions

Figure 4-10 illustrates the overturning deformation kinematics and the force resistance mechanics. Noting that the height from the base to the equipment c.g. is identified as a factor, γ ,

times the overall equipment height, h , the effective aspect ratio is defined as $e = \gamma h / b$ where b is the base width between support attachment points. In general, it is assumed that $e > 1$. The total horizontal displacement, δ_t , of the equipment c.g. is the sum of the equipment deformation, δ_f , and the deformation due to the rigid body rotation of the equipment base is defined by the rotational kinematics as, $\delta_r = e\delta_w$, where δ_w is the deformation of the weld in the vertical direction. Consideration of the force mechanics indicates that the overturning moment is resisted by the weld force times the base width and also reduced by the restoring moment of the dead weight of the equipment. The dead weight restoring moment acts to create a horizontal force dead-band in the effective horizontal resistance function associated with the weld deformation, since the weld will not be stressed until the overturning moment created by the lateral inertia force exceeds the dead weight restoring moment.



Deformation Kinematics:

$$e = \gamma h / b$$

$$\delta_r = \gamma h \delta_w / b = e \delta_w$$

$$\delta_t = \delta_f + \delta_r$$

Force Mechanics:

$$F_t(\gamma h) = F_w b + W b / 2$$

F_H = Horizontal force applied to mass, M

$$F_H = F_t - W / (2e) = F_w / e, F_t > W / (2e)$$

$$F_H = 0, F_t \leq W / (2e), \delta_r = 0$$

Figure 4-10
Deformation Kinematics and Force Mechanics

Figure 4-11 shows the effective horizontal resistance function associated with the weld deformation. For large aspect ratios and high equipment response levels, the effect of the dead weight restoring force will be small and can be conservatively ignored. This is consistent with the common design practice of designing post-installed anchorages to resist the full overturning moment without consideration of dead weight restoring effects. The stiffness, or slope of the resistance function, can be related to the stiffness of the weld support component as, $K_R = K_w / e^2$, which is demonstrated in Figure 4-11.

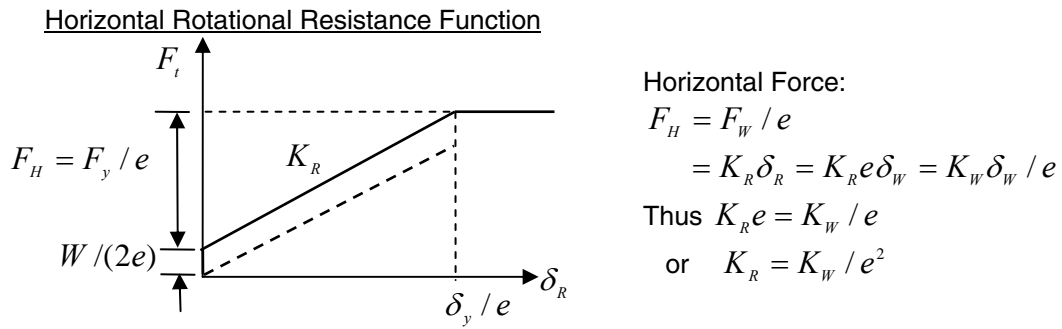


Figure 4-11
Horizontal Rotational Resistance Function

The equipment/anchorage system may now be idealized as series resistance function consisting of a linear equipment resistance and a non-linear effective rotational weld attachment resistance (ignoring dead weight restoring effects) as shown in Figure 4-12. This is similar to the Shear Resistance Model developed above except that the non-linear weld deformations are scaled by the aspect ratio, e , and the yield level force applied to the equipment mass is denoted as, F_y .

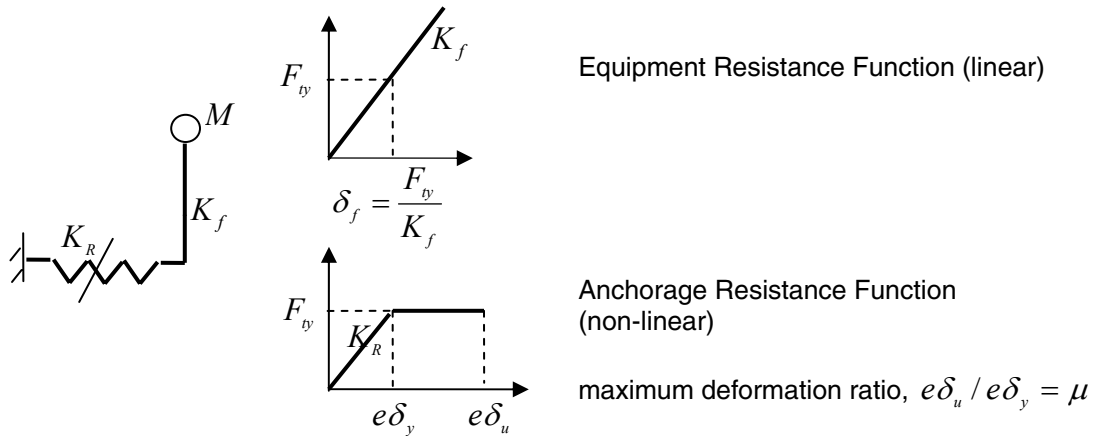


Figure 4-12
Basic Overturning Resistance Model

If the effective series resistance is considered, the quarter cycle resistance function shown in Figure 4-13 results with series stiffness, K^* , defining the yield deformation, δ_y^* , and secant stiffness, K_s , defining the maximum total deformation, δ_u^* . As was the case in the Shear Resistance Model, the force level is the same in each resistance component of the Overturning Resistance Model.

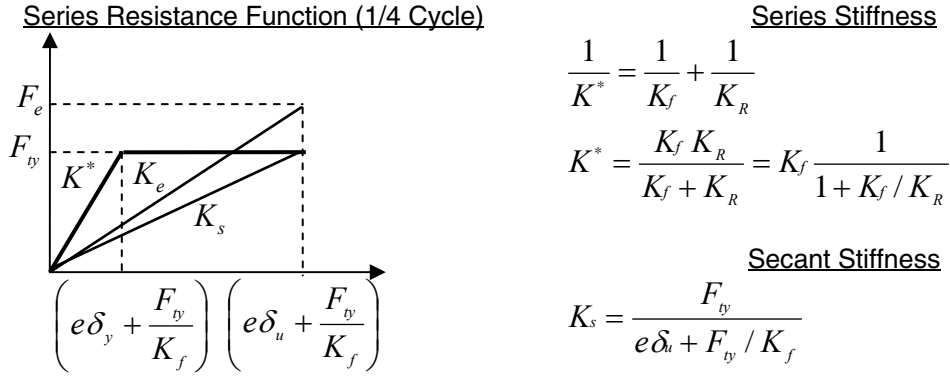


Figure 4-13
Quarter Cycle Series Resistance Function

Given that the dead weight restoring effects are conservatively ignored, the quarter cycle resistance function can be used to define the full cycle hysteretic loop shown in Figure 4-14. The equivalent system has an effective stiffness, K_e , which is less than the linear stiffness, K^* , and greater than the minimum secant stiffness, K_s , as shown in Figure 4-13. It should also be noted that the rotational inertia of the equipment is ignored in the overturning model.

Full Reverse Cycle Hysteretic Loop

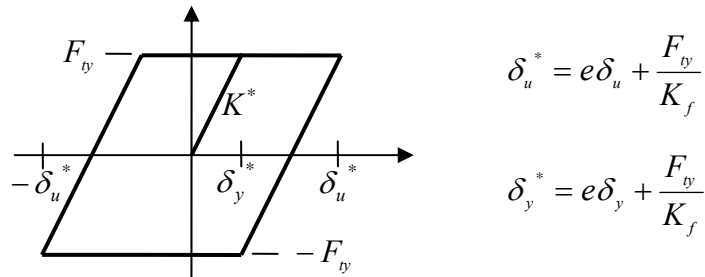


Figure 4-14
Cyclic Hysteretic Behavior

Again we define the secant frequency as $f_s = \frac{1}{2\pi} \sqrt{K_s / M}$, thus the ratio of secant stiffness to equipment stiffness for the overturning model may be represented as

$$X = \frac{K_s}{K_f} = \left(\frac{f_s}{f_f} \right)^2 = \frac{F_{ty}}{K_f (F_{ty} / K_f + e\delta_u)} = \frac{1}{1 + \frac{e\delta_u K_f}{F_{ty}}} = \frac{1}{1 + e(2\pi f_f)^2 \delta_u / \frac{F_{ty}}{M}}$$

If we represent the yield force normalized by the equipment mass as the response acceleration causing the initial yield level force, or $SA_y = F_y / M$, then the secant ratio may be expressed as

$$X = \frac{1}{1 + \frac{(2\pi f_f)^2 \delta_u}{SA_y / e}} \quad \text{(Equation 4-7)}$$

Comparison of eq. 4-7 to the secant ratio used for the Shear Resistance Model, eq. 4-6 indicates that the only difference between the shear and overturning models is the reduced response acceleration, SA_y / e , causing the initial yield level force. With this one change, the remainder of the equivalent linear model development and the relationships developed for the input scaling approach or spectral de-amplification approach of the shear resistance model are directly applicable to the Overturning Resistance Model.

Non-Linear Response Correlation

The prior EPRI study (Reed et al, 1993) established that an equivalent linear evaluation model could be developed to represent the non-linear response of an equipment item idealized as a linear SDOF system with a non-linear anchorage component. The compliance of the system is represented as a series resistance function of the linear equipment resistance and non-linear anchorage resistance. The anchorage resistance is idealized as a bi-linear (elasto-plastic) function with yield force, F_y , ultimate deformation, δ_u , and yield deformation, $\delta_y = \delta_u / \mu$, where μ is the maximum deformation ratio. The simplified model, developed in the foregoing, begins with the specification of system secant stiffness ratio, X , which is the case of the Shear Resistance Model, is

$$X = \frac{1}{1 + \frac{(2\pi f_f)^2 \delta_u}{SA_y}} \quad \text{(Equation 4-8)}$$

where f_f is the equipment frequency and, $SA_y = F_y / M$, given the equipment mass, M .

For the Overturning Resistance Model, the secant ratio is

$$X = \frac{1}{1 + \frac{(2\pi f_f)^2 \delta_u}{SA_y / e}} \quad \text{(Equation 4-9)}$$

where, $e = \gamma h / b$, is the equipment aspect ratio and $SA_y = F_y / M$. The system equivalent stiffness ratio, X_e , is then given by

$$X_e = 1 - (1 - X)^a \quad \text{(Equation 4-10)}$$

where a is a parameter to be established by response correlation. The frequency of the equivalent system, f_e , is then

$$f_e = f_f \sqrt{X_e} \quad \text{(Equation 4-11)}$$

The damping of the equivalent system, β_e , is determined by the set of equations

$$\beta_e = \frac{X}{X_e} [X^{1/2} \beta_f + b \beta_h], \quad \beta_h = \frac{2}{\pi} (1 - X) \left(1 - \frac{1}{\mu} \right) \quad \text{(Equation 4-12)}$$

where, β_f , is the equipment damping ratio and b is a parameter to be established by response correlation. Considering the input scaling approach, the system is proportioned such that, $SA_y = SA(f_f, \beta_f)$, where $SA(f_f, \beta_f)$ is the input motion response spectrum value for the equipment frequency and damping. Having determined the equivalent system frequency and damping, the input motion response spectrum value for the equivalent system can be determined as $SA(f_e, \beta_e)$. The non-linear input scale factor, F_u , is then given as

$$F_u = \frac{X_e}{X} \frac{SA(f_f, \beta_f)}{SA(f_e, \beta_e)} \quad \text{(Equation 4-13)}$$

To establish the parameters, a and b , Reed et al (1993) conducted extensive non-linear time-history response correlation analyses using the program DRAIN2D (Kannan and Powell, 1985). An ensemble of 15 time-histories was selected to represent a wide range of possible earthquake motions: high frequency content, low frequency content, narrow-band spectra, wide-band spectra, etc. Table 4-1 identifies the time-histories used. Two records were artificial, with the remainder being actual recorded earthquake records. Review of the response spectra provided in Reed et al (1993) indicates that at least 9 of the records selected have substantial high frequency content greater than 10 Hz. One-third of the selected records are associated with ENA earthquakes. The purpose for including low frequency records was to demonstrate that small inelastic deformations do not affect the response of low frequency systems. The yield force level, F_y , of the anchorage component was set at 7.5 kips/in with an ultimate deformation of $\delta_u = 0.0105$ inch and a yield level of $\delta_y = 0.001$ inch ($\mu = 10.5$), representing a 3/16 inch fillet weld under transverse loading, based on the relationships developed by Lesik and Kennedy (1988, 1990) from static test data. Two sets of models, one for the shear resistance case (denoted as sliding in the EPRI study) and one for the overturning resistance case (denoted as rocking in the EPRI study), were generated with series resistance functions determined to provide support

yield levels at the reference input motion levels for equipment frequencies f_f of 2, 5, 8, 13, 18, and 25 Hz. The equipment damping was selected as $\beta_f = 0.04$. For the overturning case, the equipment aspect ratio was selected as $e = 3.35$. Given the 6 models for each case, the 15 inputs were scaled until yield occurred in the model. This established the reference input level that initiates yielding of the weld. Then, each input motion was further scaled to establish the non-linear input scale factor, F_μ , for each model. Thus, a matrix of 90 values of input scale factor was obtained for both the shear resistance case and the overturning resistance case. Then, using eqs. 4-8 through 4-13, the values of F_μ corresponding to each model and input motion spectra were computed using different values of parameters, a and b , until an optimum set of values was obtained for each case. The parameter values:

$$a = 1.6$$
$$b = 0.3$$

were found to produce mean ratios of F_μ generated by time-history analysis and F_μ generated using the equivalent linear models which were very close to unity with COVs of 0.106 for the shear resistance model and 0.160 for the overturning resistance model. That the same a and b values were obtained for separate response correlation analyses for the shear resistance model and overturning resistance model should have been expected, since, as shown previously, the two models differ only in the values of modified response acceleration, SA_y or SA_y / e , associated with the initial yield level of each model.

The models developed in the prior study and represented herein, are valid for horizontal input motion only. Vertical motion is a special case since the dead weight effect must first be overcome before any anchorage loading can occur. The consideration of vertical input motion would require 1) the development of the appropriate model modifications, 2) the non-linear response determination using the DRAIN2D program and a suite of time-history records, and 3) the correlation of the non-linear response with an equivalent linear model developed for vertical motion effects.

Table 4-1
Time History Records Used for Response Correlation Analysis (Reed et al, 1993)

No.	Earthquake	Date	Station Name	Direction
1	R.G. 1.60 (Artificial)	<i>Low Frequency Spectra</i>		_____
2	Olympia, WA	04/13/1949	Highway Test Labs	N86E
3	Parkfield, CA	06/27/1966	Cholame No. 2	N65E
4	Tabas, Iran	09/16/1978	Tabas	Trans.
5	Imperial Valley, CA	10/15/1979	E.C. Array No. 5	140
6	Nahanni, Canada	12/23/1985	Site 1	Long.
7	Saguenay, Canada	11/25/1988	Site 20	Long.
8	Gazli, USSR	05/17/1976	Karakyr Point	East
9	Bear Valley, CA	09/04/1972	Melendy Ranch	N29W
10	Gazli, USSR	05/17/1976	Karakyr Point	North
11	Saguenay, Canada	11/25/1988	Site 16	Long.
12	Leroy Modified	<i>Frequency Shifted</i>		_____
13	Leroy, Ohio	01/31/1986	Perry NPP Basemat	South
14	New Brunswick, Canada	03/31/1982	Mitchell Lake	28
15	Artificial	<i>High Frequency Spectra</i>		_____

5

HIGH FREQUENCY STRUCTURAL RESPONSE BEHAVIOR

Response of Building Mounted Components

Figure 5-1 illustrates the fundamental considerations that are used for the determination of seismic response of building mounted components. The ground motion causes the response of the structure, which, in turn, causes the response of the structure mounted equipment items. Reed et al (1993) postulated that any equipment response reduction should be applied as a modification to the ground motion spectrum, which would then be used to define a time history for determination of in-structure spectra that implicitly incorporate the effects of non-linear behavior of anchorages. The motivation for this approach is that structural models have inherent limitations for computing high frequency response, thus the effects of the high frequency content of the structure response motion should be incorporated at the input level rather than the response level. This approach requires that the structure amplification, as measured by the ratio of an in-structure spectrum to input spectrum, be included in the application of the models developed in Chapter 4.

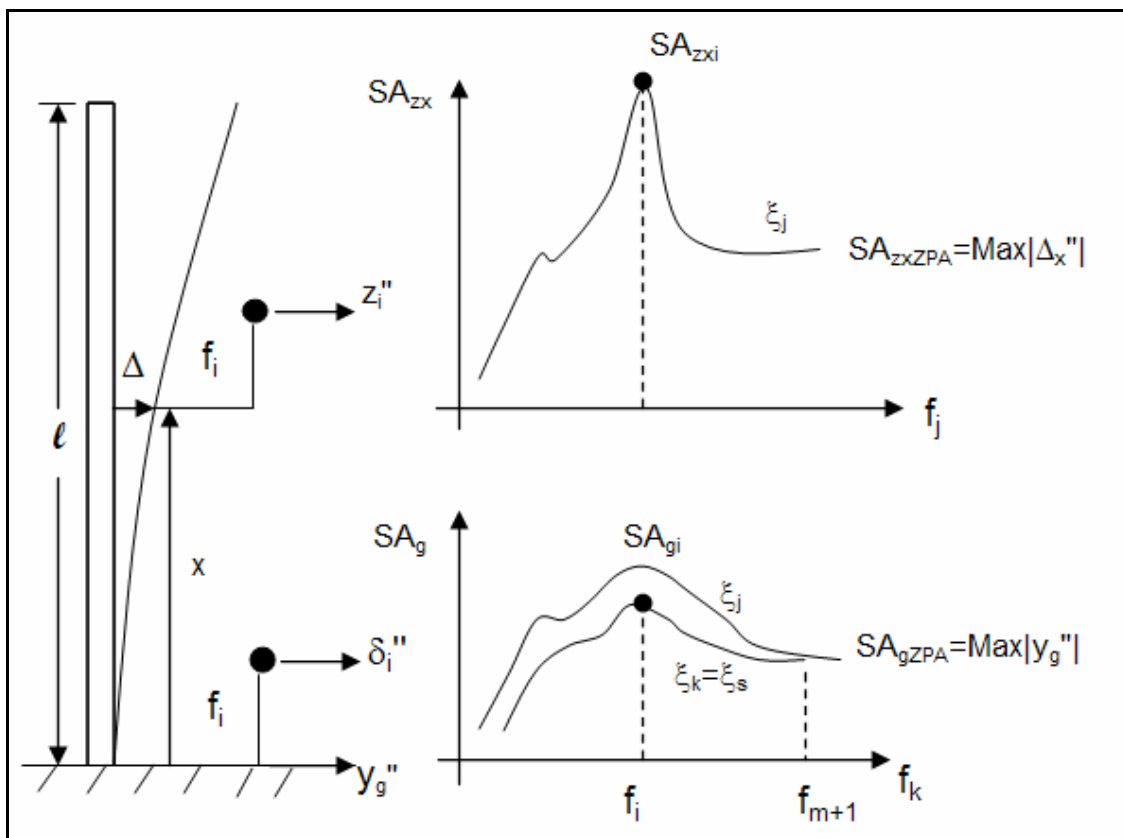


Figure 5-1
Response of Structure Mounted Oscillator

Based on a simple example, Reed et al (1993) concluded that structural amplification effect was approximately a factor of 2 for frequencies greater than 10 Hz if the fundamental frequency of the structure is less than 10 Hz. The purpose of the following sections is to further study the amplification of motion expected within a typical nuclear plant structure and to provide a definitive basis for recommending an amplification factor for use in the determination of the inelastic effects on equipment response.

Base Input Response Spectra

The response of a single-degree-of freedom (SDOF) oscillator with natural frequency f_k mounted on the input base is governed by the equation:

$$\delta_k'' + 2\xi_k \omega_k \delta_k' + \omega_k^2 \delta_k = -y_g''$$

where $\omega_k = 2\pi f_k$ is the circular frequency of the oscillator; ξ_k is the oscillator damping; δ_k , δ_k' , δ_k'' are the relative displacement, relative velocity, and relative acceleration of oscillator mass (throughout this report, v' will denote the first derivative with respect to time and a'' will denote the second derivative with respect to time); and y_g'' is the absolute acceleration of the base defined over $t = 0, T$ where T is the duration of the motion. The absolute acceleration of the oscillator mass is given by $A_{gk} = \delta_k'' + y_g''$ and the peak response over duration of motion is denoted by the spectral acceleration $SA_{gk} = \text{Max}|A_{gk}|$. The plot of SA_{gk} as a function of f_k for a given value of ξ_k is the base input response spectrum. At some frequency, termed the zero period acceleration (ZPA) cutoff frequency, f_{ZPA} , the frequency content of the motion becomes negligible (or the Nyquist frequency of the digitized acceleration record is reached). For oscillator frequencies greater than f_{ZPA} , the spectral acceleration of the oscillator will be the peak acceleration of the base, or $SA_{gZPA} = \text{Max}|y_g''|$.

Structure Response

Given a structure characterized by a modal representation (eigenvalue decomposition) with mode frequencies f_{si} , modal participation factors Γ_i , mode shape $\phi_i(x)$, and modal damping values, ξ_{si} , then the relative response of a structure location at elevation x is given by:

$$\Delta_x'' = \sum_1^n \Gamma_i \phi_i(x) \delta_i''$$

where δ_i'' is the relative acceleration of the SDOF ground mounted oscillator with frequencies $f_k = f_{si}$ and damping $\xi_k = \xi_{si}$. The summation is taken over the set of n modes which characterize the structure. The absolute acceleration of the structure location is given by $A_x = \Delta_x'' + y_g''$ or

$$A_x = \sum_1^n \Gamma_i \phi_i(x) \delta_i'' + y_g''$$

Since the mode shape values satisfy the identity $\sum_1^n \Gamma_i \phi_i(x) = 1.0$, we may write

$$A_x = \sum_1^n \Gamma_i \phi_i(x) [\delta_i'' + y_g''] = \sum_1^m \Gamma_i \phi_i(x) [\delta_i'' + y_g''] + \sum_{m+1}^n \Gamma_i \phi_i(x) [\delta_i'' + y_g'']$$

where the summation has been partitioned into two parts: 1) $i = 1, m$ which has modal frequencies less than the ZPA cutoff frequency of the base input motion and 2) $i = m+1, n$ which

encompasses the remainder set of frequencies that are equal to or greater than the ZPA cutoff frequency. We note that for $f_k \geq f_{m+1} = f_{ZPA}$, the relative response of the ground mounted oscillator is negligible, or

$\delta_i'' \approx 0$, and that $\sum_{m+1}^n \Gamma_i \phi_i(x) = [1 - \sum_1^m \Gamma_i \phi_i(x)]$. Thus, we may write:

$$A_x = \sum_1^m \Gamma_i \phi_i(x) [\delta_i'' + y_g''] + [1 - \sum_1^m \Gamma_i \phi_i(x)] y_g'' = \sum_1^m \Gamma_i \phi_i(x) A_{gi} + [1 - \sum_1^m \Gamma_i \phi_i(x)] y_g'' \quad \text{(Equation 5-1)}$$

where A_{gi} is the absolute acceleration of the SDOF ground mounted oscillator with frequencies $f_k = f_{si}$ and damping $\xi_k = \xi_{si}$.

In-Structure Response Spectra

The response of a SDOF oscillator with natural frequency f_j mounted on the structure at location x is governed by the equation:

$$z_j'' + 2\xi_j \omega_j z_j' + \omega_j^2 z_j = -A_x$$

where $\omega_j = 2\pi f_j$ is the circular frequency; ξ_j is the oscillator damping; z_j, z_j', z_j'' are the relative displacement, relative velocity, and relative acceleration of the in-structure oscillator mass; and A_x is the absolute acceleration of the of the structure location x . The absolute acceleration of the in-structure oscillator mass is given by $A_{z_{xj}} = z_j'' + A_x$ and the peak response over duration of motion is denoted by the spectral acceleration $SA_{z_{xj}} = \text{Max}|A_{z_{xj}}|$. The plot of $SA_{z_{xj}}$ as a function of f_j for a given value of ξ_j is the in-structure response spectrum for an oscillator located at structure position x . For oscillator frequencies greater than f_{ZPA} , the spectral acceleration of the oscillator will be the peak acceleration of the structure at position x , or $SA_{z_{xZPA}} = \text{Max}|A_x|$.

Amplification of Building Mounted Components

The amplification of the in-structure oscillator, at location x , due to the filtering effect of the structure motion may be measured by the ratio of the in-structure response spectrum to the base input response spectrum for the same damping value ξ_j , or

$$AF_x(f_j) = SA_{z_{xj}}/SA_{gi}(\xi_j) \quad \text{(Equation 5-2)}$$

As can be noted from the above development, the in-structure response spectrum ordinate at each frequency, f_j is the sum of the contribution of the response of each structure mode, i . The response of the in-structure mounted SDOF oscillator may then be idealized as the resulting weighted sum of several cascaded SDOF oscillators. Given that the modes are well separated, the amplification factor, AF_x , will have a maximum when the in-structure oscillator is equal or tuned to a structure mode frequency, or $f_j = f_{si}$.

An alternate approach to estimate the amplification of the in-structure oscillator may be based on the random vibration results developed by Crandall and Mark (1963) for a cascaded set of SDOF systems (i.e., uncoupled oscillators) with white noise base motion input. If the motion of the in-

structure position is expressed as, $A_x = \sum_1^m \Gamma_i \phi_{ix} A_i$, then each mode component may be considered

as an independent input to the in-structure oscillator, and thus the contribution of each mode component to the in-structure oscillator response can be considered as the response of two cascaded SDOF systems. The output of the first stage, or structure modal component response, is used as input to the second stage which is the response spectrum oscillator (on the structure) with frequency f_j . The output of the second stage is the modal component of the floor response spectrum ordinate. Now, given that the base input motion for the first stage is characterized as white noise, the root-mean-square (RMS) response of the first and second stage may be obtained from the white noise results presented in Crandall and Mark (1963) for a two-SDOF cascade. Denoting the first stage response as A_{xiRMS} , and the second stage response as A_{zjRMS} , the functional relations presented by Crandall and Mark (1963) may be utilized to obtain an amplification factor which compares the uncoupled response of the in-structure oscillator to the structure response at the point of attachment. We denote this cascade amplification function as the response ratio

$$AF_c = \frac{A_{zjRMS}}{A_{xiRMS}} \left(\frac{f_j}{f_i}, \xi_i, \xi_j \right)$$

which is a function of the frequency ratio, and damping values of the two SDOF systems. The maximum or peak value of the first stage output is the structure modal acceleration response component, $SA_{xi} = \Gamma_i \phi_{xi} SA_{gi}(\xi_{si})$, where $SA_{gi}(\xi_{si})$ is the base input response spectrum ordinate at f_i with damping ξ_{si} . The maximum response of each stage may also be represented by the notation

$$SA_{xi} = \Gamma_i \phi_{xi} SA_{gi}(\xi_{si}) = P_{gi} A_{xiRMS}$$

$$SA_{zj} = P_{zj} A_{zjRMS}$$

where P_{zxi} and P_{gij} are Peak Factors introduced by Vanmarke (1976). Using the above equations, the modal floor response component may be expressed in terms of the modal structure response as:

$$SA_{zji} = AF_c \Gamma_i \phi_{xi} [P_{zj} / P_{gi}] SA_{gi}(\xi_{si})$$

Vanmarke (1976) showed that the peak factors, P , corresponding to a given exceedance level (such as 84%) may be considered, in general, as approximately constant for a damped oscillator over the frequency range 5-50 Hz. Vanmarke (1976) also showed that the ratio P_z/P_g was approximately 0.8-0.9. It is conservative to take this ratio as unity. Now given the tuned case of $f_i = f_j$, the modal contribution associated with the tuned mode will dominate the oscillator response

$$SA_{zj} \approx AF_c(1, \xi_{si}, \xi_j) \Gamma_i \phi_{xi} SA_{gi}(\xi_{si})$$

If this response value is normalized by the ground spectral acceleration associated with the in-structure oscillator damping, $SA_{gj}(\xi_j)$, then

$$SA_{zj}/SA_{gj}(\xi_j) = AF_c(1, \xi_{si}, \xi_j) \Gamma_i \phi_{xi} [SA_{gi}(\xi_{si})/SA_{gj}(\xi_j)]$$

and a bounding approximation for the spectral amplification of the in-structure oscillator, AF_x , may be identified as

$$AF_x(f_i/f_j=1) = AF_c(1, \xi_{si}, \xi_j) \Gamma_i \phi_{xi} [SA_{gi}(\xi_{si})/SA_{gj}(\xi_j)] \quad \text{(Equation 5-3)}$$

Using the equations (or interpolation of graphic figures) presented in Crandall and Mark (1963), AF_c may be determined, for the tuned case ($f_j/f_i=1$) with a structural damping value of $\xi_{si} = 0.07$ and an oscillator damping value of $\xi_{si} = 0.05$, as $AF_c = 6.53$. McGuire et al (2001) provide an empirical relation (discussed in Chapter 6, eq. 6-3) for estimation of spectra for any damping

ratio given the design spectrum is developed for 5% damping. Application of this relation to expected CEUS rock site response spectra will indicate that the ratio, $SA_{gi}(0.05)/SA_{gi}(0.07)$, may be approximated by a value ≈ 0.9 for the frequency range 10-60 Hz. Thus, an estimate of spectral amplification for the tuned case can be obtained, given the modal factor, $\Gamma_i \phi_{xi}$.

When the in-structure oscillator frequency exceeds f_{ZPA} , the spectral amplification factor becomes, $AF_x = \text{Max}|A_x|/SA_{gZPA}$, which may be approximated as

$$AF_x \approx \left\{ \sum_1^m [\Gamma_i \phi_i(x) SA_{gi}/SA_{gZPA}]^2 + [1 - \sum_1^m \Gamma_i \phi_i(x)]^2 \right\}^{1/2} \quad \text{(Equation 5-4)}$$

It should be noted that for the frequency range $f_j > f_{ZPA}$, the spectral amplification factor is a constant value which simply indicates that the in-structure oscillator is undergoing the structure motion at the attachment point without response amplification. In this case, the acceleration can be viewed as pseudo-static loading on the oscillator mass.

Modeling of Structures for Response Determination

The usual procedure used by analysts to obtain in-structure response spectra in nuclear plant structures is to construct a finite element model of the structure with lumped mass inertia which adequately represents the distribution of mass of the structure/contents and which provides a sufficient representation of the stiffness of the major components that resist the inertial loads generated by earthquake ground motion. The structures are designed to maintain elastic material response for extreme design events such as earthquake. Normally, the mass is lumped according to the natural concentrations occurring at the floors of the structure which are spaced at 15-20 ft. intervals. The resulting mass and stiffness arrays are used to form an eigenvalue problem, which yields fixed base frequencies and mode shapes along with the participation factors associated with base input motion. The normal mode method described above is then used to determine the in-structure response using a ground motion acceleration time history that yields ground response spectra that closely match the specified design spectra. While a coarse lumping is sufficient to capture the fundamental modes, the higher modes are only approximately determined. In order to demonstrate the effect of modeling discretization, two different models of the same idealized structure were prepared. Most nuclear plant buildings are cylindrical or box type concrete structures characterized by thick walls with building height that is approximately equal to the plan dimensions. As an example, a fixed-base, free-standing cylinder with height of 165', an outer diameter of 150', and an approximate three foot thickness was chosen as representative of nuclear structures. This example structure is illustrated in Figure 5-2. The dimensionless ratio, $I/(AL^2)$, where I is the moment of inertia of the thick-walled cylinder cross-section, A is the area of the cross-section, and L is the free-standing height of the cylinder, may be computed as approximately $I/(AL^2)=0.1$. Most plant structures will have configurations that yield $I/(AL^2)$ values that fall within the range 0.08-0.12. The cylinder may be idealized as a uniform vertical cantilever beam within uniform cross-section (ignoring any shell modes).

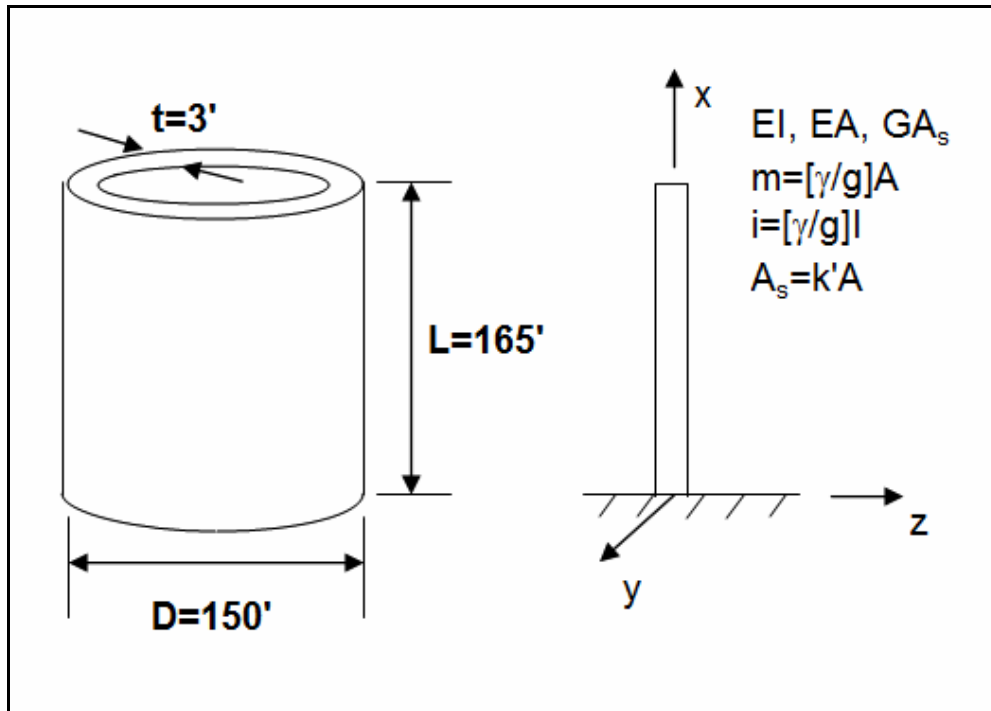


Figure 5-2
Example Representative Plant Structure

Structures of this configuration have lateral deformations that are predominately due to shear, thus the effective shear area, $A_s = k'A$ must be defined. According to Cowper (1966), the shape factor k' for a thick-walled cylinder may be taken as $k' = 2(1+\nu)/(4+3\nu)$, where ν is Poisson's ratio. Given the mass per unit length, $m = (\gamma/g)A$ and the rotary inertia per unit length, $i = (\gamma/g)I$, the remainder of the problem variables may be specified if $E = 35 \times 10^5$ psi, $\nu = 0.2$, and weight density $\gamma = 150$ lb/ft³ (typical for concrete). Noting that $G = E/[2(1+\nu)]$, the dimensionless ratio $E/(k'G)$ may be computed as $E/(k'G) = 4.6$.

Two alternate discretizations of the representative structure model are shown in Figure 5-3. In Case 1, 8 nodes are spaced at eight equal element length elements ($\Delta L = 20$ ft.-7.5in.) while Case 2 has 33 equal element length elements ($\Delta L = 5$ ft.). The properties of both models were entered into the SAP2000 (2003) finite element code using beam elements specified by E , ν , I , A , and $A_s = k'A$. The masses and rotary inertias were lumped at the nodes according to the tributary distribution $m\Delta L$ and $i\Delta L$. The first 12 resulting horizontal mode frequencies and product of participation factor and mode shape ($\Gamma_i \phi_i[x]$) are tabulated in Table 5-1 for selected locations on the modeled structure. As can be noted, the first three modes of both cases have reasonable agreement of frequencies with the $\Gamma_i \phi_i$ values beginning to deviate significantly for the third and higher modes. This example indicates that the normal lumped mass models used for nuclear plant structures will have reasonable accuracy up to about 25 Hz but for response accuracy with input frequency content up to 100 Hz, such models will require much higher discretization.

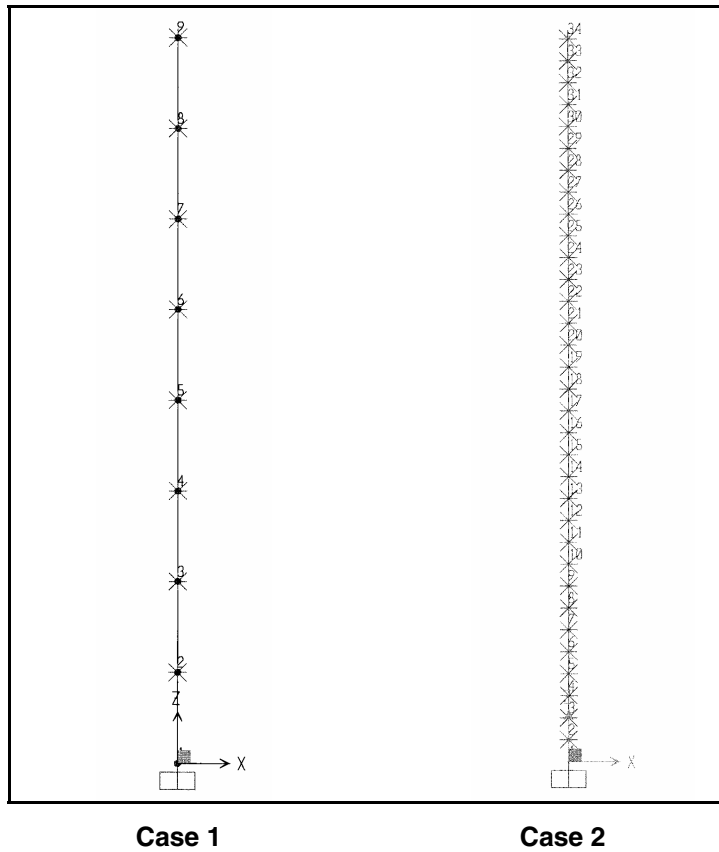


Figure 5-3
Finite Element Idealization of Representative Nuclear Structure

Table 5-1
Comparison of GammaPhi ($\Gamma_i\phi_i[x]$) Computed for Two Alternate Model Discretizations

Case 1

Horz. Mode	f, Hz	f/f ₁	x/L=1	x/L=0.5
			$\Gamma_i\phi_i$	$\Gamma_i\phi_i$
1	6.030	1.000	1.34108	0.73034
2	15.663	2.597	-0.37478	0.36257
3	25.333	4.201	-0.11690	0.09837
4	34.184	5.669	0.24733	-0.16263
5	46.611	7.730	-0.13528	-0.11040
6	49.424	8.196	-0.01991	0.00101
7	57.857	9.595	0.09941	0.06808
8	65.702	10.896	-0.06797	0.04883
9	71.390	11.839	0.03762	-0.02559
10	74.107	12.290	-0.01174	-0.01065
11	77.647	12.877	0.00163	0.00036
12	102.690	17.030	-0.00065	-0.00026

Sum GammaPhi	0.99982	1.00003
---------------------	---------	---------

Case 2

Horz. Mode	f, Hz	f/f ₁	x/L=1	x/L=0.51
			$\Gamma_i\phi_i$	$\Gamma_i\phi_i$
1	6.047	1.000	1.34635	0.71128
2	15.795	2.612	-0.37840	0.37204
3	25.582	4.230	-0.12738	0.11803
4	35.353	5.846	0.26696	-0.15215
5	49.351	8.161	-0.06923	-0.08107
6	51.303	8.484	-0.11610	-0.07109
7	65.343	10.805	0.13957	0.07180
8	78.316	12.951	-0.07298	0.07024
9	81.511	13.479	-0.04020	0.03009
10	93.656	15.487	0.09554	-0.04372
11	107.600	17.793	-0.08061	-0.07322
12	111.050	18.364	-0.00093	-0.00145

Sum GammaPhi	0.96257	0.95077
---------------------	---------	---------

Structure Amplification Study

As outlined above, the determination of the spectral amplification of a structure mounted oscillator may be determined by the modal analysis time-history method using the following sequence of equations:

$$\delta_j'' + 2\xi_j\omega_j\delta_j' + \omega_j^2\delta_j = -y_g'', \quad \omega_j = 2\pi f_j, \quad A_{gj} = \delta_j'' + y_g'' \quad \text{(Equation 5-5)}$$

$$SA_{gj} = \text{Max}|A_{gj}| \quad \text{(Equation 5-6)}$$

$$\delta_i'' + 2\xi_i\omega_i\delta_i' + \omega_i^2\delta_i = -y_g'', \quad \omega_i = 2\pi f_i, \quad A_i = \delta_i'' + y_g'' \quad \text{(Equation 5-7)}$$

$$A_x = \sum_1^m \Gamma_i\phi_i(x)A_i + [1 - \sum_1^m \Gamma_i\phi_i(x)]y_g'' \quad \text{(Equation 5-8)}$$

$$z_j'' + 2\xi_j\omega_jz_j' + \omega_j^2z_j = -A_x \quad \text{(Equation 5-9)}$$

$$A_{zj} = z_j'' + A_x \quad \text{(Equation 5-10)}$$

$$SA_{zj} = \text{Max}|A_{zj}| \quad \text{(Equation 5-11)}$$

$$AF_x(f_j) = SA_{zj}/SA_{gj} \quad \text{(Equation 5-12)}$$

In general, the peak amplification will occur for the tuned case, $f_j=f_i$. The accuracy of the in-structure oscillator response is primarily determined by the accuracy of the m modal frequencies, f_i , and the m products of the modal participation factors and mode shape function, $\Gamma_i\phi_i$. The frequency content of the ground acceleration, y_g'' , is also an important contributor to spectral amplification. The fundamental frequency of most nuclear plant structures of substantial size will be less than 10 Hz. The amplification characteristics of such structures, due the higher modes, do not appear to have been fully studied in the past for the case of ground motion input at the base. The response generated by the structural finite element models used was simply accepted. In addition, the input motions used had ZPA cutoff frequencies of approximately 33 Hz, thus the higher modes were not fully excited. In order to study the effect of high frequency modes (i.e., greater than 10 Hz) on a structure with fundamental frequency less than 10 Hz, it was decided to study the horizontal response of a fixed-base uniform cantilever beam for input time history motions that are characteristic of motions now expected to occur on CEUS rock sites. It was also decided to use analytical solutions rather than finite element models. Most texts on structural dynamics [e.g., Jacobsen and Ayre (1958)] present eigenvalue solutions for uniform beams idealized as continuous elastic bodies. Usually three cases are discussed: 1) flexural beams (also known as an Euler-Bernoulli beams) in which the deformation is due to bending strain of the cross-section, 2) shear beams in which the deformation is due to shearing strain of the cross-section, and 3) and Timoshenko beams in which the deformation is taken as the sum of bending and shear deformations. The solutions are provided as modal frequencies (f_i) and mode shapes (eigenfunctions $\phi_i[x]$) which are determined by the boundary conditions (a vertical cantilever is free at the top and fixed or built-in at the base). The modal frequencies can be expressed as

known ratios times the fundamental frequency which, in some cases, is a simple formula involving the section properties (I, A_s), length (L), uniform mass per unit length (m, i), and the elastic properties (E, G). It is to be noted that a continuous elastic body has an infinite set of modal frequencies in contrast to the discrete set of frequencies determined with a finite element model. The mode shapes $\phi_i[x]$ are expressed as analytic functions of elementary form (\sin, \cos, \sinh, \cosh) which in turn are functions of beam position (x/L) and parameters involving the section properties, unit mass, and elastic material properties. The participation factors for a uniform beam undergoing base input may be defined, in general, as

$$\Gamma_i = \int_0^L \phi_i(x/L) dx / \int_0^L [\phi_i(x/L)]^2 dx \quad \text{(Equation 5-13)}$$

For continuous beams, the eigenfunction normalization, $\int_0^L [\phi_i(x/L)]^2 dx = L$, is commonly used.

The values of participation factors Γ_i for each mode i may be computed using the corresponding eigenfunctions. For the flexure and shear beams, the eigenfunctions are simple analytic forms which can be readily integrated to obtain values of the participation factors, however, the eigenfunctions for the Timoshenko beam are algebraically complicated requiring numerical integration to obtain values of the participation factors. For a flexure beam, the controlling parameter is the ratio $EI/(mL^4)$ while for a shear beam the controlling parameter is the ratio $k'AG/mL^2$. The Timoshenko beam requires specification of two parameters $I/(AL^2)$ and $E/(k'G)$ in addition to either of the parameters $EI/(mL^4)$ or $k'AG/mL^2$. For general details of the governing equations for determining the modal frequencies, eigenfunctions, and participation factors, the reader is referred to the large body of texts and technical review papers (e.g., Han et al (1999), Papadopoulos and Trujillo (1980), Jacobsen, (1938)) on this subject. The general results are summarized below.

Flexure Beam

For a flexure beam, the fundamental frequency may be computed with the formula

$$\omega_{f1}^2 = (2\pi f_{f1})^2 = (1.875)^4 EI/(mL^4) \quad \text{(Equation 5-14)}$$

As can be noted from the above formula, the specification of the first mode frequency, f_{f1} , is sufficient to specify the controlling parameter for the flexure beam. Further, the higher mode frequencies can be specified as ratios of the first mode frequencies. The following Table 5-2 provides the mode frequency ratios, f_i/f_{f1} , mode participation factors, Γ_i , and product of participation factor and mode shape, $\Gamma_i\phi_i$, for representative beam positions. The accompanying Figure 5-4 shows the distribution of $\Gamma_i\phi_i$ over the structure height. For the flexure beam, the second mode peak occurs at $x/L = 0.47$ and has a maximum value, $\Gamma\phi = 0.625$.

Table 5-2
Modal Parameters for Flexure Beam

mode i	f_i/f_n	Γ_i	$\Gamma_i\phi_i (x/L=0.9)$	$\Gamma_i\phi_i (x/L=0.5)$	$\Gamma_i\phi_i (x/L=0.47)$	$\Gamma_i\phi_i (x/L=0.20)$
1	1.000	0.7830	1.35050	0.53169	0.47792	0.10002
2	6.267	0.4339	-0.45455	0.61937	0.62508	0.26128
3	17.547	0.2544	0.11628	0.01002	0.09427	0.30760
4	34.386	0.1819	0.01893	-0.25725	-0.24288	0.27423

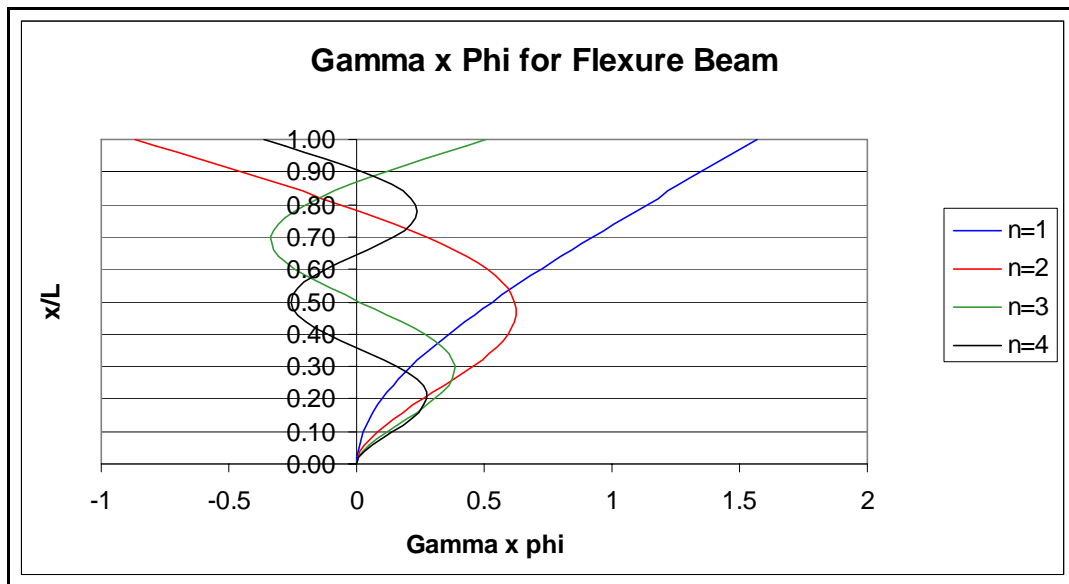


Figure 5-4
Distribution of GammaPhi ($\Gamma_i\phi_i[x]$) for Flexure Beam as a Function of Beam Position

Shear Beam

For a shear beam, the fundamental frequency is determined with the formula

$$\omega_{s1}^2 = (2\pi f_{s1})^2 = (\pi/2)^2 k' AG / (mL^2) \quad \text{(Equation 5-15)}$$

In a similar manner, the specification of the first mode frequency, f_{s1} , is sufficient to specify the controlling parameter for the shear beam along with higher mode frequencies specified as increasing odd number ratios of the first mode frequencies. The following Table 5-3 provides the first seventeen mode frequency ratios, f_i/f_{s1} , mode participation factors, Γ_i , and product of participation factor and mode shape, $\Gamma_i\phi_i$, for representative beam positions. The accompanying

Figure 5-5 shows the distribution of $\Gamma_i \phi_i$ for the first six modes over the structure height. For the shear beam, the second mode peak occurs at $x/L = 0.33$ and has a maximum value, $\Gamma \phi = 0.424$.

Table 5-3
Modal Parameters for Shear Beam

mode i	f_i/f_{s1}	Γ_i	$\Gamma_i \phi_i (x/L=0.9)$	$\Gamma_i \phi_i (x/L=0.5)$	$\Gamma_i \phi_i (x/L=0.33)$	$\Gamma_i \phi_i (x/L=0.20)$
1	1	0.9003	1.25756	0.90032	0.63662	0.39345
2	3	0.3001	-0.37815	0.30011	0.42441	0.34336
3	5	0.1801	0.18006	-0.18006	0.12732	0.25465
4	7	0.1286	-0.08258	-0.12862	-0.09095	0.14715
5	9	0.1000	0.02213	0.10004	-0.14147	0.04372
6	11	0.0818	0.01811	0.08185	-0.05787	-0.03577
7	13	0.0693	-0.04446	-0.06926	0.04897	-0.07924
8	15	0.0600	0.06002	-0.06002	0.08488	-0.08488
9	17	0.0530	-0.06673	0.05296	0.03745	-0.06059
10	19	0.0474	0.06619	0.04739	-0.03351	-0.02071
11	21	0.0429	-0.05988	-0.04287	-0.06063	0.01874
12	23	0.0391	0.04932	-0.03914	-0.02768	0.04479
13	25	0.0360	-0.03601	0.03601	0.02546	0.05093
14	27	0.0333	0.02141	0.03335	0.04716	0.03815
15	29	0.0310	-0.00687	-0.03105	0.02195	0.01357
16	30	0.0290	-0.00643	-0.02904	-0.02054	-0.01269
17	33	0.0273	0.01752	0.02728	-0.03858	-0.03121

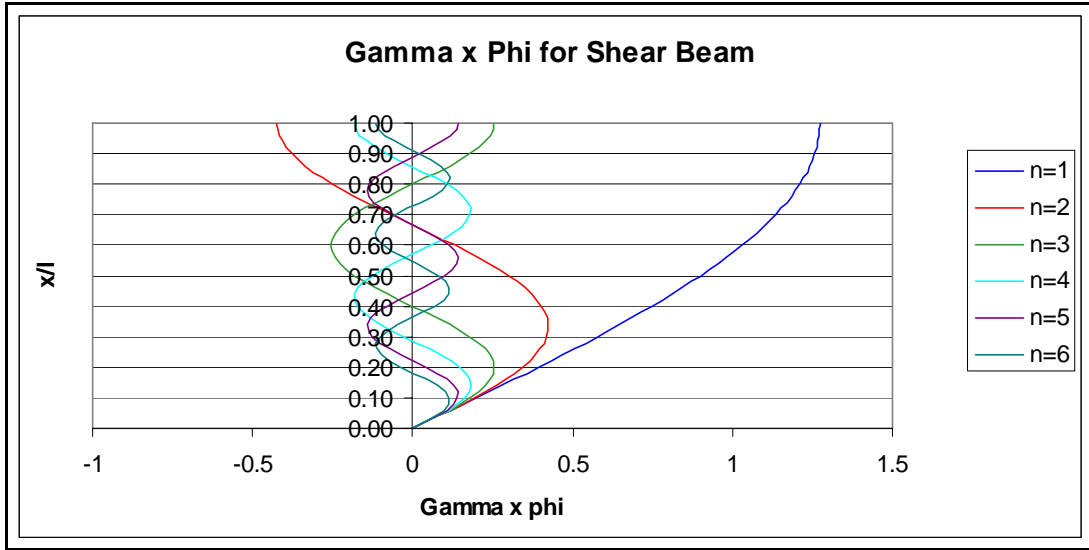


Figure 5-5
Distribution of GammaPhi ($\Gamma_i \phi_i[x]$) for Shear Beam as a Function of Beam Position

Timoshenko Beam

For a Timoshenko beam, the fundamental frequency cannot be expressed as a simple formula. There are actually two pairs of related general solutions (ϕ_i, ψ_i) which apply depending upon whether the mode frequency is less or greater than a critical frequency given by the ratio of the controlling parameters:

$$\omega_c^2 = [k'AG/mL^2] / [I/(AL^2)]$$

In addition, to determine the participation factors, the eigenfunction normalization used in the denominator of eq. 5-13, must be modified to be,

$$\int_0^L [\phi_i(x/L)]^2 dx + I/(AL^2) \int_0^L [\psi_i(x/L)]^2 dx = L \quad \text{(Equation 5-16)}$$

in the case of the Timoshenko beam. Given specification of the two controlling parameters $I/(AL^2)$ and $E/(k'G)$, either of the other parameters $EI/(mL^4)$ or $k'AG/mL^2$, may be determined by computing the fundamental frequency of an assumed shear beam (eq. 5-15), or the fundamental frequency of an assumed flexure beam (eq. 5-14). The reduced fundamental frequency of the Timoshenko beam may then be numerically determined as a factor times the shear beam fundamental frequency, $\omega_{T1} = C_{Ts} \omega_{s1}$, or as a factor times the flexure beam fundamental frequency, $\omega_{T1} = C_{fs} \omega_{f1}$. Given the specification of the first mode frequency, f_{T1} , the higher modes can be determined as ratios. Further, the higher mode frequencies can be specified as ratios of the first mode frequencies f_i/f_{T1} . For this study, the controlling parameters were chosen to match the values of the representative plant structure used in the finite element discretion study, $I/(AL^2) = 0.1$ and $E/(k'G) = 4.6$. The following Table 5-4 provides the mode frequency ratios, f_i/f_{T1} , mode participation factors, Γ_i , and product of participation factor and mode shape, $\Gamma_i \phi_i$, for representative positions over the height of a Timoshenko beam. The accompanying Figure 5-6

shows the distribution of $\Gamma_i \phi_i$ over the structure height. For the Timoshenko beam, the second mode peak occurs at $x/L = 0.38$ and has a maximum value, $\Gamma \phi = 0.413$.

Table 5-4
Modal Parameters for Timoshenko Beam

$I/(AL^3)=0.1, E/(k'G) = 4.6, f_{T1} = 0.823 f_{s1} = 0.542 f_{T1}$

mode i	f_i/f_{T1}	Γ_i	$\Gamma_i \phi_i (x/L=0.9)$	$\Gamma_i \phi_i (x/L=0.51)$	$\Gamma_i \phi_i (x/L=0.33)$	$\Gamma_i \phi_i (x/L=0.20)$
1	1.000	0.8445	1.25896	0.75020	0.54773	0.27064
2	2.618	0.3986	-0.22770	0.36187	0.41346	0.30534
3	4.207	0.1471	-0.13435	0.07537	0.14629	0.13398
4	5.872	0.1798	0.17567	-0.18077	0.03743	0.23940
5	8.168	0.0948	-0.01134	-0.07773	-0.06137	0.08466
6	8.520	0.1013	-0.07197	-0.05413	-0.10619	0.08579
7	10.879	0.1000	0.02431	0.11008	-0.11106	0.04507
8	13.066	0.0620	-0.04987	0.07926	0.09056	0.06687
9	13.545	0.0502	0.00006	0.02166	0.01162	-0.01397
10	15.733	0.0691	-0.04410	-0.08147	0.09715	-0.07842
11	18.160	0.0591	0.05824	-0.04344	0.03767	-0.08143
12	18.464	0.0145	0.00260	-0.00197	0.00149	-0.00527
13	20.623	0.0529	-0.06622	0.06502	-0.04938	-0.06045
14	23.016	0.0464	0.06242	0.02994	-0.06037	-0.01890
15	23.643	0.0081	0.00237	0.00093	-0.00194	-0.00124
16	25.480	0.0428	-0.05963	-0.05419	-0.00196	0.01886
17	27.913	0.0391	0.04894	-0.02287	0.05063	0.04438
18	28.794	0.0025	0.00033	0.00025	0.00022	0.00045
19	30.354	0.0359	-0.03605	0.04664	0.03584	0.05045
20	32.772	0.0332	0.02090	0.01671	-0.01854	0.03787

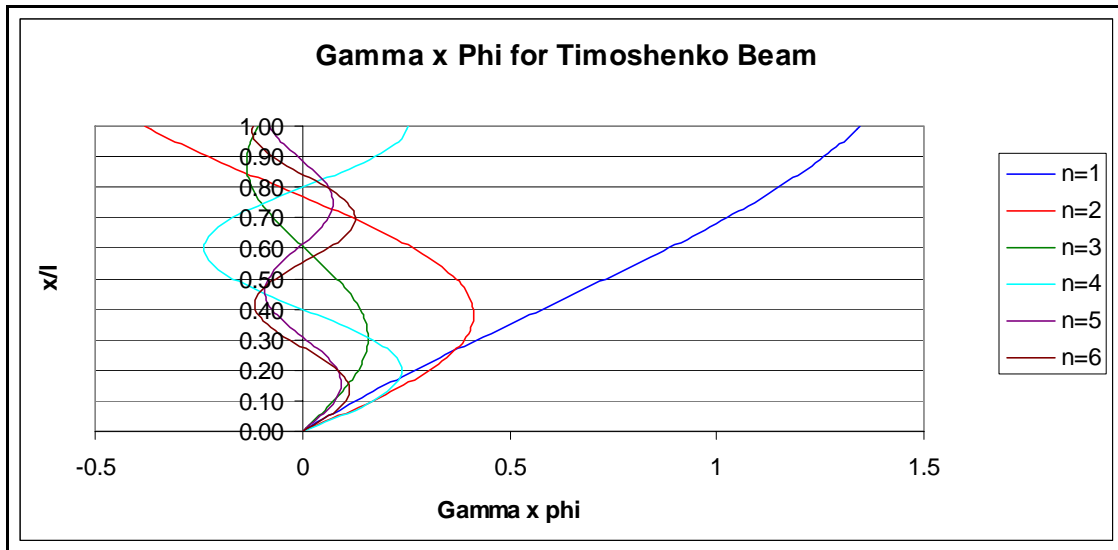


Figure 5-6
Distribution of GammaPhi ($\Gamma_i \phi_i[x]$) for Timoshenko Beam as a Function of Beam Position

For the representative plant structure considered previously behaved as a shear beam the first mode frequency would be computed using eq. 5-15, resulting in a value $f_{s1} = 7.35$ Hz. The Timoshenko beam frequency would be $f_{T1} = 0.823 f_{s1} = 6.049$ Hz which is almost identical to the frequency of the Case 2 finite element model. In general, most plant structures will have response behavior that closer to a Timoshenko beam idealization rather than a flexure or shear beam idealization. Since the controlling parameters are the same as the Case 2 model, the mode frequency ratios and $\Gamma_i \phi_i$ values for $x/L=0.51$ given in Table 5-4 are the exact analytical solution values that can be compared to the refined finite element model results (higher discretion Case 2) given in Table 5-1. As can be noted, the frequency ratios are in general agreement up to the 10th mode, but the $\Gamma_i \phi_i$ values deviate for the 3rd and higher modes. Thus, the modal response computed with a more refined finite element model would not yield the same high frequency response as the analytical solution due to different weighting factors (i.e., $\Gamma_i \phi_i$) being applied to the response contribution of each mode.

Selection of Time-History Motions for Amplification Study

In order to study the effect of high frequency modes (i.e., greater than 10 Hz) on structures with fundamental frequencies less than 10 Hz, it is important to select input time history motions that have input power concentrated in the greater than 10 Hz range. Three acceleration time-histories were chosen that are distinguished by their high frequency content:

1. Time-History Motion 1: An artificial time-history motion that is compatible with a horizontal design spectrum used in Europe for hard rock sites (SKI, 1992). This time-history has been used to evaluate the various structures of several European nuclear plants sited on hard rock. It has an approximate duration of 6 seconds and is scaled to an approximate peak acceleration of 0.1 g as shown in Figure 5-7. The response spectrum of the motion for 5% damping is shown in Figure 5-8. The frequency content of the time-history is concentrated in the 10-20 Hz range with a PGA cut-off frequency of approximately 50 Hz.

2. *Time-History Motion 2*: A time-history motion that was developed to match an example response spectrum that is representative of the horizontal spectra that are expected for a CEUS rock site. An actual recorded rock record was used as the seed motion. The record was windowed to isolate the portion of the motion associated with the shear wave and then modified to have a response spectrum compatible with the example spectrum. The time-history is defined for an approximate 10-second window and has an approximate peak acceleration of 0.55 g as shown in Figure 5-9. The response spectrum of the motion for 5% damping is shown in Figure 5-10. As can be noted in Figure 5-10, time-history yields a response spectrum that is close to the design spectrum with a PGA cut-off frequency of approximately 100 Hz

3. *Time-History Motion 3*: An actual earthquake time-history recorded on rock during the 1982 Miramichi, New Brunswick, Ca, aftershock sequence. The record is denoted as the 3/12/82 Mitchell Lake Road Component 28. This record is one of the Eastern North America motions used by Reed et al (1993) for the model correlation discussed in Chapter 4. The time-history is has an approximate 8 second duration and has an approximate peak acceleration of 0.24 g as shown in Figure 5-11. The frequency content of the time-history is concentrated in the 20-60 Hz range with a PGA cut-off frequency of approximately 85 Hz.

Amplification Study Procedure

The amplification study consisted of determining the horizontal response of analytic fixed-base uniform cantilever beams represented as three beam types 1) a flexure beam, 2) a shear beam, and 3) a Timoshenko beam. Four fundamental frequencies cases of ~3, 5, 7, and 9 Hz were chosen for each beam type. An additional frequency case of 6.05 Hz was chosen for the Timoshenko beam to match the representative plant structure. For each beam type and selected fundamental frequency, all modes up to 100 Hz were considered. A summary of the fundamental frequencies selected and resulting mode frequencies used for each beam type are provided in Table 5-5. The spectral amplification, as defined by eq. 5-2, was computed for each beam type and fundamental frequency, for 10 positions (ranging from $x/L=0.2$ to $x/L=0.9$) by repeated application of the modal time history method represented by eqs. 5-7 through 5-12 using the theoretical mode frequencies, mode shapes, and participation factors presented above. All structure modes were assumed to have 7% structural damping with both the ground and in-structure spectra having default values of 5% damping. Spectral amplification functions, as a function of frequency, were determined using each selected time-history input motion. Figure 5-13 shows the set of amplification functions determined for a Timoshenko beam, with a fundamental frequency of 5 Hz, using the Time-History 2 (example CEUS rock design motion). It can be noted that, for the greater than 10 Hz range, the maximum amplification for each frequency is associated with different beam positions. Figure 5-14 shows the envelope of maximum spectral amplification for all positions for the Timoshenko beam case shown in Figure 5-13. Overall, the study resulted in 39 separate sets of amplification functions (3 beam types, 4 fundament frequencies, 3 input time histories plus three additional cases). The amplification functions for each beam type, fundamental frequency, and input motion are provided in Appendix A.

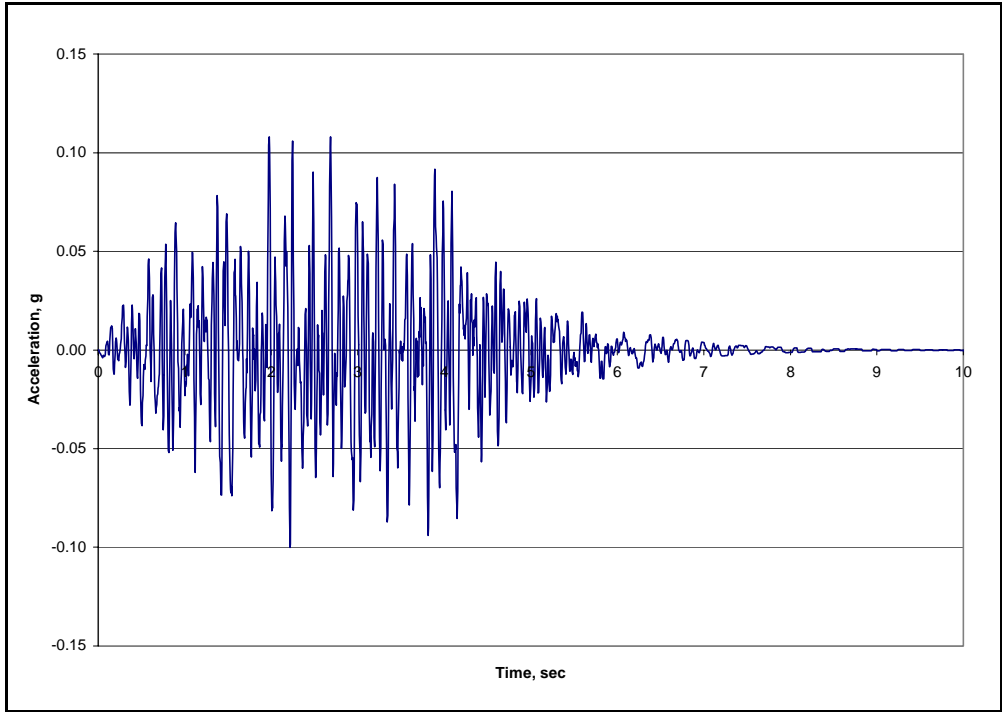


Figure 5-7
Time History 1: Compatible European Hard Rock Design Motion

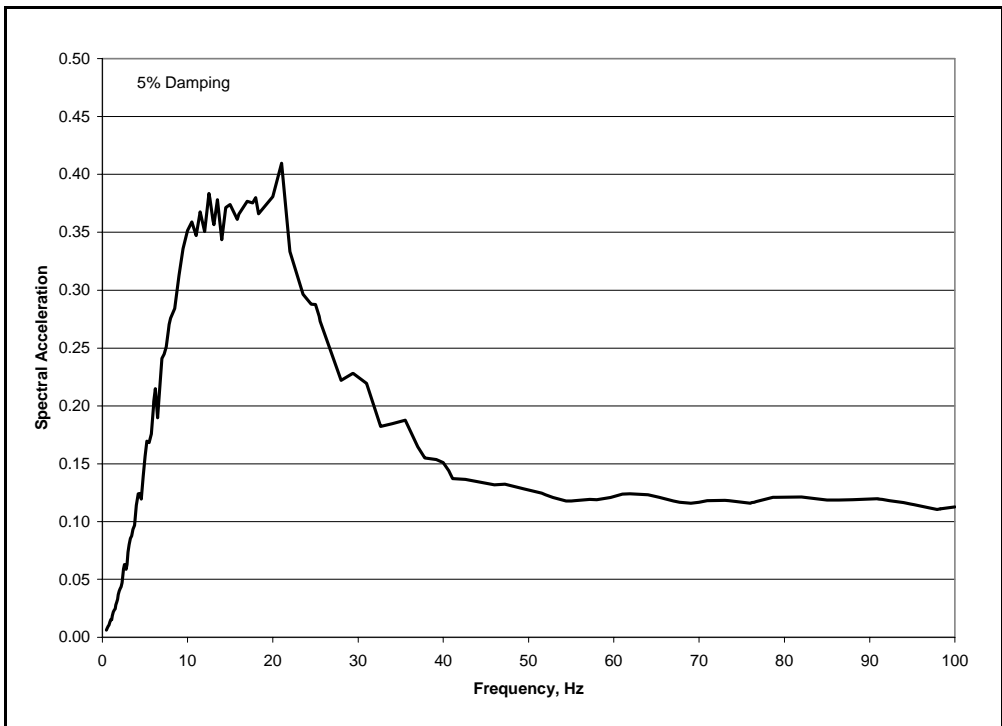


Figure 5-8
Response Spectrum for Time History 1

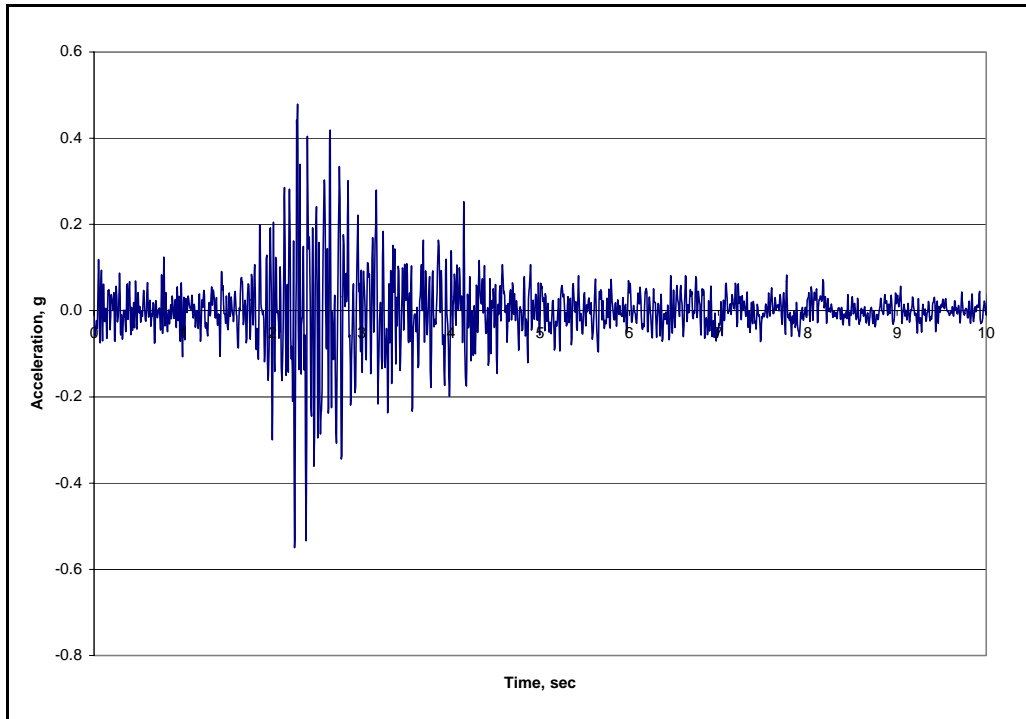


Figure 5-9
Time History 2: Example CEUS Rock Design Motion

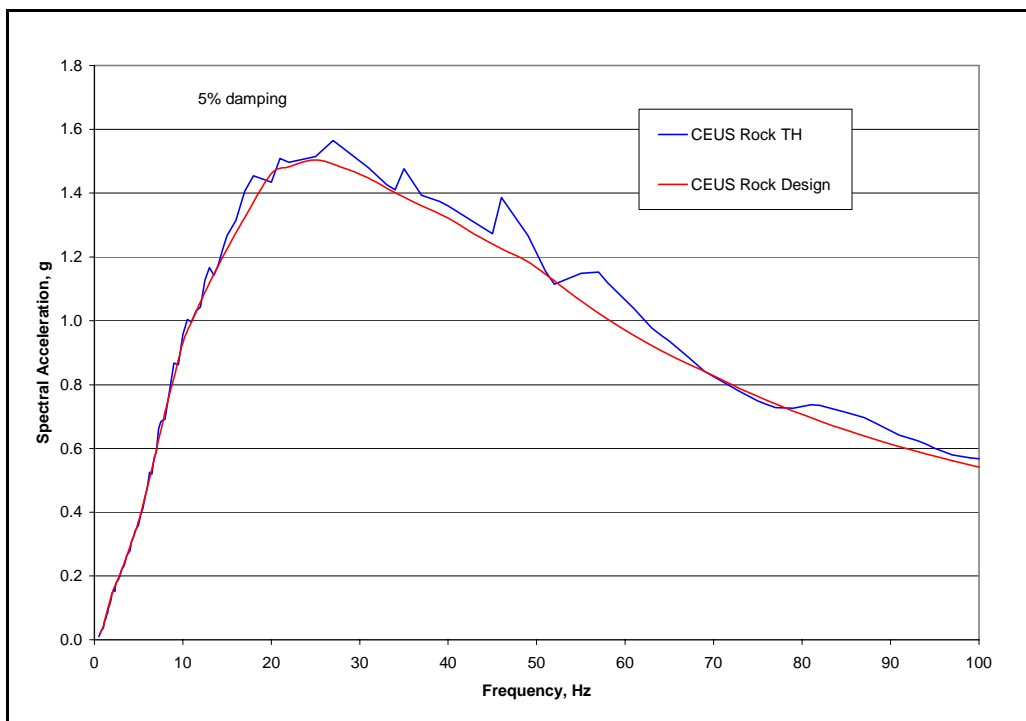


Figure 5-10
Response Spectrum for Time History 2

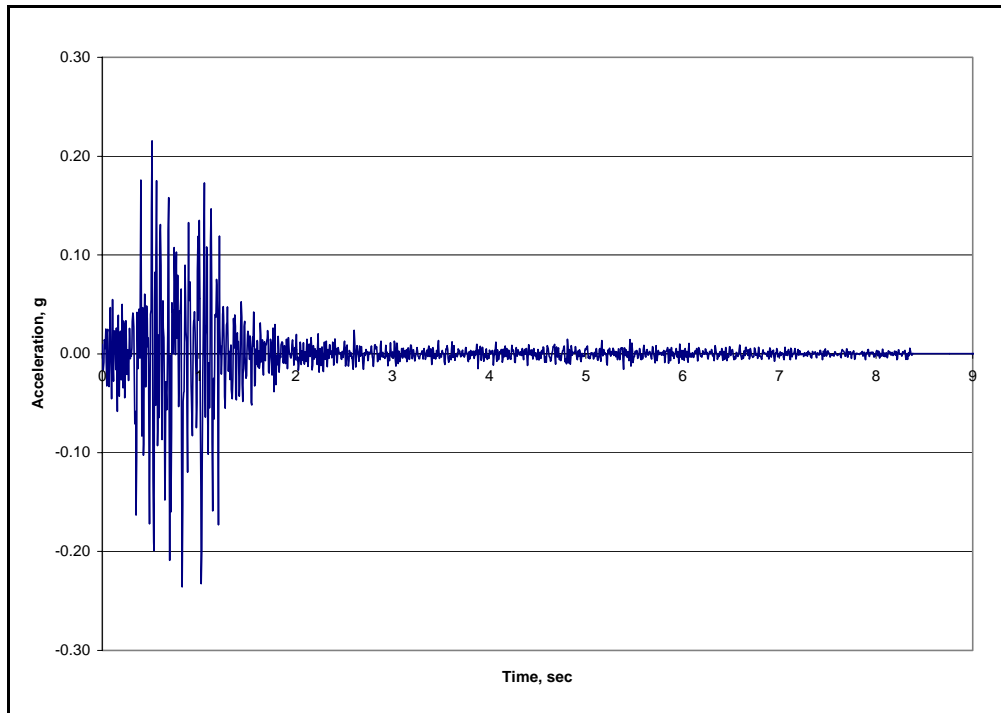


Figure 5-11
Time History 3: ENA Rock Motion, 1982 New Brunswick, CA
Mitchell Lake Road Component 28 (3/12/82)

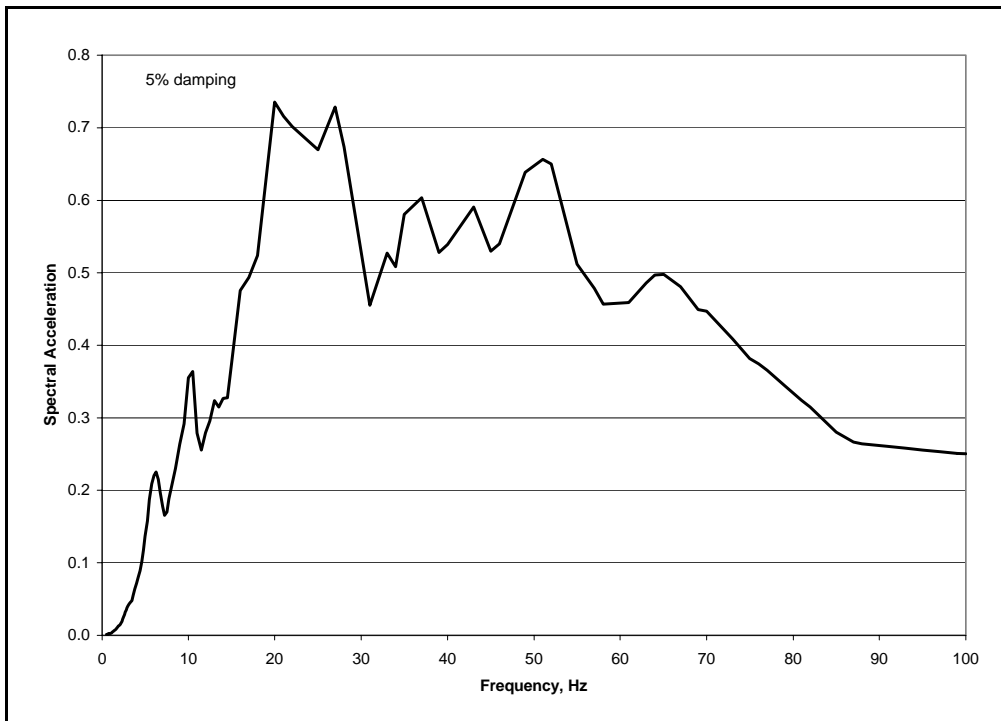


Figure 5-12
Response Spectrum for Time History 3

**Table 5-5
Beam Frequencies Selected for Amplification Study**

Flexure Beam Modes				
Mode	Beam1	Beam2	Beam3	Beam4
1	2.9 Hz*	5 Hz	7 Hz	9 Hz
2	18.2 Hz	31.3 Hz	43.87 Hz	56.4 Hz
3	50.9 Hz	87.7 Hz		
4	99.7 Hz			

* A frequency of 2.9 Hz was selected to allow for four modes to be included

Shear Beam Modes				
Mode	Beam1	Beam2	Beam3	Beam4
1	3 Hz	5 Hz	7 Hz	9 Hz
2	9 Hz	15 Hz	21 Hz	27 Hz
3	15 Hz	25 Hz	35 Hz	45 Hz
4	21 Hz	35 Hz	49 Hz	63 Hz
5	27 Hz	45 Hz	63 Hz	81 Hz
6	33 Hz	55 Hz	77 Hz	99 Hz
7	39 Hz	65 Hz	91 Hz	
8	45 Hz	75 Hz		
9	51 Hz	85 Hz		
10	57 Hz	95 Hz		
11	63 Hz			
12	69 Hz			
13	75 Hz			
14	81 Hz			
15	87 Hz			
16	93 Hz			
17	99 Hz			

Table 5-5 (Continued)
Beam Frequencies Selected for Amplification Study

Timoshenko Beam Modes					
Mode	Beam1	Beam2	Beam3	Beam4	Beam5
1	3.00 Hz	5 Hz	7.00 Hz	9 Hz	6.05 Hz
2	7.85 Hz	13.09 Hz	18.32 Hz	23.56 Hz	15.84 Hz
3	12.62 Hz	21.03 Hz	29.45 Hz	37.86 Hz	25.45 Hz
4	17.61 Hz	29.36 Hz	41.10 Hz	52.84 Hz	35.52 Hz
5	24.50 Hz	40.84 Hz	57.17 Hz	73.51 Hz	49.42 Hz
6	25.56 Hz	42.6 Hz	59.64 Hz	76.68 Hz	51.54 Hz
7	32.64 Hz	54.4 Hz	76.16 Hz	97.91 Hz	65.82 Hz
8	39.20 Hz	65.33 Hz	91.56 Hz		79.05 Hz
9	40.63 Hz	67.72 Hz	94.81 Hz		81.84 Hz
10	47.20 Hz	78.67 Hz	*		95.19 Hz
11	54.48 Hz	90.79 Hz	*		
12	55.39 Hz	92.32 Hz	*		
13	61.87 Hz				
14	69.05 Hz				
15	70.93 Hz				
16	76.44 Hz				
17	83.74 Hz				
18	86.38 Hz				
19	91.06 Hz				
20	98.32 Hz				

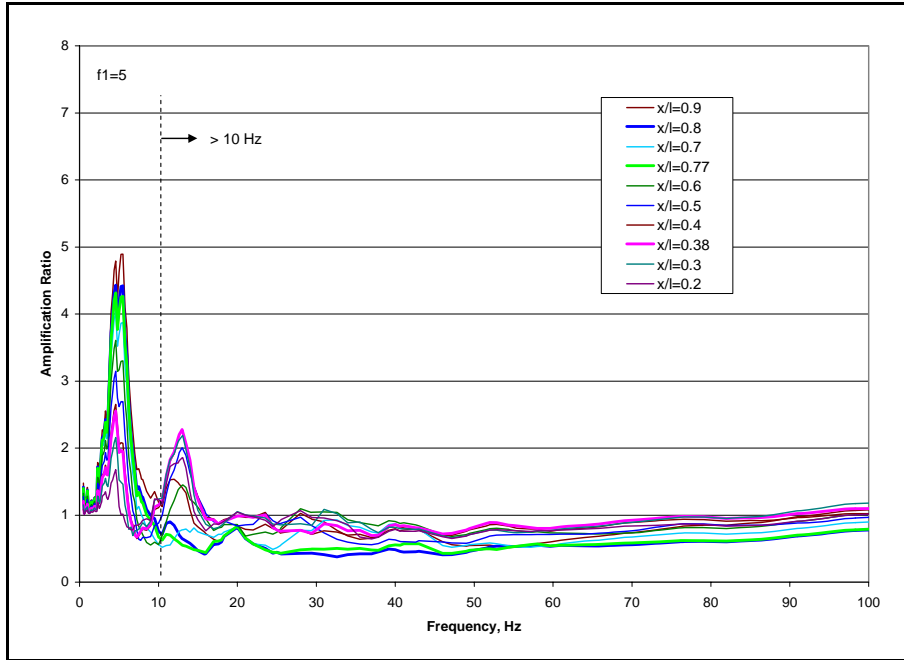


Figure 5-13
Example Spectral Amplification for Timoshenko Beam with $f_1 = 5$ Hz, Time History Input 2
(Example CEUS Rock Design Motion)

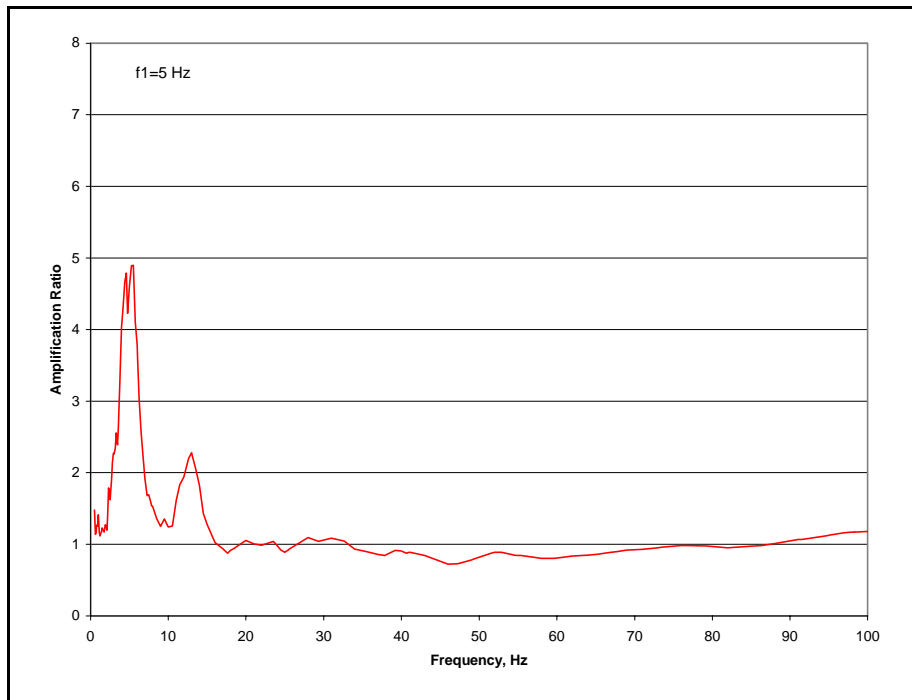


Figure 5-14
Maximum Amplification for Timoshenko Beam with $f_1 = 5$ Hz, Time History Input 2
($0.2 \leq x/L \leq 0.9$)

Amplification Study Results

Figures 5-15 through 5-19 compare the envelopes of maximum amplification for each beam case. Both the shear beam and Timoshenko beam have amplification less than 2.5 for higher modes with frequencies greater than about $\sqrt{2}$ times the fundamental frequency of the beam. For Time-History 1, the amplification functions appear to rise to a constant value for frequencies greater than about 40 Hz. This is due to the PGA cutoff frequency of Time-History 1 being approximately 50 Hz. In general, if the ground input has a PGA cutoff frequency less than 100 Hz, the amplification ratio at the PGA cutoff frequency or higher is simply the ratio of the in-structure ZPA to the ground PGA, as indicated by eq. 5-4, and should not be interpreted as an oscillator amplification. It can be noted that the flexural beam has higher amplification values than either the shear or Timoshenko type beams. The reason for this behavior of the flexure beam is due to the higher $\Gamma\phi$ values for the second mode compared to the other beam types. For example, the flexure beam has a second mode response which is a factor of $0.625/0.413 = 1.51$ times higher than the Timoshenko beam. This increased level of response is not considered as representative of nuclear plant structural configurations.

The observed amplification values may be verified by considering the random vibration estimate of spectral amplification provided by eq. 5-3. If $AF_c = 6.53$, $SA_{gt}(0.05)/SA_{gt}(0.07) \approx 0.9$, and $\text{Max}|\Gamma_2\phi_2| = 0.413$, then the spectral amplification of the in-structure oscillator mounted in a Timoshenko beam for the tuned frequency case is $AF_x = 6.53(0.9)(0.413) = 2.42$. Figure 5-19 shows that this estimate is in good agreement with the maximum response of the representative Timoshenko beam for frequencies greater than 10 Hz and less than the PGA cutoff frequency. Thus, it is recommended that a generic structural spectral amplification factor be conservatively estimated as a value of 2.5 for frequencies greater than 10 Hz if the fundamental frequency of the structure is less than 10 Hz.

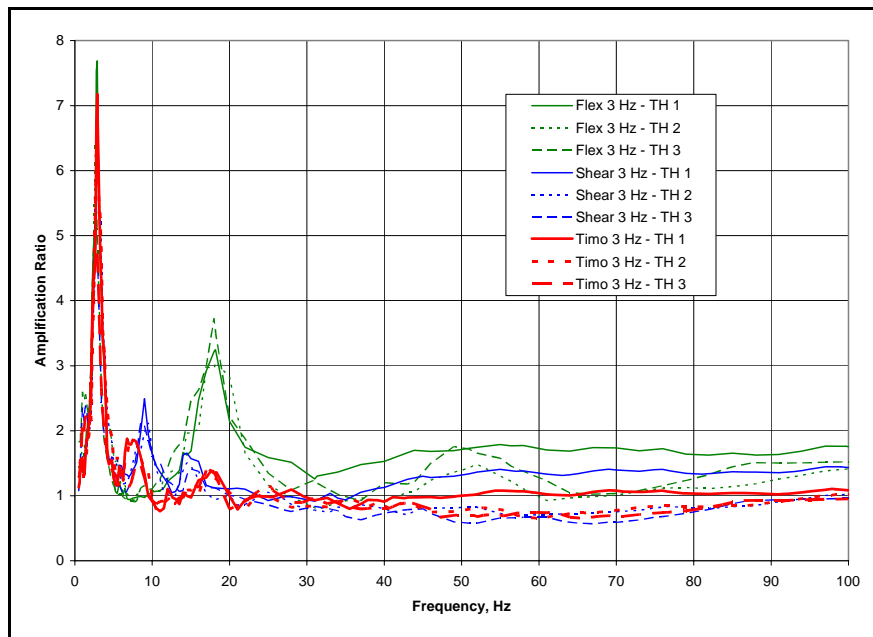


Figure 5-15
Comparison of $f_1 = 3$ Hz Beam Response

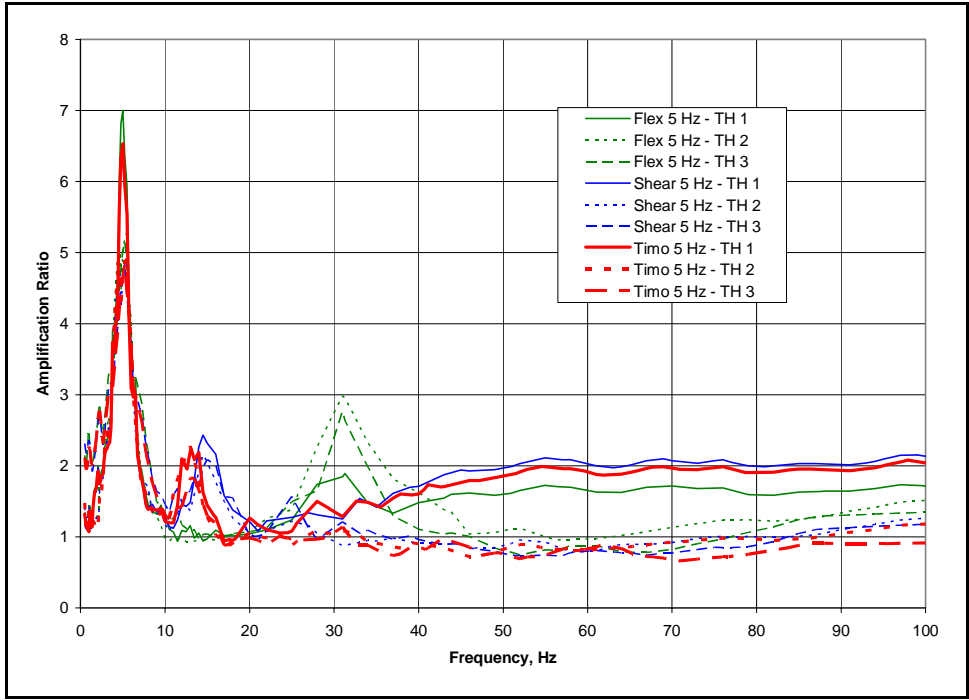


Figure 5-16
Comparison of $f_1 = 5$ Hz Beam Response

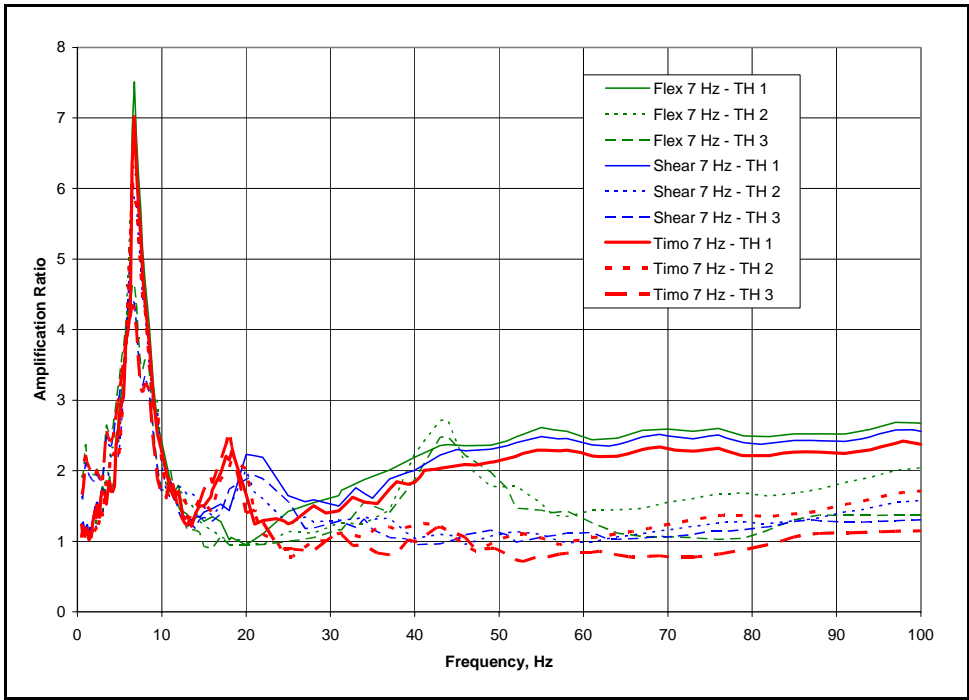


Figure 5-17
Comparison of $f_1 = 7$ Hz Beam Response

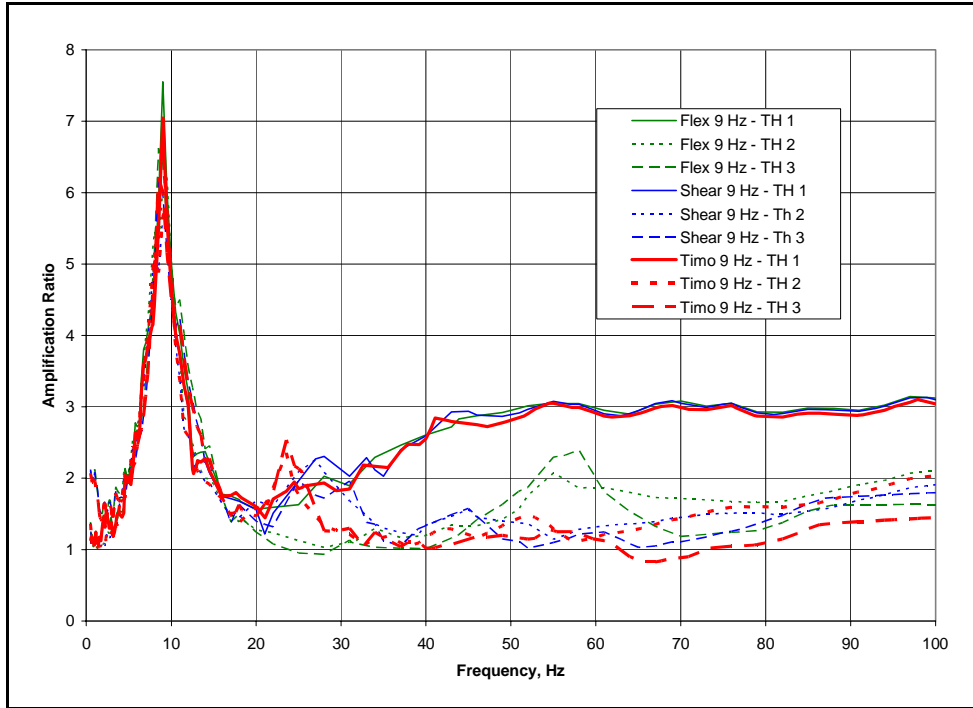


Figure 5-18
Comparison of $f_1 = 9$ Hz Beam Response

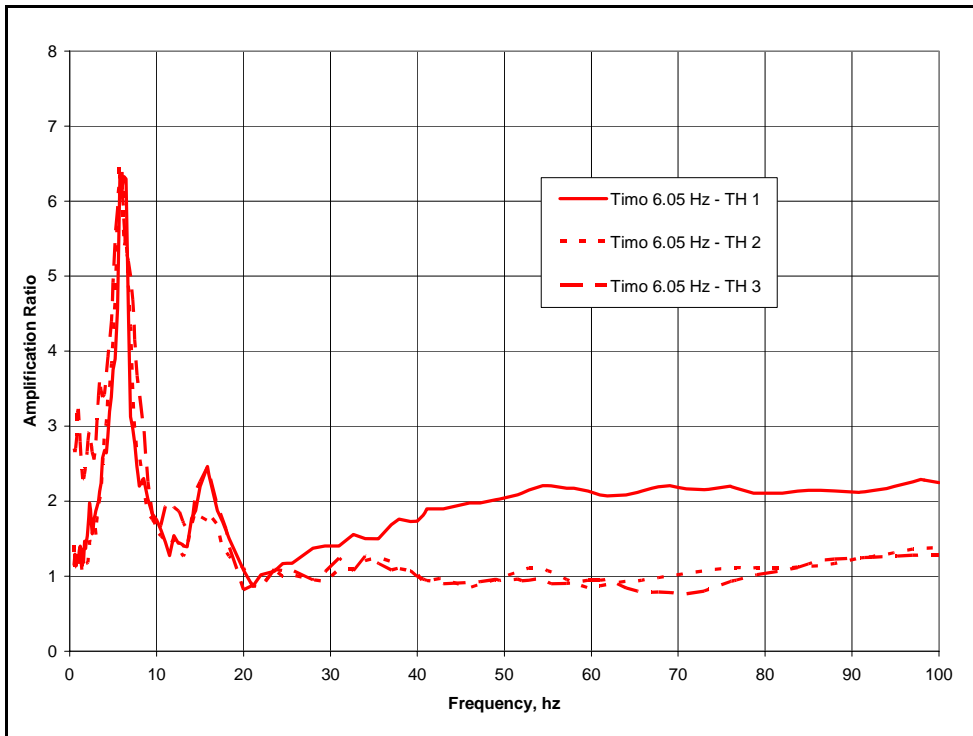


Figure 5-19
Comparison of $f_1 = 6.05$ Hz Timoshenko Beam Response

6

APPLIED RESPONSE MODIFICATION PROCEDURE

Seismic Margin Factor

The equations governing the estimation of non-linear response for both the Shear Resistance Model and the Overturning Resistance Model using the equivalent linear system methodology were developed in Chapter 4. Chapter 3 demonstrated that the design margin for welds designed using current LRFD procedures is approximately a value of 1.6 for fillet welds loaded in transverse shear. Chapter 5 demonstrated that the expected spectral amplification for equipment mounted in a typical plant structures was approximately 2.5 for equipment with frequencies greater than about 10 Hz mounted in plant structures with fundamental frequencies less than 10 Hz. As indicated in Chapter 4, the spectral de-amplification approach is used to find a modified level of design acceleration that reflects the response attenuation caused by the presence of a negligible deformation non-linearity in the anchorage load path. In order to apply the spectral de-amplification approach developed in Chapter 4, the input spectral acceleration must correspond to the motion that causes the actual yield capacity level of the model and not the motion which is associated with the lower design strength level. Following the approach used by Reed et al (1993), the ground level response spectra must first be scaled up to represent the motion at the base of the equipment within the structure. Then, an additional scale factor must be considered to allow the design level motion to be increased to the actual yield level motion. Thus, for the case of the Shear Resistance Model, the yield capacity spectral acceleration would be taken as

$$SA_y = SA_c = F_{SM} SA_r \quad \text{(Equation 6-1)}$$

where SA_y is the modified design spectral acceleration and F_{SM} is a scale factor that represents both the design margin and the structural amplification. Thus, F_{SM} would range from a value of 1.6 to 4 [2.5(1.6)=4]. In the case of the Overturning Resistance Model, the yield capacity spectral acceleration for the anchorage component would be taken as

$$SA_y / e = SA_c / e = (F_{SM} / e) SA_r \quad \text{(Equation 6-2)}$$

where the equipment aspect ratio, e , acts to reduce the yield level of the anchorage component in the model. Aspect ratios of equipment can vary widely, but are generally in the range 1-4. Thus, F_{SM} / e can be considered as a combined factor, which ranges from 0.4 [1.6/4=0.4] to 1.6 [4/1=4]. Thus, the entire set of scale factors $\{ F_{SM}, F_{SM} / e \}$ can be represented by the range of values 0.4-4.

Response Modification Procedure

The sequential application of the non-linear set of eqs. 4-8 through 4-13, which govern the estimation of the equivalent linear response of either model, allows development of an iterative

to calculate modified values of design spectral acceleration, SA_r . Table 6-1 provides the procedure steps for the calculation methodology. Note that the scale factors, either F_{SM} or F_{SM}/e , and each equipment frequency, f_f , are considered as given values and that the default value of equipment damping is set at $\beta_f = 0.05$. The design spectra, $SA(f_f, \beta_f)$, is also a known function. Similarly, values for ultimate displacement capacity, $\delta_u = 0.01$ inch, and maximum deformation ratio, $\mu = 10$ are default values associated with an assumed minimum 3/16 inch weld loaded in transverse shear. Steps 5 and 6 are eqs. 4-10 and 4-12 using the parameters, $a = 1.6$ and $b = 0.3$, which are the empirical model correlation factors discussed in Chapter 4. Step 8 is represents the estimation of the spectral acceleration $SA(f_e, \beta_e)$ by a function denoted as $G(f_e, \beta_e)$. This is a key step in this calculation sequence, since the iteration requires repeated estimation of the spectral acceleration, $SA(f_e, \beta_e)$, for any value of f_e and β_e . In general, design spectra are specified at a default value of damping; often 5% is used. McGuire et al (2001) provide an empirical relation for $G(f_e, \beta_e)$ that allows estimation of spectra for any damping for frequencies greater than 5 Hz in the form:

$$SA(f_e, \beta_e) = \{PGA^2 + [SA(f_e, 0.05)^2 - PGA^2][(1 + 4.9\beta_e f_e D)/(1 + 0.05 f_e D)]^{0.82}\}^{1/2} \quad \text{(Equation 6-3)}$$

where $PGA = SA(100, 0.05)$ and D is the duration of motion. A value of D within the range 5-10 provides the same approximate value of $SA(f_e, \beta_e)$, thus $D = 10$ is recommended. Using eq. 6-3, values of spectral acceleration may be estimated for any damping ratio given the design spectrum is developed for 5% damping. Other functional forms for $G(f_e, \beta_e)$ can also be used such as interpolation between spectra developed for damping values greater than 5%. In general, the value of equivalent damping computed in step 7 will be less than 0.12, thus, only generation of spectra with damping in the range 5-12% is required. The check step using the relation, $ABS|SA_{r_{i+1}} - SA_{r_i}| > Tol$, where Tol is a set convergence tolerance number, say 10^{-6} , allows the solver option of a spreadsheet to be used for compute the modified spectra over a range of frequencies, in general greater than 8 Hz, for each F_{SM} or F_{SM}/e value. The convergence of the procedure is also rapid enough to allow hand calculation as illustrated by the example calculation shown in Table 6-2.

Application of Response Modification Procedure

An example design spectrum that is representative of the spectra that are expected for a CEUS rock site is shown in Figure 6-1. The spectrum is specified by pairs of spectral acceleration and frequency values indicated by the data markers in Figure 6-1. The function $SA(f_f, \beta_f)$ is determined by interpolation between the data points. The peak value occurring at approximately 25 Hz was chosen for the application of the response modification procedure illustrated by the Table 6-2 example. Given the design spectral values for 22 Hz, 25 Hz, and 100 Hz (PGA), the procedure begins by assuming that the value of SA_r is equal to $SA(f_f, \beta_f)$. The procedure steps are identified in Table 6-2. At the end of each sequence of steps 1-11, the new value of SA_r is used to start the iteration sequence. As can be noted, convergence to four place accuracy occurs in six iterations. For the final calculation sequence, the starting value of SA_r is equal to the

ending value. Step 8a is simply the interpolation of the function $SA(f_f, \beta_f)$ for the value associated with f_e which is between 22 Hz and 25 Hz. Linear interpolation of $\log SA$ and $\log f$ values is assumed. Then, step 8 uses eq. 6-3 to compute the value of $SA(f_e, \beta_e)$. Also shown in Table 6-2, is the spreadsheet solver (Excel, 2003) solution. The solver add-in function of Excel forces the target cell to an approximate zero value by making small changes to the initial value of SA_r , specified as the changing cell. The solver function accomplishes the automatic calculation of the manual iteration sequence shown in Table 6-2.

The full computation of a modified spectrum ($F_{SM} = 3$) is shown in Table 6-3. The full modified spectrum is also shown in Figure 6-1 together with the unmodified spectrum. As can be noted, a modified spectrum can be established with good accuracy by doing the calculations at approximate 3 Hz intervals. The de-amplification factors F_μ are approximately 1.0 for frequencies less than about 10 Hz and for frequencies greater than about 85 Hz. The frequency shift and increased damping due to the non-linear behavior of the anchorage component can be noted by tracking the values of f_e and β_e . For frequencies greater than about 88 Hz, values of $F_\mu < 1.0$ are not allowed, thus the elastic design spectrum is followed. Steps 8a-8d identify the frequencies and spectral acceleration values that are interpolated in step 8e to obtain the value of $SA(f_e, \beta_e)$. Step 8 uses eq. 6-3 to compute the value of $SA(f_e, \beta_e)$.

Since, in general, a set of reduced curves for $\{F_{SM}, F_{SM}/e\}$ within the range of values 0.4-4 must be computed, it was decided to compute a set of reduced curves for different spectral shapes and also different spectral amplitudes. Figure 6-2 shows three different spectra (5% damping): 1) a representative CEUS rock site design spectrum, 2) a design spectrum which is representative of the spectra that are expected for a CEUS soil site, and 3) a design spectrum used in Europe for hard rock sites (SKI, 1992). These spectra are all scaled to 0.75g at 10 Hz which is the approximate spectra value at 10 Hz for a RG 1.60 spectrum with 5% damping and a PGA equal to 0.3g. As can be noted, the European hard rock spectrum has a PGA cut-off frequency of 50 Hz, in contrast to the CEUS spectra that have a 100 Hz PGA cut-off frequency. A full set of modified curves was computed for each of these design spectra for three cases: 1) scaled by a factor equal to 1.5, 2) scaled by a factor equal to 1.0, and 3) scaled by a factor equal to 0.67.

Figures 6-3, 6-5, and 6-7 show the variation of CEUS rock site design spectra for different values of damping (5%-12%) generated with eq. 6-3. Figures 6-4, 6-6, and 6-8 show the results for the corresponding modified CEUS rock spectra generated for each case. Examining Figure 6-4 (1.5 factored case) indicates that, in general, the upper bound envelope of all the modified spectra should be used as the reduced design spectrum. This is designated as the bounding case in Figure 6-4. For frequencies less than about 9 Hz, the design spectrum is unreduced. For frequencies within the range 10-58 Hz, the shear resistance case with $F_{SM} = 4$ governs, while for the 58-78 Hz range, the overturning case with $F_{SM}/e = 0.4$ governs. For frequencies greater than 78 Hz, the unreduced design spectrum is used. For the 1.0 and 0.67 factored cases the behavior is similar, except that the crossover occurs for different values of F_{SM}/e and the crossover frequency shifts down. The crossover of the different models was noted by Reed et al (1993) but

the limiting value in the higher frequency range was handled in a different manner by assuming no reduction less than the peak value of the 10% damped design spectrum divided by 1.6. If the envelope of all model cases is taken, then the consideration of such a bound is unnecessary.

Figures 6-9, 6-11, and 6-13 show the variation of design spectra for different values of damping (5%-12%) generated with eq. 6-3 for the three levels of CEUS soil site spectra. Figures 6-10, 6-12, and 6-14 show the results for the corresponding modified CEUS soil site spectra. The same crossover behavior can be noted but the reductions are less dramatic since the high frequency content of the motion is weak compared to the rock case. This should be expected since the effect of increased damping on the design spectrum is also smaller than the rock case.

Figures 6-15, 6-17, and 6-19 show the variation of the European hard rock design spectra for different values of damping (5%-12%). Figures 6-16, 6-18, and 6-20 show the results for the corresponding modified European hard rock spectra. Here, the design spectra are defined for each damping level (SKI, 1992) and the use of eq. 6-3 is not required. Values of spectra for intermediate damping can be simply interpolated from the specified design spectra using linear interpolation of $\log SA$ and $\log f$ values. The effect of the PGA cutoff being at 50 Hz can be seen with the reduction confined to the 10 -34 Hz range. The crossover behavior of the various model cases is more complex with different model cases governing each factored modified spectrum.

In general, all three spectra shapes show the similar modification behavior with maximum reductions ranging from 14% to 33%. With regard to the effects of spectra amplitude, there is a tendency for a lower level design spectrum to have slightly greater reduction than the higher level design spectrum with the same shape.

Application of Modified Design Spectrum

Figure 6-21 shows the overall reduced design spectrum (envelope of all model cases) for the representative CEUS rock site considered as the example modification case shown in Figure 6-1. Following the recommendations of Reed et al (1993), this reduced design spectra would then be used to define the modified input motion for generation of in-structure response spectra that have the effect of non-linear response implicitly incorporated. This could be accomplished in either of three ways: 1) Generate time-histories that are compatible with the modified design spectrum for use in generation of in-structure spectra using modal time-history analysis, 2) generate a PSD function which is compatible with the modified design spectrum for use in generation of in-structure spectra by direct methods based on random vibration theory, or 3) generate an input motion transfer function which is determined by the square-root of the ratio of PSDs that are respectively compatible with the reduced design spectrum and the unreduced design spectrum.

A companion EPRI study (EPRI, 2005) has considered the effects of random spatial variation of ground motion on the response of structure with a large foundation. The coherency of motion between two separated points varies considerably as a function of both separation distance and frequency. When considered from a soil-structure interaction perspective, a large foundation must move as a unit, thus the motion of the foundation is modified from the free-field motion. This phenomenon, based on empirical data gathered from seismic instrument arrays, has the effect of reducing the high frequency content of motion. Stated simply, a large foundation will average the high frequency motion which differs from point to point in the free field. Figure 6-22

shows the incoherency reduced response spectrum that results (ERPR, 2005) when a massless rigid foundation (150 foot square) is subjected to an average free-field motion that has the unreduced design spectrum shown in Figure 6-21. As can be noted, there is a substantial reduction in both spectral amplitude and frequency content, particularly in the 20-50 Hz range. This incoherency reduced motion, denoted as the scattered foundation motion, would then be used as input to the remainder of the soil-structure interaction problem involving foundation/structure inertia response and structure response feedback. All mounted equipment would then be subjected to the reduced motion. If the additional response modification due to non-linear equipment anchorage behavior is to be included, then it is the scattered foundation motion that must be further modified. While the design spectrum modified for non-linear equipment anchorage effects shown in Figure 6-21 has a maximum reduction of approximately 30%, the maximum reduction of the incoherency reduced scattered motion is 19%. For the scattered motion, the frequency region of 30-50 Hz, which for the design spectrum had large reduction for inelastic effects, has been effectively removed by the loss of motion coherency. The scattered motion can only be further reduced for non-linear equipment anchorage response effects in the 10 -25 Hz range. To be consistent with the procedure used for the development of the incoherency reduced scattered motion, it is recommended that an additional transfer function be generated which represents the additional response modification due to inelastic effects and then applied to the Fourier transform of the scattered foundation motion. This transfer function may be determined as the square-root of the ratio of PSDs that are respectively compatible with the inelastic reduced scattered spectrum and the scattered foundation spectrum. Each transfer function will be unique and depend on the frequency content of the scattered foundation motion.

Table 6-1
Modified Spectrum Calculation Procedure

Given F_{SM} , F_{SM}/e , f_f , let $\beta_f = 0.05$, $SA(f_f, \beta_f)$, $\delta_u = 0.01$ inch, $\mu = \delta_u/\delta_y = 10$

1. Assume SA_{ri}
2. $SA_C = F_{SM} SA_{ri}$, or $SA_C = (F_{SM}/e) SA_{ri}$
3. $A = (2\pi f_f)^2 \delta_u / SA_C$
4. $X = 1/(1+A)$
5. $X_e = 1 - (1-X)^{1.6}$
6. $\beta_e = (X/X_e) [X^{1/2} \beta_f] + (0.6/\pi) (1-X)(1-1/\mu)$
7. $f_e = f_f (X_e)^{1/2}$
8. $SA(f_e, \beta_e) = G(f_e, \beta_e)$
9. $F_\mu = (X/X_e) [SA(f_f, \beta_f)/SA(f_e, \beta_e)]$
10. $SA_{ri+1} = SA(f_f, \beta_f)/F_\mu$
11. $ABS|SA_{ri+1} - SA_{ri}| > Tol \sim 10^{-6}$
12. $SA_r = SA_{ri+1}$

Table 6-2
Example Calculation of Modified Spectrum at 25 Hz

$F_{SM} = 3, \beta_r = 0.05, \delta_u = 0.01, \mu = 10$

Given		Procedure Steps											
		1	2	3	4	5	6	7	8a	8	9	10	11
f_r	SA_r	SA_r	SA_c	A	X	X_c	β_c	f_c	$SA(f_c, 0.05)$	$SA(f_c, \beta_c)$	F_u	SA_r	Target
22	1.4830												
25	1.5043	1.5043	4.5130	0.1416	0.8760	0.9646	0.0619	24.5530	1.5013	1.3943	1.1880	1.2663	0.23802
		1.2663	3.7989	0.1682	0.8560	0.9550	0.0636	24.4310	1.5005	1.3800	1.2161	1.2370	0.02929
		1.2370	3.7111	0.1722	0.8531	0.9535	0.0639	24.4123	1.5003	1.3780	1.2202	1.2329	0.00412
		1.2329	3.6987	0.1727	0.8527	0.9533	0.0639	24.4096	1.5003	1.3777	1.2207	1.2323	0.00059
		1.2323	3.6969	0.1728	0.8526	0.9533	0.0639	24.4092	1.5003	1.3777	1.2208	1.2322	0.00008
		1.2322	3.6967	0.1728	0.8526	0.9533	0.0639	24.4091	1.5003	1.3777	1.2208	1.2322	0.00001
100	0.5417												
Solver Solution		1.23221	3.69664	0.17283	0.85264	0.95329	0.06395	24.40913	1.50032	1.37767	1.22084	1.23221	2.5E-07

↑
Iteration
↓

Table 6-3
Full Reduction of Example Design Spectrum

$F_{SM} = 3, \beta_f = 0.05, \delta_u = 0.01, \mu = 10, PGA = SA(100, 0.05) = 0.5417$

Given		Procedure Steps															
		1	2	3	4	5	6	7	8a	8b	8c	8d	8e	8	9	10	11
f_r	SA_r	SA_r	SA_r	A	X	X_r	β_r	f_r	f_r	$SA(f_r, 0.05)$	f_r	$SA(f_r, 0.05)$	$SA(f_r, 0.05)$	$SA(f_r, \beta_r)$	F_u	SA_r	Target
10	0.9307	0.8817	2.6452	0.0386	0.9628	0.9948	0.0537	9.9741	9	0.8215	10	0.9307	0.9278	0.9111	1.0555	0.8817	7.63E-07
11	0.9978	0.9388	2.8163	0.0439	0.9579	0.9937	0.0541	10.9654	10	0.9307	11	0.9978	0.9955	0.9738	1.0629	0.9388	2.44E-07
13	1.1185	1.0346	3.1039	0.0557	0.9473	0.9910	0.0552	12.9412	11	0.9978	13	1.1185	1.1150	1.0824	1.0810	1.0346	8.66E-07
15	1.2251	1.1131	3.3393	0.0689	0.9356	0.9876	0.0563	14.9064	13	1.1185	15	1.2251	1.2202	1.1750	1.1006	1.1131	8.13E-07
17	1.3230	1.1795	3.5386	0.0835	0.9229	0.9834	0.0575	16.8587	15	1.2251	17	1.3230	1.3162	1.2568	1.1216	1.1795	2.67E-08
20	1.4614	1.2647	3.7941	0.1078	0.9027	0.9760	0.0594	19.7582	17	1.3230	20	1.4614	1.4506	1.3673	1.1555	1.2647	2.25E-07
22	1.4830	1.2607	3.7821	0.1308	0.8843	0.9683	0.0611	21.6483	20	1.4614	22	1.4830	1.4793	1.3804	1.1763	1.2607	4.92E-07
25	1.5043	1.2322	3.6966	0.1728	0.8526	0.9533	0.0639	24.4091	22	1.4830	25	1.5043	1.5003	1.3777	1.2208	1.2322	2.5E-07
28	1.4807	1.1732	3.5196	0.2277	0.8145	0.9325	0.0673	27.0386	25	1.5043	28	1.4807	1.4879	1.3431	1.2621	1.1732	1.88E-07
31	1.4477	1.1064	3.3193	0.2960	0.7716	0.9059	0.0709	29.5046	28	1.4807	31	1.4477	1.4636	1.2989	1.3084	1.1064	4.54E-07
34	1.4016	1.0407	3.1222	0.3785	0.7254	0.8736	0.0746	31.7782	31	1.4477	34	1.4016	1.4352	1.2533	1.3468	1.0407	2.57E-07
37	1.3608	0.9784	2.9351	0.4768	0.6771	0.8362	0.0783	33.8335	31	1.4477	34	1.4016	1.4040	1.2081	1.3908	0.9784	5.13E-07
40	1.3218	0.9259	2.7778	0.5888	0.6294	0.7957	0.0818	35.6811	34	1.4016	37	1.3608	1.3782	1.1706	1.4275	0.9259	5.47E-07
43	1.2713	0.8818	2.6453	0.7145	0.5833	0.7535	0.0850	37.3263	37	1.3608	40	1.3218	1.3563	1.1392	1.4418	0.8818	5.6E-08
46	1.2260	0.8442	2.5327	0.8541	0.5394	0.7107	0.0880	38.7788	37	1.3608	40	1.3218	1.3371	1.1124	1.4522	0.8442	6.92E-08
49	1.1850	0.8126	2.4378	1.0068	0.4983	0.6683	0.0906	40.0583	40	1.3218	43	1.2713	1.3207	1.0899	1.4583	0.8126	8.74E-08
52	1.1250	0.7828	2.3484	1.1770	0.4593	0.6262	0.0930	41.1482	40	1.3218	43	1.2713	1.3018	1.0671	1.4372	0.7828	4.28E-07
55	1.0618	0.7579	2.2738	1.3599	0.4237	0.5860	0.0952	42.1034	40	1.3218	43	1.2713	1.2858	1.0482	1.4009	0.7579	8.6E-07
58	1.0052	0.7370	2.2111	1.5552	0.3914	0.5482	0.0970	42.9422	40	1.3218	43	1.2713	1.2722	1.0324	1.3638	0.7370	2.71E-07
61	0.9543	0.7193	2.1580	1.7626	0.3620	0.5128	0.0987	43.6808	43	1.2713	46	1.2260	1.2606	1.0190	1.3266	0.7193	4.32E-08
64	0.9082	0.7042	2.1127	1.9818	0.3354	0.4798	0.1001	44.3333	43	1.2713	46	1.2260	1.2506	1.0076	1.2895	0.7042	1.42E-07
67	0.8662	0.6913	2.0738	2.2127	0.3113	0.4493	0.1013	44.9118	43	1.2713	46	1.2260	1.2419	0.9979	1.2531	0.6913	2.92E-07
70	0.8275	0.6801	2.0402	2.4552	0.2894	0.4211	0.1024	45.4264	43	1.2713	46	1.2260	1.2343	0.9895	1.2168	0.6801	7.54E-07
73	0.7877	0.6703	2.0109	2.7090	0.2696	0.3951	0.1034	45.8858	43	1.2713	46	1.2260	1.2276	0.9823	1.1752	0.6703	1.76E-07
76	0.7509	0.6618	1.9853	2.9741	0.2516	0.3711	0.1042	46.2974	46	1.2260	49	1.1850	1.2217	0.9759	1.1347	0.6618	9.24E-07
79	0.7171	0.6543	1.9628	3.2503	0.2353	0.3490	0.1050	46.6675	46	1.2260	49	1.1850	1.2165	0.9704	1.0960	0.6543	5.72E-07
82	0.6860	0.6476	1.9429	3.5378	0.2204	0.3285	0.1056	47.0012	46	1.2260	49	1.1850	1.2118	0.9655	1.0592	0.6476	8.66E-07
85	0.6573	0.6417	1.9252	3.8362	0.2068	0.3097	0.1062	47.3033	46	1.2260	49	1.1850	1.2077	0.9612	1.0242	0.6417	5.28E-07

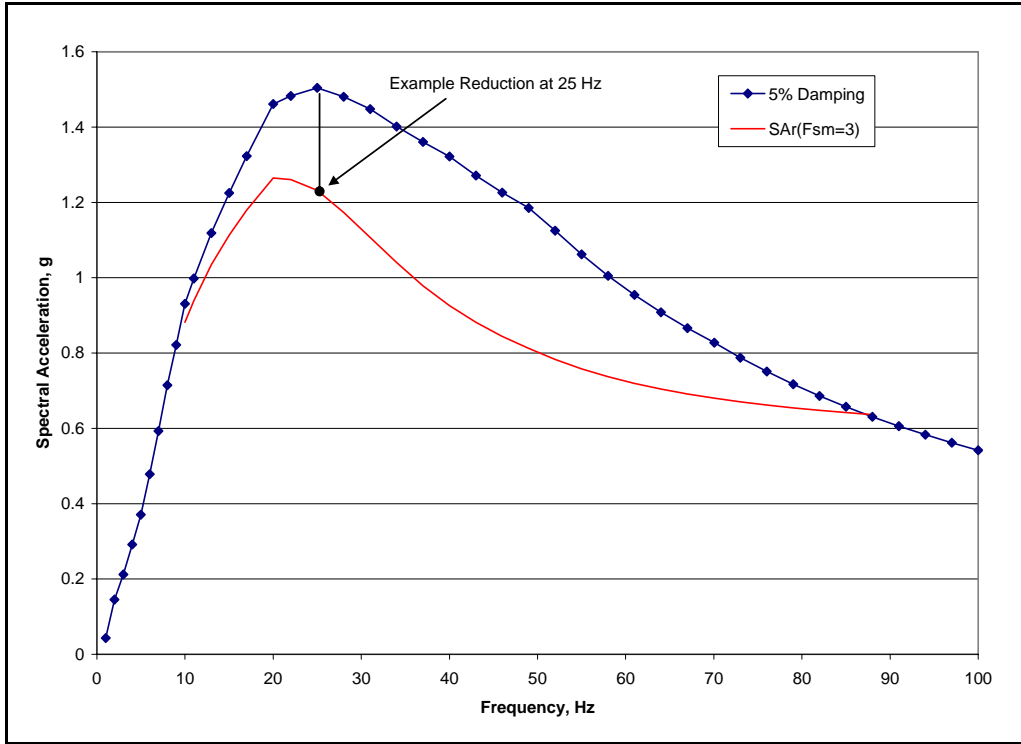


Figure 6-1
Example CEUS Site Design Spectrum

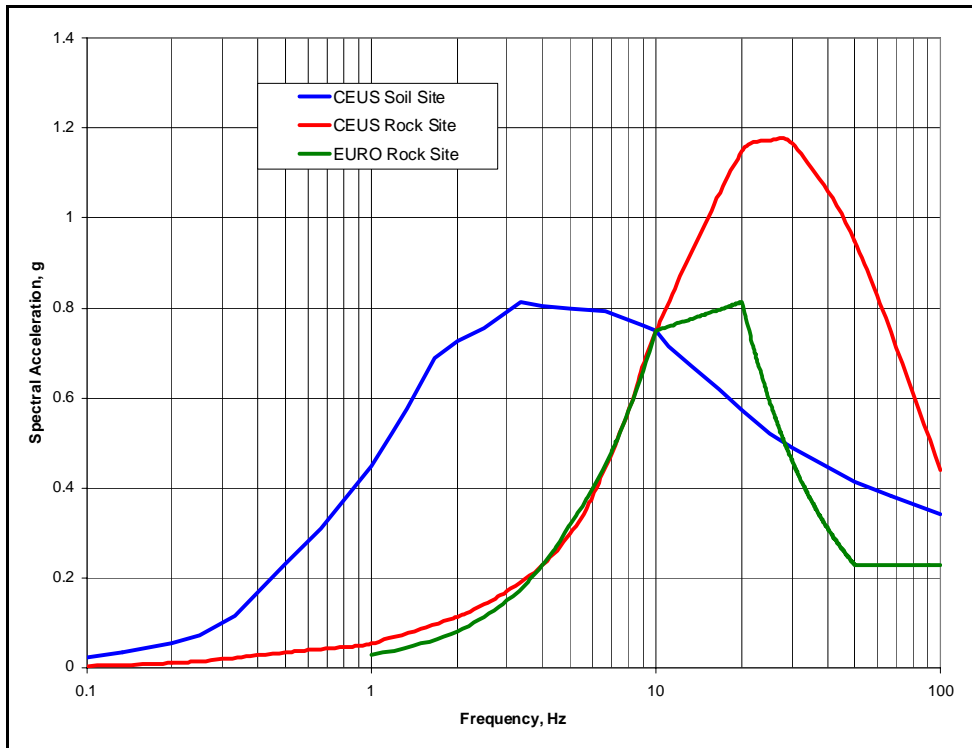


Figure 6-2
Ground Motions Considered

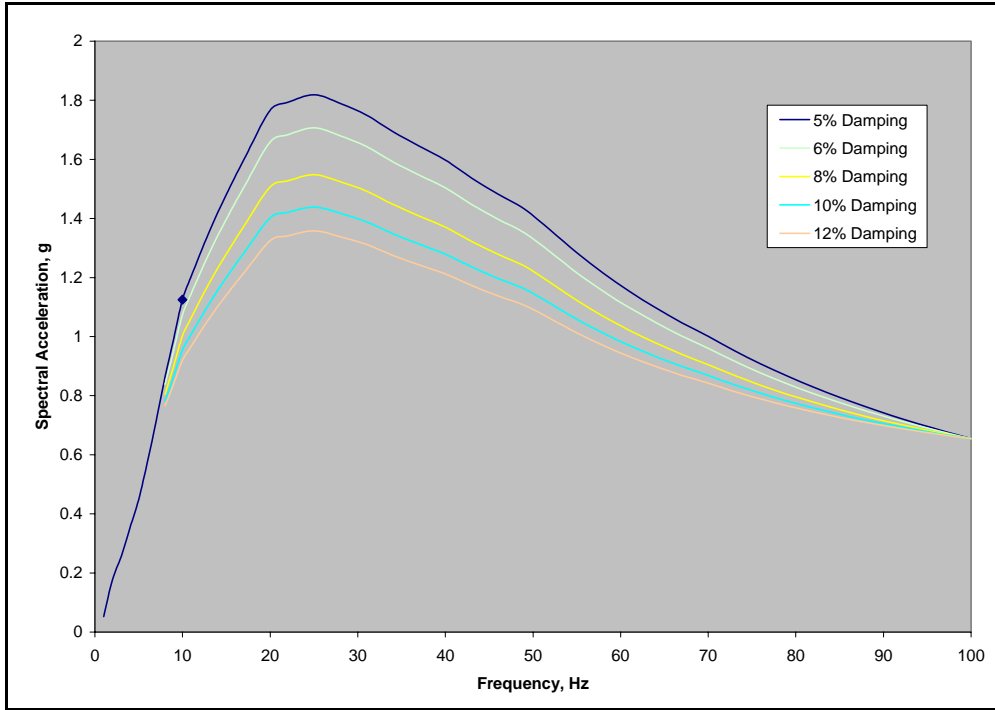


Figure 6-3
CEUS Rock Site Spectra
(5% Spectrum Normalized to 1.5 x 0.75g at 10Hz)

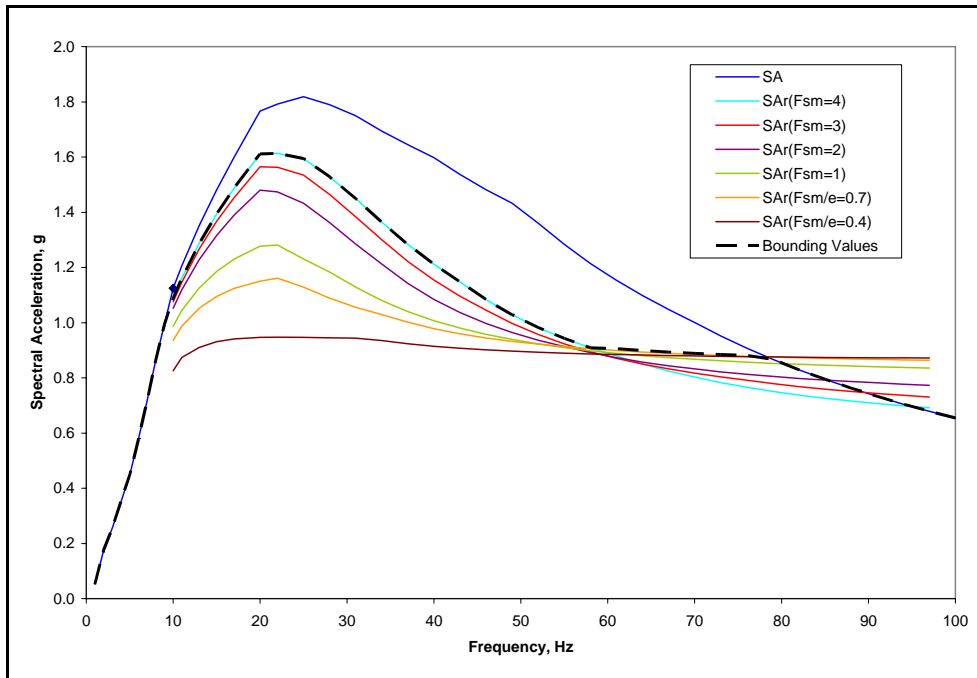


Figure 6-4
CEUS Rock Site Modified Spectra
(Unreduced Spectrum Normalized to 1.5 x 0.75g at 10 Hz)

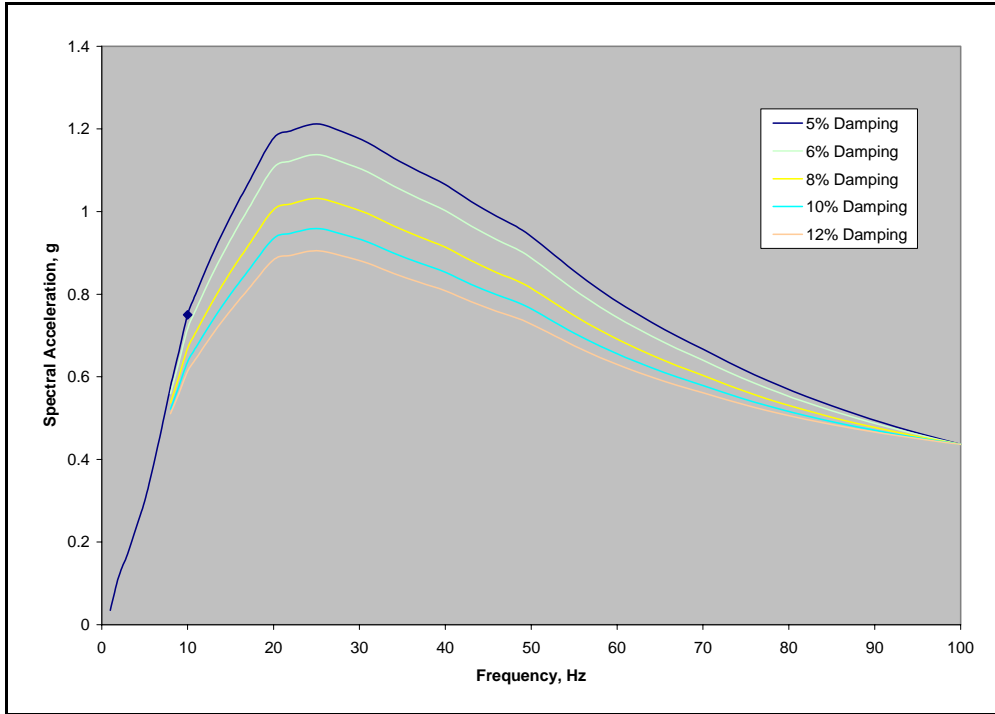


Figure 6-5
CEUS Rock Site Spectra
(5% Spectrum Normalized to 1.0 x 0.75g at 10 Hz)

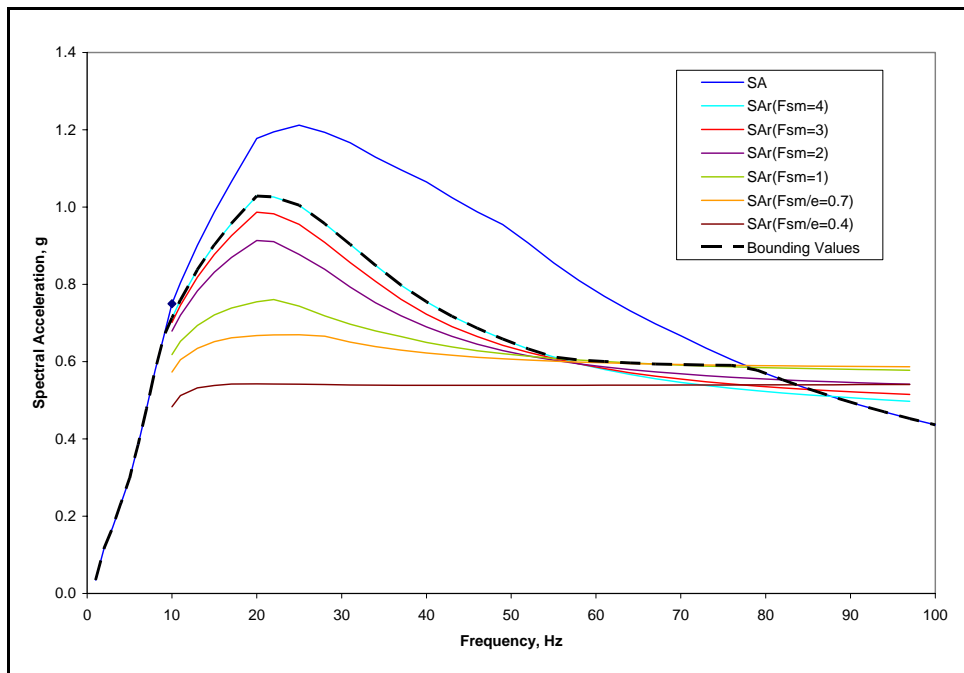


Figure 6-6
CEUS Rock Site Modified Spectra
(Unreduced Spectrum Normalized to 1.0 x 0.75g at 10 Hz)

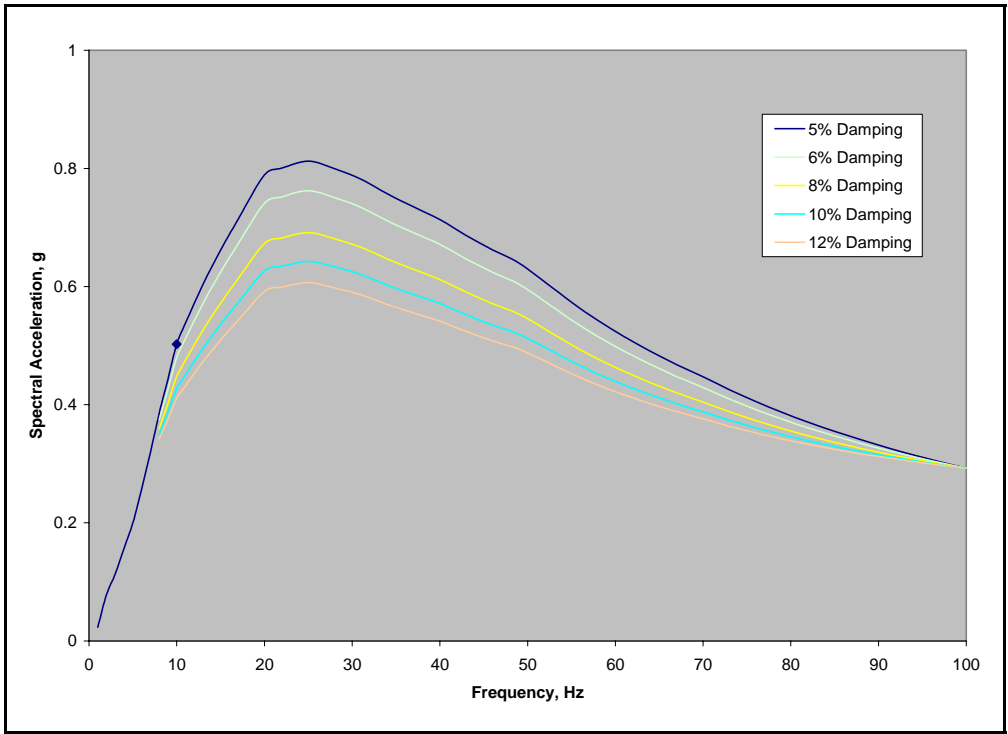


Figure 6-7
CEUS Rock Site Spectra
(5% Spectrum Normalized to 0.67 x 0.75g at 10 Hz)

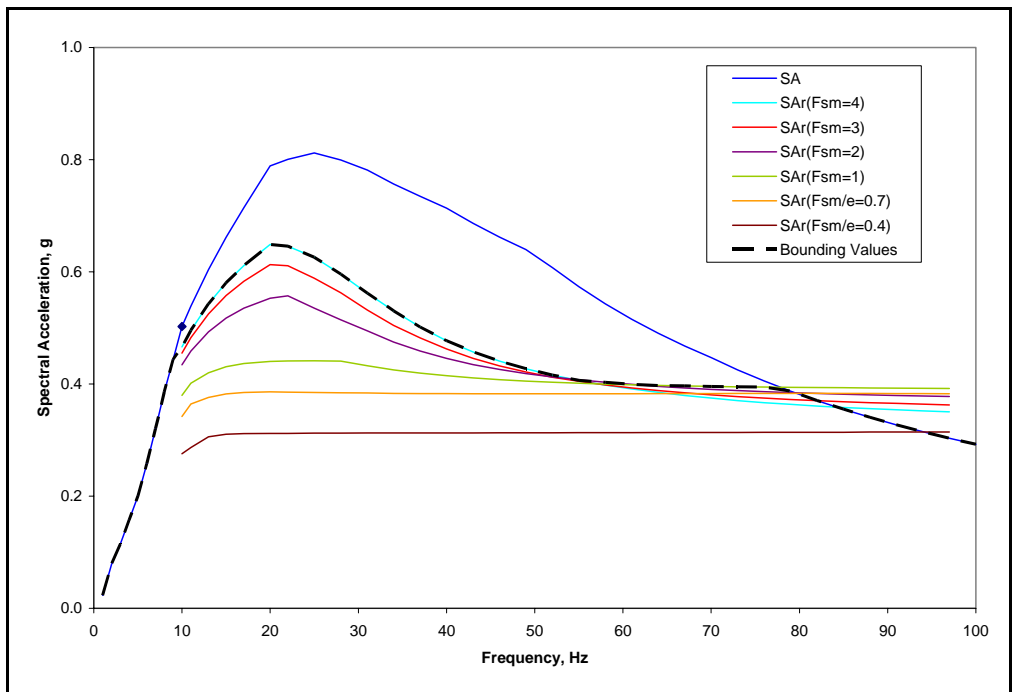


Figure 6-8
CEUS Rock Site Modified Spectra
(Unreduced Spectrum Normalized to 0.67 x 0.75g at 10 Hz)

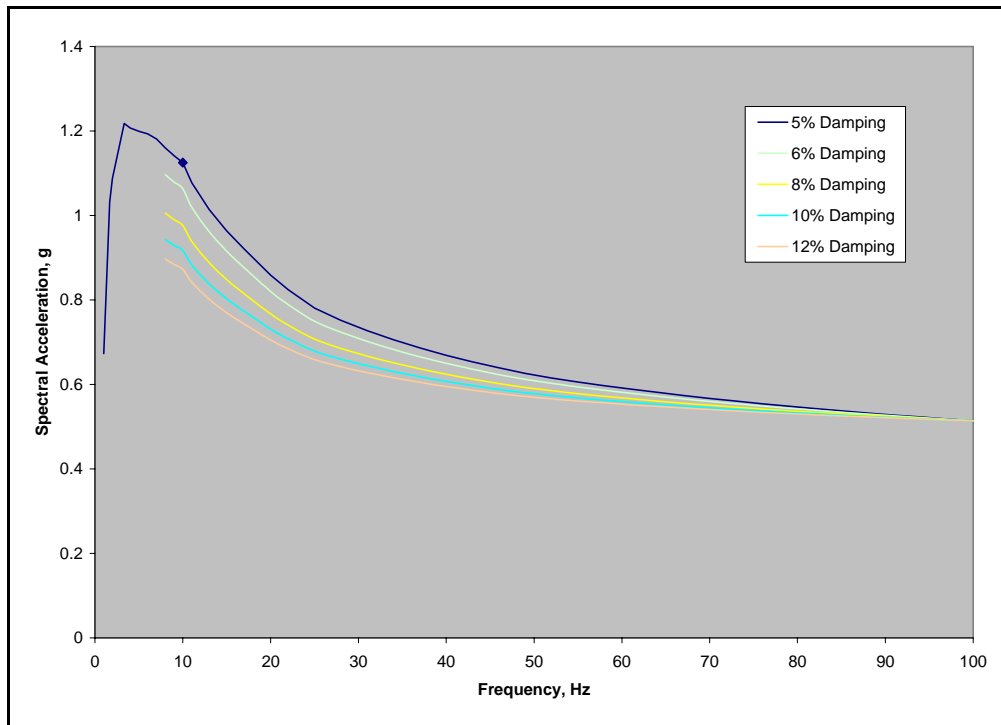


Figure 6-9
CEUS Soil Site Spectra
(5% Spectrum Normalized to 1.5 x 0.75g at 10 Hz)

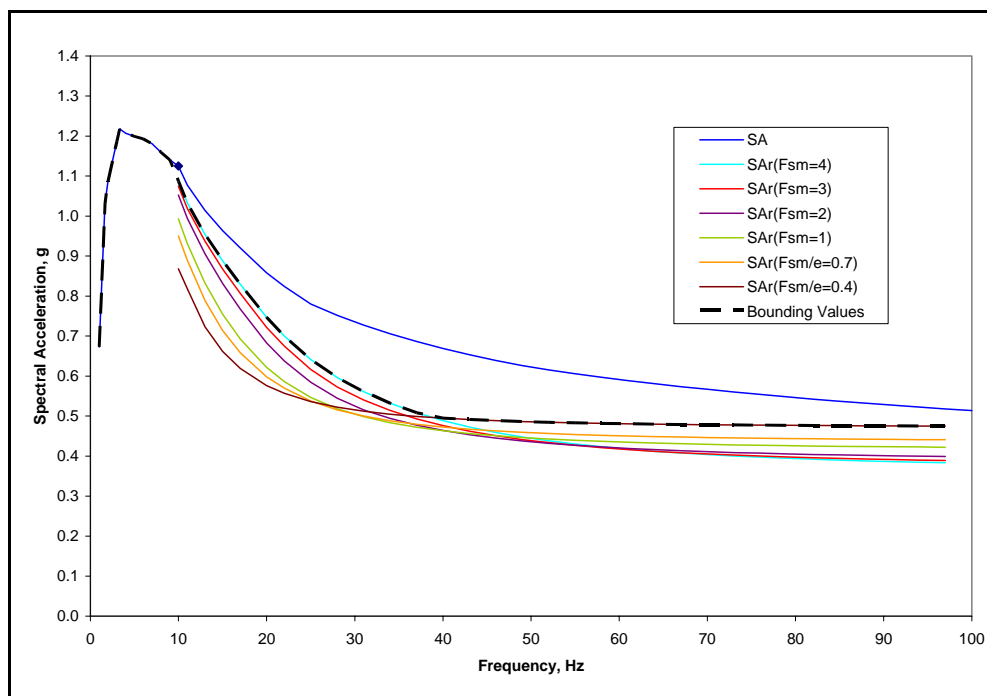


Figure 6-10
CEUS Soil Site Modified Spectra
(Unreduced Spectrum Normalized to 1.5 x 0.75g at 10 Hz)

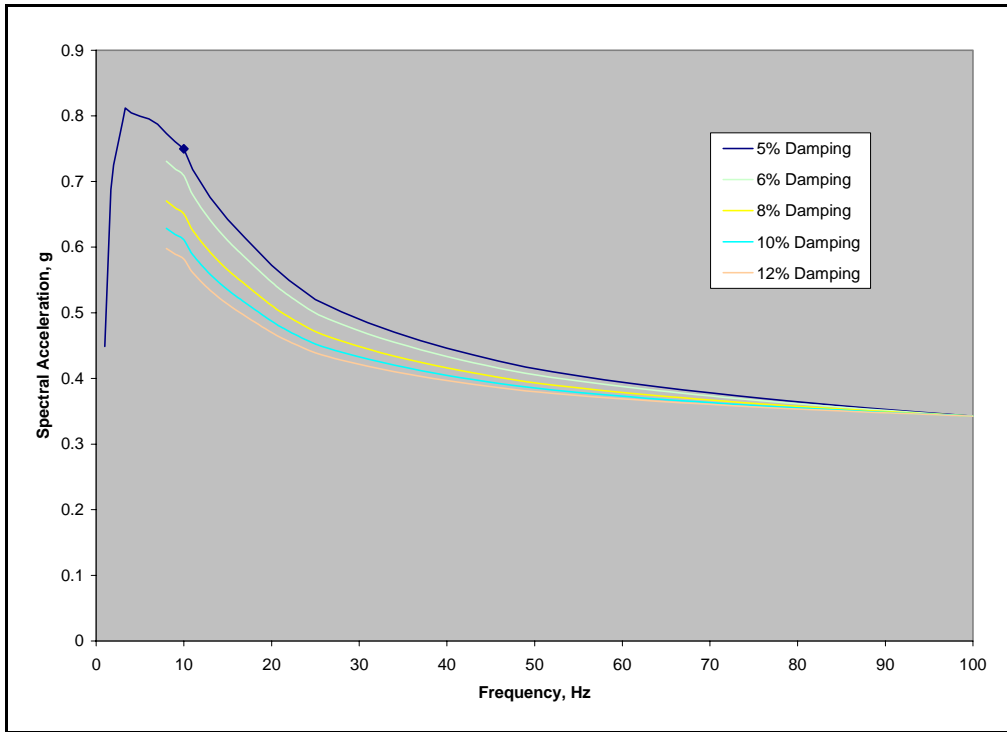


Figure 6-11
CEUS Soil Site Spectra
(5% Spectrum Normalized to 1.0 x 0.75g at 10 Hz)

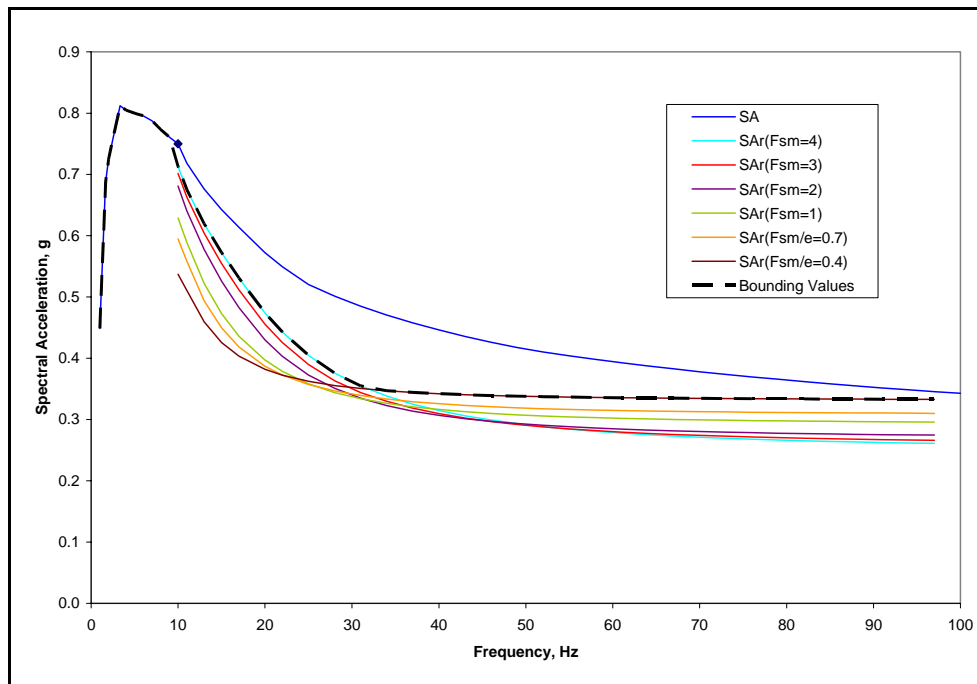


Figure 6-12
CEUS Soil Site Modified Spectra
(Unreduced Spectrum Normalized to 1.0 x 0.75g at 10 Hz)

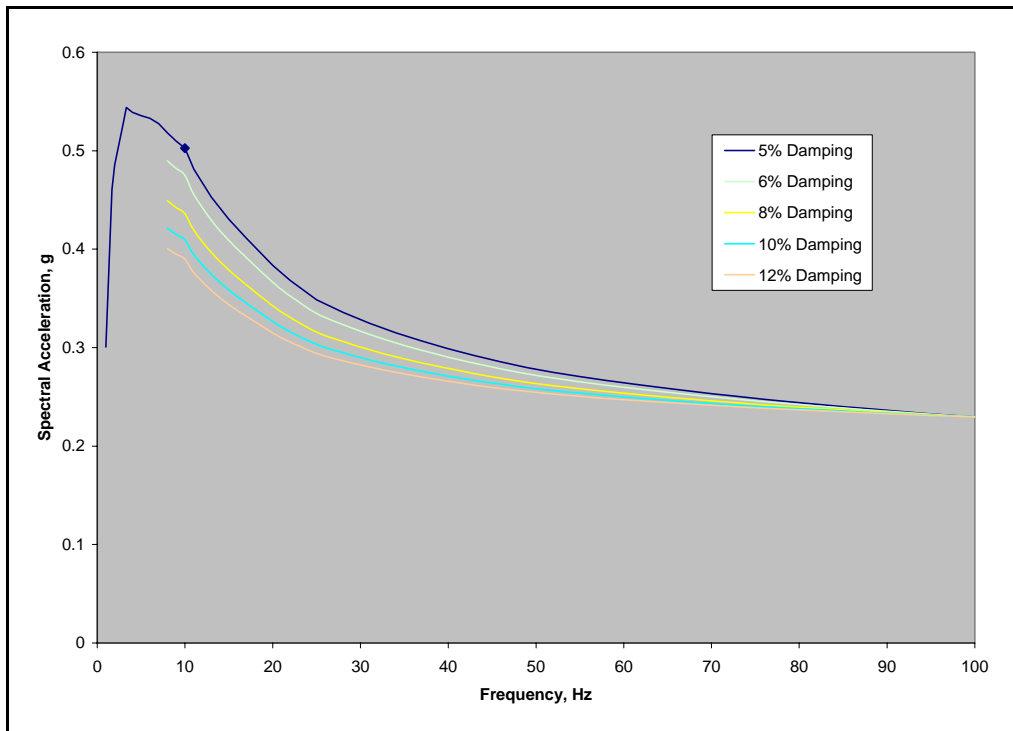


Figure 6-13
CEUS Soil Site Spectra
 (5% Normalized to 0.67 x 0.75g at 10 Hz)

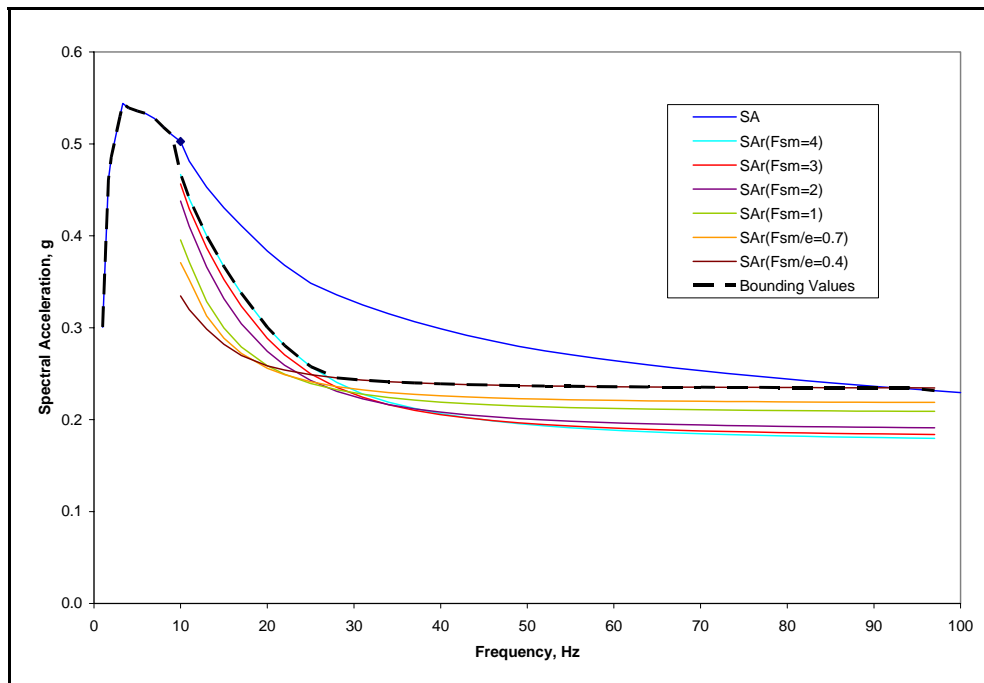


Figure 6-14
CEUS Soil Site Modified Spectra
 (Unreduced Spectrum Normalized to 0.67 x 0.75g at 10 Hz)

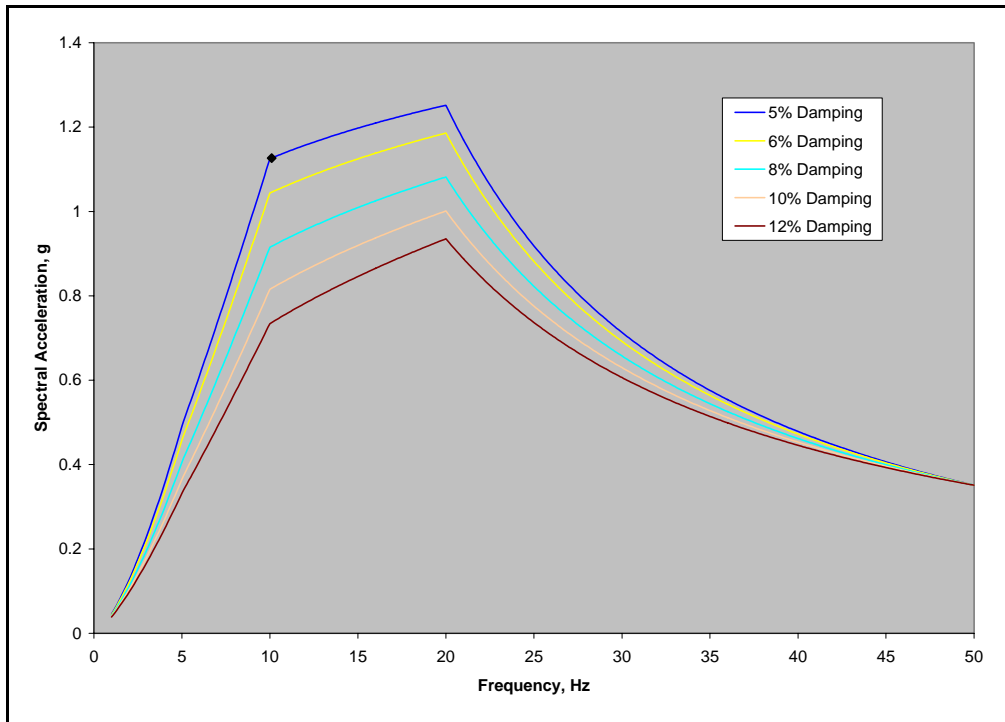


Figure 6-15
European Horizontal Hard Rock Spectra
(5% Horizontal Spectrum Normalized to 1.5 x 0.75g at 10 Hz)

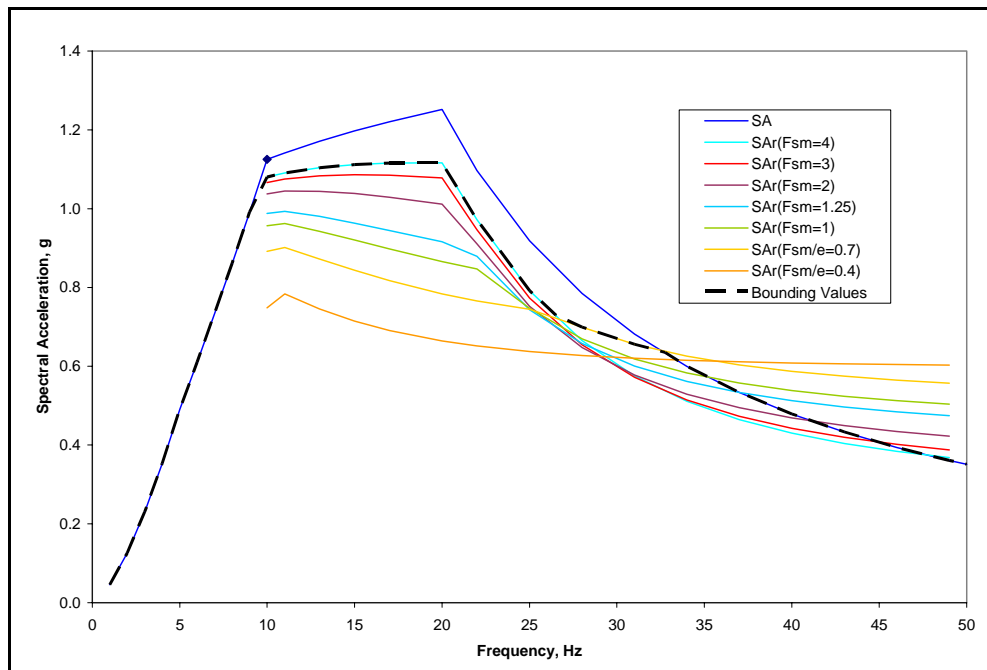


Figure 6-16
European Horizontal Hard Rock Modified Spectra
(Unreduced Horizontal Spectrum Normalized to 1.5 x 0.75g at 10 Hz)

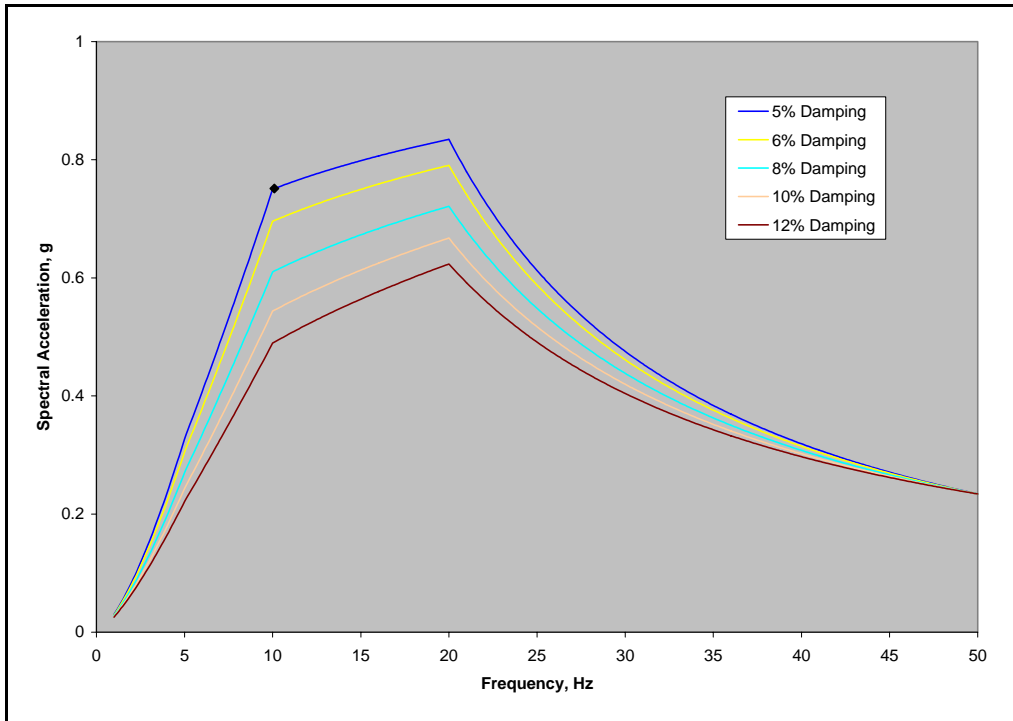


Figure 6-17
European Horizontal Hard Rock Spectra
 (5% Horizontal Spectrum Normalized to 1.0 x 0.75g at 10 Hz)

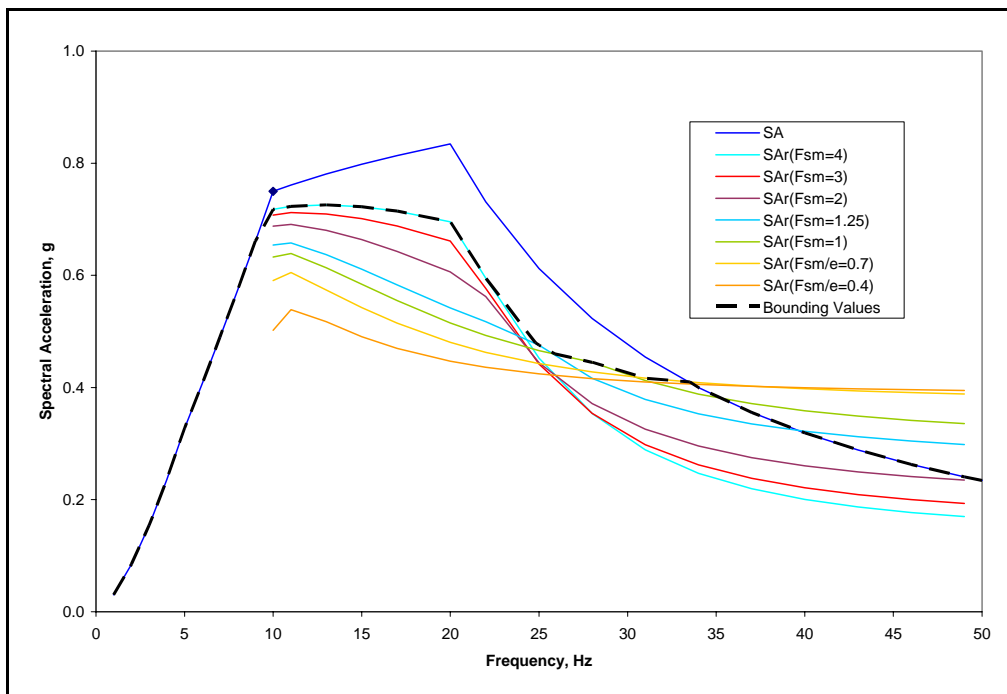


Figure 6-18
European Horizontal Hard Rock Modified Spectra
 (Unreduced Horizontal Spectrum Normalized to 1.0 x 0.75g at 10 Hz)

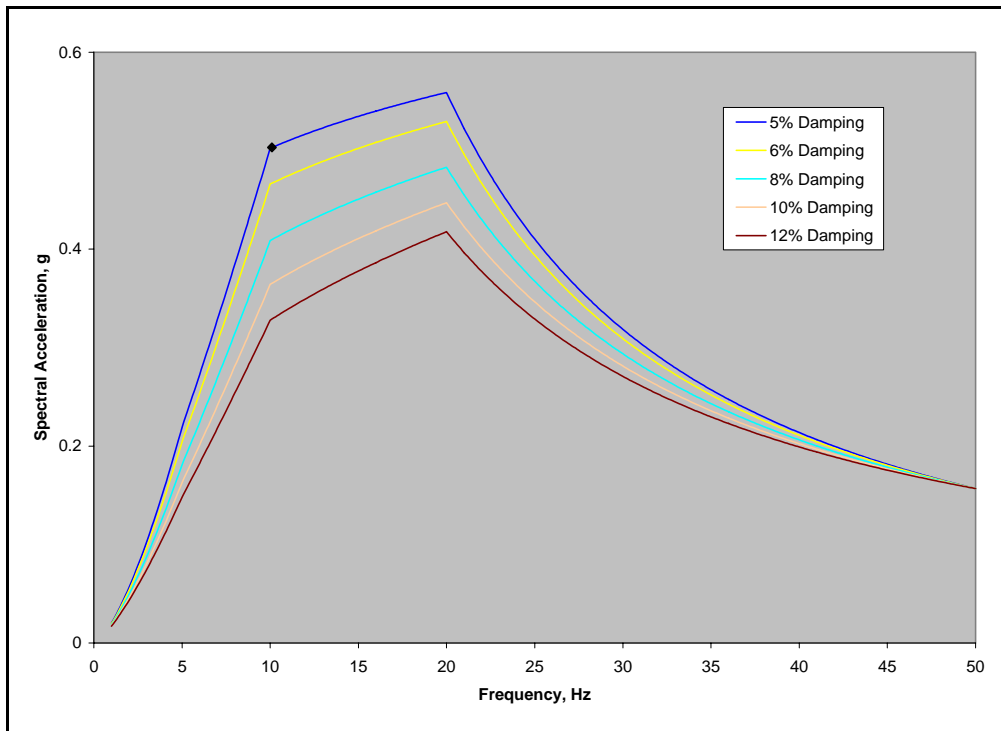


Figure 6-19
European Horizontal Hard Rock Spectra
 (5% Horizontal Spectrum Normalized to 0.67 x 0.75g at 10 Hz)

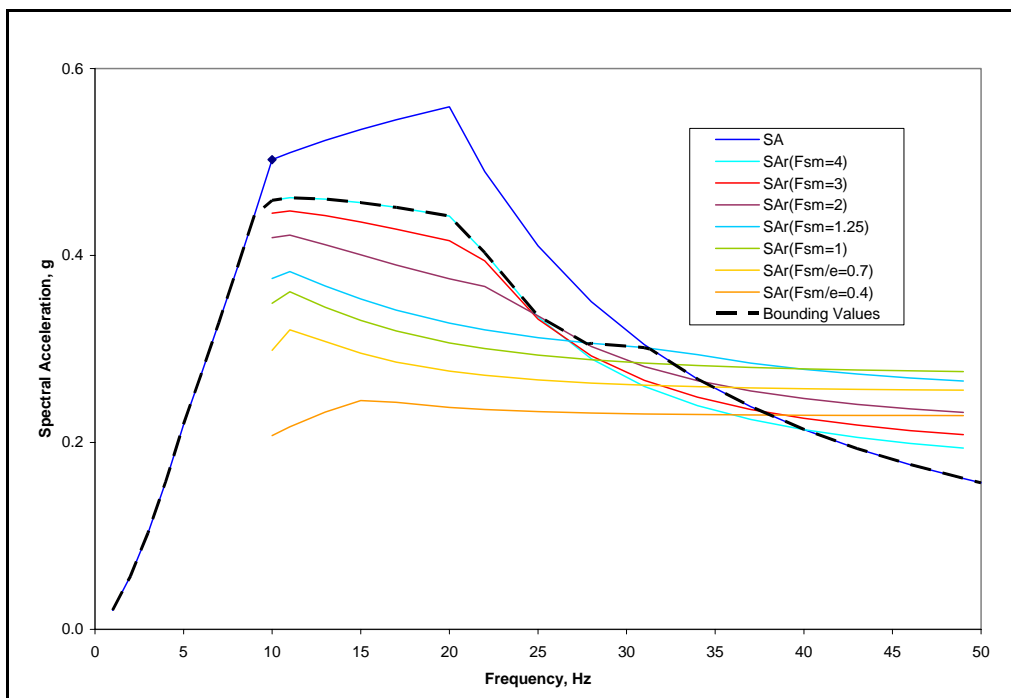


Figure 6-20
European Horizontal Hard Rock Modified Spectra

(Unreduced Horizontal Spectrum Normalized to 0.67 x 0.75g at 10 Hz)

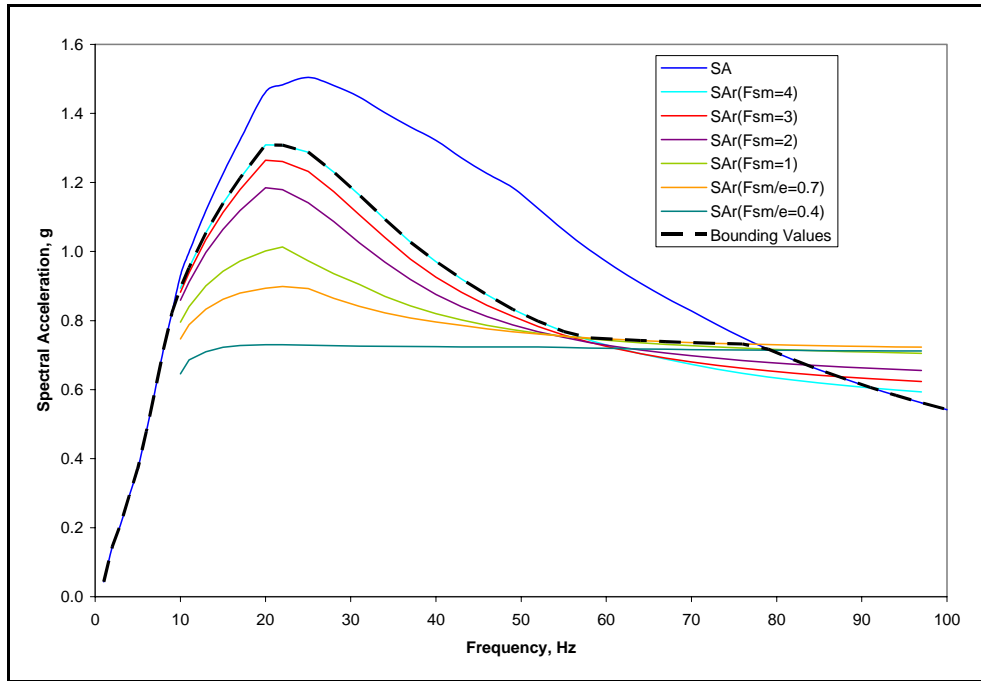


Figure 6-21
Development of Free-Field CEUS Rock Site Design Spectrum
(Unreduced Spectrum Normalized to 0.931g at 10 Hz)

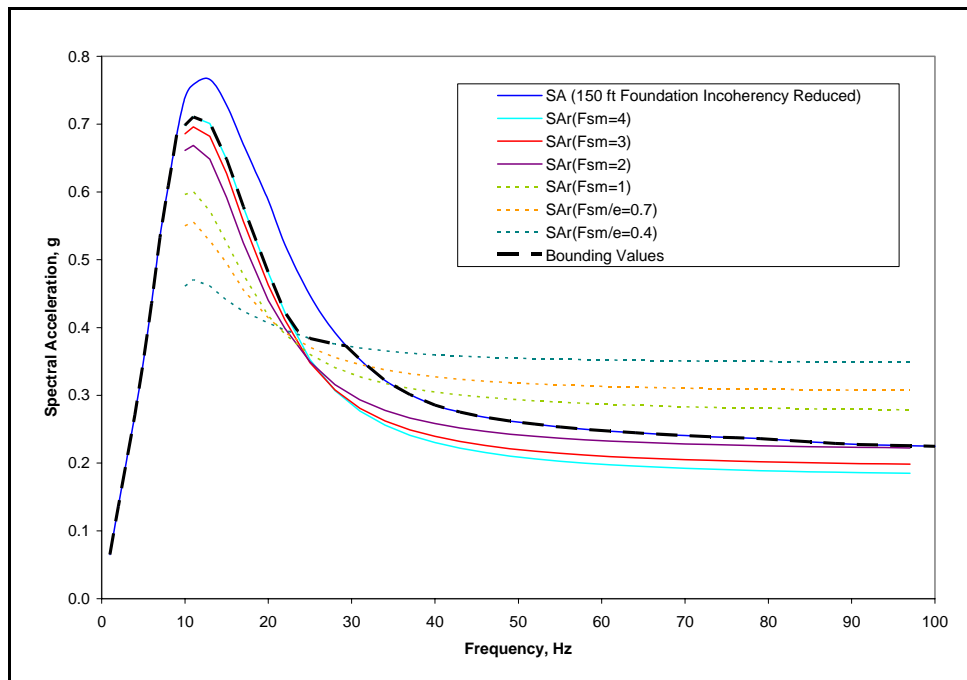


Figure 6-22
Development of 150 ft. Square Foundation on CEUS Rock Site
(Incoherence Reduced Spectrum Normalized to 0.74g at 10 Hz)

7

LIMITING AND FUNCTIONAL FAILURE MODES

Limit State Behavior

The foregoing has considered the equipment response modification that occurs when the non-linear cyclic behavior of the anchorage limit state is considered. If the design strength (factored nominal strength) of the anchorage component is equal to or greater than the required strength determined using the reduced seismic demand, then the equipment load path has the necessary design margin to assure that the probability of exceeding the maximum limit state deformation is sufficiently low. It is important to note that the response modification is determined using the limit state resistance function. For the unreduced design case, the maximum limit state deformation is directly obtained using the demand applied as an assumed static load. For the reduced case, reverse cycling of the demand along the path to the maximum limit deformation results in high frequency energy dissipation which in turn reduces the demand. The reduced demand then allows the anchorage component to be sized for lower design strength than the component designed for the unreduced demand. For the case of a fillet weld with minimum leg size, the design strength is a function of the weld length. But as noted previously, the maximum deformation of a fillet weld is independent of the weld length, thus the fillet weld sized with unreduced demand will have the same maximum limit state deformation as the weld sized for the reduced demand. Since the demand is reduced by the spectral de-amplification factor or the inverse of the response modification factor, F_{μ} , the length of the weld sized for the reduced demand will have a length that is reduced by the same factor compared to a weld sized for the unreduced demand. The ratio of the design strength to the limit state strength is approximately $R/R_r = 1/1.6 = 0.625$ as indicated in Chapter 3. The weld deformation ratio associated with this load ratio is approximately $\delta/t = 0.0057$ if the limit state load-deflection relationship given in the AISC specification is used (see Figure 3-3). For a 3/16 inch weld, this corresponds to a deformation of approximately $\delta = 0.001$ inch. Thus, both the weld sized for the reduced demand, and the weld sized for the unreduced demand, will have the same small deformation associated with the design strength levels. It should be noted that the deformation associated with the design strength component force levels is approximately the same value of displacement selected as the yield level displacement in the effective elasto-plastic resistance function used in the analyses to determine the response modification factors.

A fillet weld loaded in transverse shear was selected as a low bounding surrogate component for demonstration of the effects of negligible non-linear behavior on the high frequency response of in-structure mounted equipment. The reason for selecting the transverse loaded fillet weld is that it is the connection that has the least ultimate deformation capacity compared to other types of connections and, thus, can be considered as a bounding case representation. Due to both configuration and fit-up allowances, the limit state behavior of connections is inherently non-linear. The range of 0.001 – 0.010 inch represents the lower bound of fit-up allowances for both structures and equipment attachments in power plants. Attachment components such as bolts, screws, and welds are all present and in the aggregate can all act as sources of non-linear limit behavior. Behavior mechanisms such as bolt frictional slip can also be represented with an

effective elasto-plastic resistance function. The surrogate problem as posed, considers only the effect of a single mechanism, confined to the anchorage load path. There are, in fact, numerous other sources of non-linearity not only in the anchorage load path but also within the both the equipment and supporting structure that can act to limit high frequency response. Many connections might have other limitations imposed (such as minimum required weld length) that provide an over-strength of the connection. The selection of a transverse loaded fillet weld is meant to represent a low bounding approximation of any of several non-linear mechanisms present. The use of the lowest estimate of ultimate limit deformation provides the least equipment response reduction.

Functional Failure Modes

In general, the function of an active component during a seismic design event can only be demonstrated by a shaking table test. For other types of more passive equipment, function may be related to position retention of components or certain clearances being maintained. For these types of equipment, analysis may be sufficient to demonstrate function during a seismic event. Given that function is only required after a seismic event, then other options can be used to demonstrate post-earthquake function. If similar items in power or industrial plants have continued operation after an actual earthquake, then documentation of the event, and a conservative estimate of motion that the equipment was subjected to, may suffice to demonstrate equipment post-earthquake function. Also it is possible to show that equipment has been subjected to more severe motion for other applications (military, transportation, etc.). Equipment qualification is normally conducted using guidance provided in IEEE Std. 344 (IEEE, 2005).

The design of new plants is being accomplished in a completely different manner than the past approach used for the current generation of operating plants which resulted in the equipment of each plant being uniquely qualified. New plant designs have been pre-certified and the safety-related equipment has been limited to a smaller subset of the total plant equipment system. With regard to seismic design, the certified designs have used generic design spectra, similar to those recommended in RG 1.60, anchored to a PGA value of 0.3g. Since the certification process has been conducted over a period of several years, the design spectra were fixed and not allowed to undergo any changes. As such, the certified design spectra do not fully reflect the high frequency content of motion which recent seismic hazard studies have shown for some CEUS sites. Figure 7-1 compares an example certified design spectrum (an augmented RG 1.60 spectrum) with the incoherency reduced and corresponding non-linear response modified design spectrum developed for an example CEUS rock site. Each of these spectra represent input motion levels that would be used to generate in-structure response spectra. As can be noted in Figure 7-1, the incoherence reduced spectrum exceeds the design spectrum in the 10-24 Hz range by a maximum factor of 1.15. In general, the additional reduction due to non-linear behavior is tied to the level of the incoherence reduced spectrum and will result in approximately 15-30% additional reduction.

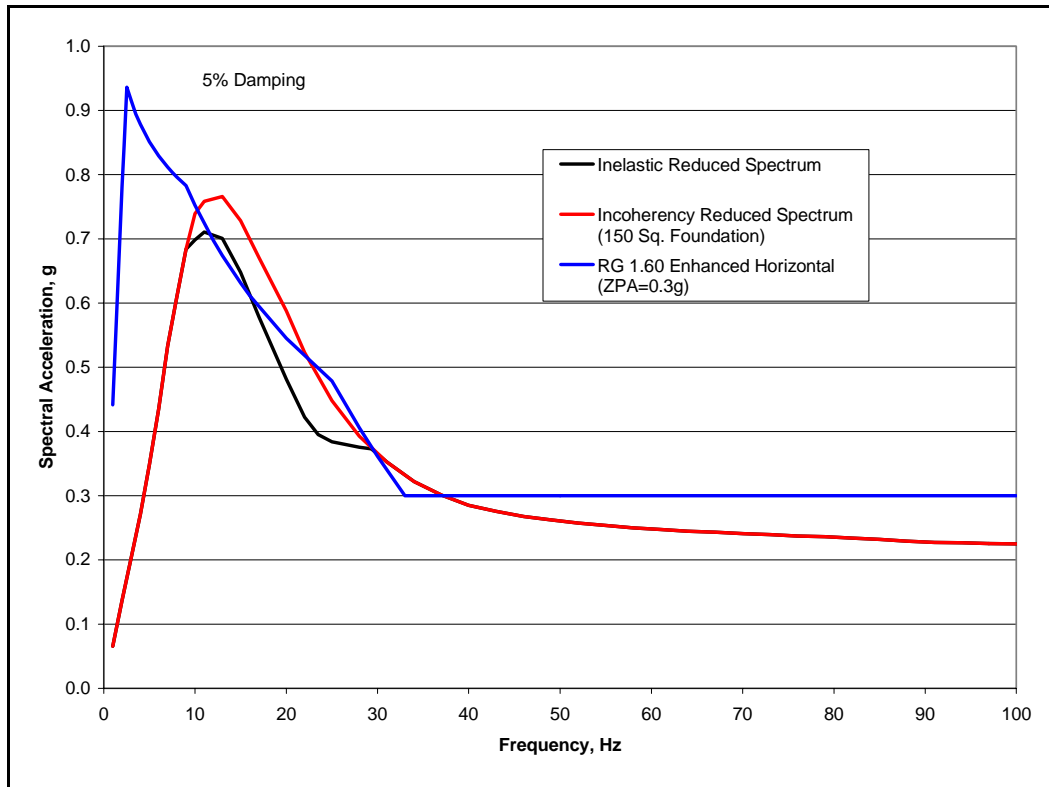


Figure 7-1
Comparison of Reduced CEUS Rock Site Spectra with Example Certified Plant Design Spectra

Reed et al (1993) recommended that spectra reduced for non-linear load path behavior should be used only for determination of structural integrity and not used to generate spectra for functional qualification of active equipment. This is true for entire equipment packages that are to be anchored, because in that case the functional qualification will need to include the same anchorage load path as to be used in the plant. Any response modification will then occur during the test. For the qualification of passive equipment, the spectrum, reduced for non-linear effects, is the appropriate basis for input motion determination.

For cases where the incoherency reduction removes much of the high frequency content of the free field ground motion, the in-structure spectra computed with finite element structure models will be reasonably accurate. Then, if the qualification level represented by the certified design in-structure spectra is exceeded, a re-qualification effort may be necessary. If the variability of the incoherence phenomenon is considered, then the foundation spectrum may be higher, particularly in the high frequency range. For these situations, in-structure spectra computed with finite element structure models will involve computation of modal response with questionable accuracy above 25 Hz. For such cases, where the scattered foundation motion is significantly higher than the certified design spectrum or if there are plant site locations, where the full unreduced site ground design spectrum needs to be specified, alternate qualification procedures will be needed to augment the qualification level represented by the certified design.

In general, at least three basic methods can be considered for dealing with motion that exceeds the certified design qualification level:

1. **Re-qualify the equipment item to the higher level input motion.** This approach would be applicable when there is a high confidence in the computed in-structure spectra. If the original qualification test was conducted with suitable margin or if the item was over tested, the original qualification test may have already accomplished the additional testing effort. Qualification testing is normally conducted with a 10% margin per IEEE Std 323 (IEEE, 2003) and it should be noted that ASCE-43 (ASCE, 2005) requires a margin of 1.4 for qualification tests. If a suitable margin is included in the original qualification test then any issues caused by differing site design motion can be easily addressed.
2. **Utilize a high frequency stress screening test.** If there is a low confidence in the computed in-structure spectra, then a generic test conducted at a sufficiently high input level can be used to screen the item for high frequency effects. The use of high level vibration stress screening has become a common practice in the manufacture of modern electrical components (DOD, 1993; Ciufu, 2005). The use of such methods is not to qualify the component for a service environment but rather to stress the component to a given level that assures that manufacturing defects (bad solder connections, etc.) are not present (Starr, 2005). In this form, the screening test is being used as a means of quality assurance. Additional stressors such as temperature rise and humidity can be included in the screening process. Highly Accelerated Life Testing (HALT) is used during product development to identify the product's flaws. Once the design is fixed, the HALT testing results are used to define a Highly Accelerated Stress Screening (HASS) test that then can be used in the normal manufacturing process to insure that flaws are not present (Child, 2004). Function checks of the product are made during the HASS test. This type of product quality assurance can be applied either to a single component or to a total assemblage of components in an enclosure. A common test level which has been used in the past for screen of military equipment is given by the Willoughby stress screening PSD spectrum which has a constant PSD level of $0.04 \text{ g}^2/\text{Hz}$ over a frequency range of 80-350 Hz. This corresponds to 3.3 g rms input motion which is a very high random vibration level. More recent criteria (DOD, 1993) tailor the random motion screening level used based on ability of the test to identify product defects. It is suggested that the concept of stress screening can also be applied to the seismic case where an equipment item has been qualified to a certified design spectrum. The actual item can be stress screened with a wide band random input motion defined over the 10-100 Hz band. If a PSD spectrum is defined as constant over the frequency range 10-50 Hz with a -3dB/octave roll off from 50-100 Hz, a PSD level of $0.001 \text{ g}^2/\text{Hz}$ to $0.005 \text{ g}^2/\text{Hz}$ would correspond to approximately 0.29 to 0.64 g rms, or roughly 0.7 to 1.6 g peak acceleration. The justification of any selected screening level would require a review of the PSDs of in-structure spectra.
3. **Use of other test data to qualify the function of equipment with increased high frequency motion.** This approach essentially uses experience data from qualification testing conducted for military, shipboard, and other transportation environments that are normally dominated by high frequency to accomplish the screening of equipment that is similar to the item being considered. It should be noted that the inclusion of high frequency motion in nuclear qualification efforts is not new. For BWR units, the SRV event is assumed to be concurrent with the seismic event. SRV spectra, in general have additional frequency content in the 20-80 Hz range. Qualification of selected equipment in existing BWR units was often performed with combined seismic and SRV spectra.

Vasudevan (1985) describes the application of available military test data (SAFEGUARD) for commercial type plant equipment to assess the operability of BWR plant equipment. Reed et al (Aug. 1991) present a summary of the SAFEGUARD test program for use in Seismic Margin Assessments or equipment fragility determinations. Gaberson et al (2000) conclude that, based on several different types of shock transient loading tests on equipment, the 5% damped pseudo-velocity spectrum is the best indicator of the damage severity of high frequency motion.

In general, the functional performance of components needs to be demonstrated for the input motion that results after accounting for foundation spatial incoherency effects. EPRI is also conducting several research tasks relative to the characterization of the seismic hazard which may also ultimately lead to some changes in the design input motion. If high frequency content is still present that significantly exceeds the certified design qualification level, then the alternate methods discussed above need to be further developed in order to provide specific recommendations. These alternate methods would be required due to the fact that the structural engineering community recognizes that it is not possible to adequately model for this level of high frequency response in our existing building models and, thus, there would be a lack of confidence in computed values of high frequency structure response.

8

SUMMARY AND CONCLUSIONS

Task S2.2 of the EPRI/DOE New Plant Seismic Issues Resolution Program has been conducted with results presented herein. The presence of nuclear plant equipment with anchorage components that have non-linear limit state resistance behavior, characterized by a negligible level of inelastic deformation, allows limited response modification resulting in reduced high frequency seismic demand for in-structure mounted equipment. In general, these response reductions range from 15% to 30% depending on the high frequency content of the ground design spectrum. This study further develops and provides key technical justification for an approach first presented in a prior EPRI study (Reed et al, 1993). The study also provides several example applications of the response modification procedure. The summary of results for each sub-task is given below.

Anchorage Component Limit State Behavior

Review of the limit state behavior of various types of anchorage components indicates that a fillet weld in transverse shear has the least deformation capacity. Based on empirical relationships correlated with test data (Lesik and Kennedy, 1990), a minimum 3/16 inch fillet weld loaded in transverse shear may be identified as the anchorage component that has the least deformation capacity (on the order of 0.010 inch).

The margin or ratio of mean capacity/design strength for a fillet weld loaded in transverse shear can be conservatively taken as a value of 1.6.

Test based weld deformation functions (now incorporated in the AISC Specification) were used to idealize the resistance function of the anchorage component as a bi-linear (elasto-plastic) function with ultimate deformation and equivalent yield deformation and corresponding strength level.

More recent test programs have shown that the actual weld deformation at fracture is at least a factor of two greater than the values predicted by the Lesik and Kennedy (1990). Thus, use of the Lesik and Kennedy estimates of weld deformation capacity will provide a conservative resistance function for use in equipment response simulations.

Based on very limited low-cycle fatigue test data for fillet welds failing through-the-throat under transverse loading, it is judged that strength degradation effects due to reverse cycle loading do not need to be incorporated into the equivalent bi-linear resistance function representing weld load-displacement behavior. A minimum 3/16 inch fillet weld should be able to sustain several fractional cycles of reverse displacement prior to reaching the failure displacement in the final cycle of the equipment response to in-structure motion caused by high frequency ground motion. This conclusion should be reviewed by a researcher active in the field of seismic testing of welded steel connections in order to strengthen the basis for the results of this study. EPRI plans to initiate this review subject to adequate funding availability.

Evaluation Models

The prior EPRI study (Reed et al, 1993) developed complex multi-parameter 2DOF models and then simplified the models to obtain a SDOF model that was then applied to an example case. This report directly develops the simplified SDOF models and their respective equivalent linearization.

Both a Shear Resistance Model and an Overturning Resistance Model were developed based on a series resistance function that represents the linear equipment resistance combined with a non-linear anchorage resistance.

For the model, the anchorage component is characterized by the spectral acceleration level, SA_y , that causes yield in the anchorage component. This notation allows the identification of two approaches for interpreting the response modification factor: 1) an input scaling factor, F_μ , or 2) a spectral de-amplification factor, $1/F_\mu$. This notation also allows the demonstration that the only difference between the shear and overturning models is the reduced yield acceleration, SA_y/e , used in the case of the overturning model where e is the aspect ratio of the equipment ($e > 1$). The prior EPRI study used correlation of non-linear response models to establish this result.

Reed et al (1993) conducted extensive non-linear time-history response correlation analyses using the program DRAIN2D (Kannan and Powell, 1985) to establish the parameters of the equivalent linear model. The resistance function derived for a 3/16 inch weld, loaded with transverse shear, was used. Review of the correlation data indicates that mean ratios of F_μ generated by time-history analysis and F_μ generated using the equivalent linear models are very close to unity with COVs of 0.106 for the shear resistance model and 0.160 for the overturning resistance model. An ensemble of 15 time-histories was used in the non-linear simulations to represent a wide range of earthquake motions: high frequency content, low frequency content, narrow-band spectra, wide-band spectra, etc. At least 9 of the records used had substantial high frequency content. One-third of the records used were associated with ENA earthquakes.

The models developed are valid for horizontal input motion only. Vertical motion is a special case since the dead weight effect must first be overcome before any anchorage loading can occur. The consideration of vertical input motion would require 1) the development of the appropriate model modifications, 2) the non-linear response determination using the DRAIN2D program and a suite of time-history records, and 3) the correlation of the non-linear response with an equivalent linear model. EPRI plans to initiate this additional model development subject to adequate funding availability.

Amplification of Structures

The basic underlying premise of the prior ERPI study (Reed et al, 1993) is that the ground motion design spectrum can be modified for high frequency non-linear effects and then used to define a time history that is, in turn, used to generate floor spectra which implicitly incorporate reductions in the high frequency response. The motivation for this indirect approach is that structural models have inherent limitations for computing high frequency response, thus the high frequency content of the floor motion is removed at the input level rather than the response level. Given that the structure remains linear, the artifice of a simple amplification scale factor is used to scale the ground spectral acceleration to represent the in-structure spectral acceleration. In the present study, several simplified structural models were used to determine a maximum amplification factor for use with the simplified equivalent linear equipment response modification models.

The measure of amplification used is the ratio of in-structure mounted oscillator response to ground mounted oscillator response assuming 5% damping in both cases. It is assumed that the fundamental mode of the structure is less than 10 Hz and that the amplification ratio being sought is for oscillators greater than 10 Hz.

The computation of the in-structure response, at a given position in the structure, is a function of the modal properties of the structure model in terms of modal frequencies and product of participation factor and normalized mode shape, $\Gamma_i \phi_i(x)$.

The finite element modeling of an example uniform cantilever structure with general dimensions typical of nuclear plant structures indicates that an increased modeling discretization is necessary to capture the high frequency modal properties. The comparison of an analytical solution (Timoshenko beam) with the high discretization finite element model indicates that, while modal frequencies are accurately captured, the $\Gamma_i \phi_i(x)$ values deviate significantly for the 3rd and higher modes. Thus, the high discretization finite element model cannot provide an accurate weighted response contribution for the high frequency modes.

To investigate the amplification of structures in the frequency range greater than 10 Hz, a series of three different types of uniform cantilever beams were used: 1) a flexure beam, 2) a shear beam, and 3) a Timoshenko beam. Four fundamental frequencies of 3 Hz, 5 Hz, 7 Hz, and 9 Hz were considered for each type of beam. Theoretical mode frequencies, mode shapes, and participation factors for modes up to 100 Hz were used to determine the response at 10 positions of each beam type and fundamental frequency for three time-history motions: 1) CEUS Rock compatible, 2) ENA actual record, and 3) European Hard Rock compatible. The resulting comparison of results indicates that the flexure beam has higher amplification than both the shear and Timoshenko beams. This is an expected result due to the difference in modal properties, however, as shown by the finite element model comparison, the Timoshenko beam is more typical of plant structures.

The structure amplification of a Timoshenko beam, as measured by the ratio of a in-structure spectrum to ground spectrum, is at most about a factor of 2.5 in the greater than 10 Hz range.

If the ground input has a PGA at frequency less than 100 Hz, the amplification ratio is simply the ratio of the in-structure ZPA to the ground PGA and is not an oscillator amplification.

Application of Response Modification Procedure

The indirect approach of modifying the base design spectrum prior to generation of floor spectra is used to account for the equipment response reduction due to anchorage non-linear effects.

It is assumed that an equipment anchorage is designed for the reduced spectral acceleration response of the equivalent linear model, SA_r . Then, the spectral acceleration at anchorage component yield, may be represented by $SA_y = F_{SM} SA_r$ for the Shear Resistance Model, or $SA_y / e = (F_{SM} / e) SA_r$ for the Overturning Resistance Model, where the factor, F_{SM} , is a scale factor that accounts for both structural amplification and the mean strength to design strength ratio.

Noting that the maximum spectral amplification is 2.5, the strength margin ratio is 1.6, and the range of e is 1-4, then the range of scale factors $\{ F_{SM}, F_{SM} / e \}$ can be represented by the range of values 0.4-4. Note that the use of a constant amplification factor is judged to provide adequate conservatism for the indirect generation of reduced floor spectra. This is identified as an assumption requiring verification. EPRI plans to initiate a verification study subject to adequate funding availability.

The equivalent linear model with the spectral de-amplification approach is used to obtain the modified elastic spectral values. A 12 step iterative procedure is defined for calculation of the reduced spectral value for each frequency greater than about 10 Hz. Both the shear and overturning models are computed with the same procedure. The procedure is easily adapted to a spreadsheet application which can be accomplished as a manual iteration or automated with a spreadsheet solver add-in.

The modification procedure was applied to three different spectral shapes scaled to different values. In general, the curves for each scale factor cross over each other indicating that different scaling factors or models govern in various frequency ranges. The upper envelope of the various model cases is chosen at the reduced spectrum. At some higher frequency, the unreduced design spectrum is used.

In general, spectral reductions of 15-30% are achieved for CEUS spectra with the procedure over the approximate frequency range 10-80 Hz.

The additional modification of base input spectra for inelastic response behavior should be done on the spatial coherence reduced spectrum associated with the scattered foundation motion.

Limiting and Functional Failure Modes

A small fillet weld, loaded transversely in shear was selected as the surrogate anchorage component since such welds are commonly used to anchor electrical cabinets and since they have the least deformation capacity. The selection of a transverse loaded fillet weld is meant to represent a lower bound approximation of any of several non-linear mechanisms present. The use of the lowest ultimate limit deformation in the reduction procedure provides the least equipment response reduction, i.e., a conservative approach. In general, this type of reduction of high frequency response due to negligible amounts of non-linear deformation also occurs in both civil and equipment structural systems, however, the models for the behavior would be different.

In general, a spectrum reduced for non-linear load path behavior should be used only for determination of structural integrity and not used to generate spectra for functional qualification of active equipment. For the qualification of passive equipment, the spectrum, reduced for non-linear effects, is the appropriate basis for input motion determination.

The safety related equipment for new plants are to be qualified for in-structure spectra generated for a certified design spectrum which may or may not envelop a site specific design spectrum. If after reductions due to spatial motion incoherency are applied, exceedances of the certified qualification level exist, then other options should be considered, such as evaluation of existing certified qualification test spectra for additional high frequency test motion, or review of other test data to provide the needed assurance of function, or performance of a stress screening test that properly accounts for function during a motion that conservatively exceeds the anticipated high frequency structure motion. Specific guidance on these recommended options could be generated in future phases of this project if the results of the design ground motion for representative plants show significant exceedances in the high frequency region relative to the certified design spectrum.

Recommendations

The following tasks have been identified as necessary to support the findings of this Task S2.2 effort. EPRI is committed to the performance of these additional tasks, subject to availability of appropriate funding, in order to broaden the application of these methods and to provide further verification of the procedures developed.

- An expert review of the effects of low-cycle fatigue on fillet weld performance is recommended to ensure the fillet weld capacities have been appropriately characterized within this study.
- The current methodology presented in this study applies to horizontal response reduction only. A suitable model development is recommended for the reduction of vertical in-structure response spectra.
- Indirectly reduced in-structure response spectra, generated with ground motion consistent with a reduced ground design spectrum, should be compared to directly reduced in-structure response spectra, generated with ground motion consistent with an unreduced ground design spectrum. This comparison is necessary to validate the recommended indirect reduction approach.

9

REFERENCES

AISC, *Specification for Structural Steel Buildings*, ANSI/AISC 360-05, American Institute of Steel Construction, Chicago, Illinois, 2005.

ASCE, *Seismic Design Criteria for Structures, Systems, and Components in Nuclear Facilities*, ASCE/SEI 43-05, ASCE Standard, American Society of Civil Engineers, Reston, Virginia, 2005

Ballio, G. and Castiglioni, C. A., “A Unified Approach for the Design of Steel Structures Under Low and/or High Cycle Fatigue”, *Journal of Constructional Steel Research*, Vol. 34, p.p. 75-101, Elsevier, 1995.

Bowman, M. D. and Quinn, B. P., “Examination of Fillet Weld Strength”, *Engineering Journal*, American Institute of Steel Construction, Vol. 31, No. 3, p.p. 98-108, 1994.

Callele, L. J., “Strength and Behavior of Multi-Oriented Fillet Weld Connections”, *Structural Engineering Report 255*, University of Alberta, Canada, February 2005.

Child, J., “Vibration Tests Techniques Shake the Status Quo”, *COTS Journal*, <http://cotsjournalonline.com>, April 2004.

Ciufo, C. A., “Despite Questions of Validity, HALT and HASS Remain Prevalent”, *COTS Journal*, <http://cotsjournalonline.com>, February 2005.

Cowper, G. R., “The Shear Coefficient in Timoshenko’s Beam Theory”, *Journal of Applied Mechanics*, American Society of Mechanical Engineers, Vol. 33, p.p.335-340, June 1966

Crandall, S. H. and Mark, W. D., *Random Vibration in Mechanical Systems*, Academic Press, New York, New York, 1963.

DOD, *Environmental Stress Screening (ESS) of Electronic Equipment*, MIL-HNBK-344A, Department of Defense, Washington, D.C., 1993.

IEEE, *IEEE Standard for Qualifying Class 1E Equipment for Nuclear Power Generating Stations*, IEEE Std 323-2003, IEEE Power Engineering Society, Institute of Electrical and Electronic Engineers, New York, New York, 2003.

IEEE, *IEEE Recommended Practice for Seismic Qualification of Class 1E Equipment for Nuclear Power Generating Stations*, IEEE Std 344-2004, IEEE Power Engineering Society, Institute of Electrical and Electronic Engineers, New York, New York, 2005.

Excel 2003 Assistance, “About Solver”, <http://office.mircosoft.com/en-us/assistance>, Microsoft Corporation, 2005.

EPRI, “Effect of Seismic Wave Incoherence on Foundation and Building Response”, draft report prepared for the Electric Power Research Institute, November, 2005.

Failure Control Ltd., “Review of Low Cycle Research”, RR 207, Research Report, Health and Safety Executive, Suffolk, UK, 2004.

Ferreira, J, et al, “Low Cycle Fatigue Strength Assessment of Cruciform Welded Joints”, Journal of Constructional Steel Research, Vol. 47, p.p. 223-244, Elsevier, 1998.

Fischer Fixing Systems, “Technical Handbook”, 2nd Edition, www.fischerwerke.com, 2005.

Gaberson, H. A., et al, “Classification of Violent Environments that Cause Failure”, Shock and Vibration, Vol. 34, No. 5, p.p.16-23, May 2000.

Grondin, G. Y., et al, “Strength of Transverse Fillet Welds Made with Filler Metals without Specified Toughness”, report prepared for American Institute of Steel Construction, University of Alberta, Canada, October 2002.

Gurney, T. R. and MacDonald, K., “Literature Survey on Fatigue Strengths of Load-Carrying Fillet Welded Joints Failing in the Weld”, OTH 91 356, Offshore Technology Report, Health and Safety Executive, Suffolk, UK, 1995

Han, S. M., et al, “Dynamics of Transversely Vibrating Beams Using Four Engineering Theories”, Journal of Sound and Vibration, Vol. 225, p.p. 935-988, 1999.

Iwankiw, N. R., “Rational Basis for Increased Fillet Weld Strength”, Engineering Journal, American Institute of Steel Construction, Vol. 34, No. 2, p.p. 68-71, 1997.

Jacobsen, L. S., “Natural Frequencies of Uniform Cantilever Beams of Symmetrical Cross Section”, Journal of Applied Mechanics, American Society of Mechanical Engineers, p.p. A1-6, March 1938.

Jacobsen, L. S. and Ayre, R. S., *Engineering Vibrations*, McGraw-Hill Book Co, New York, New York, 1958

Kannan, A. E. and Powell, G. H., “DRAIN-2D: A General Computer Program for Dynamic Analysis of Inelastic Plane Structures, with User’s Guide”, EERC 73-6 and EERC 73-22, Revision 1, University of California, Berkeley, August 1985.

Kennedy, R. P., et al, “Engineering Characterization of Ground Motion – Task 1, Effects of Characteristics of Free-Field Motion on Structural Response”, NUREG/CR-3805, U. S. Nuclear Regulatory Commission, May 1984.

Klingner, R. E., et al, “Anchor Bolt Behavior and Strength During Earthquakes”, NUREG/CR-5434, U. S. Nuclear Regulatory Commission, August 1998.

Kulak, G. L., et al, *Guide to Design Criteria for Bolted and Riveted Joints*, John Wiley & Sons, New York, New York, 1987.

Lesik, D. F. and Kennedy, J. L., "Ultimate Strength of Eccentrically Loaded Fillet Welded Connections", Structural Engineering Report 159, University of Alberta, Canada, May 1988.

Lesik, D. F. and Kennedy, J. L., "Ultimate Strength of Fillet Welded Connection Loaded In Plane", Canadian Journal of Civil Engineering , Volume 17, p.p. 55-67, 1990.

McGuire, R. K. ,et al, "Technical Basis for Revision of Regulatory Guidance on Design Ground Motions: Hazard and Risk-Consistent Motions Spectra Guidelines," NUREG/CR-6728, U. S. Nuclear Regulatory Commission, May 2001.

Papadopoulos, A. P. and Trujillo, D. M., "Natural Frequency of Timoshenko Beam on Flexible Base", Journal of the Engineering Mechanics Division, American Society of Civil Engineers, Vol. 106, p.p. 307-321, April 1980.

Reed, J. W. et al, "A Criterion For Determining Exceedance of the Operating Basis Earthquake," EPRI NP-5930, Electric Power Research Institute, July 1988.

Reed, J. W. et al, "A Methodology for Assessment of Nuclear Power Plant Seismic Margin," EPRI NP-6041SL Revision 1, Electric Power Research Institute, August, 1991

Reed, J. W., et al, "Recommended Procedures to Address High-Frequency Ground Motions in Seismic Margin Assessment for Severe Accident Policy Resolution," Appendix B of "Industry Approach to Seismic Severe Accident Policy Implementation," EPRI NP-7498, Electric Power Research Institute, Palo Alto, California, November 1991.

Reed, J. W., et al, "Analysis of High-Frequency Seismic Effects," EPRI TR-102470, Electric Power Research Institute, Palo Alto, California, October 1993.

SAP2000, Version 8, Integrated Software for Structural Design, "Basic Analysis Reference Manual" Computers and Structures, Inc., Berkeley, California, 2005.

SKI Project Seismic Safety, "Characterization of Seismic Ground Motions for Probabilistic Safety Analyses of Nuclear Facilities in Sweden, Summary Report," SKI Technical Report 92:3, April 1992.

Starr, J., "Vibration Test Goals: Efficient, Effective, and Valid", COTS Journal, <http://cotsjournalonline.com>, April 2005.

Vanmarcke, E. H., "Structural Response to Earthquakes," Chapter 8 of *Seismic Risk and Engineering Decisions*, C. Lomnitz and E. Rosenblueth, Editors, Elsevier, 1976.

Vasudevan, R., "Equipment Operability Under High-Frequency Excitation", EPRI NP-3946, Electric Power Research Institute, April, 1985.

A

AMPLIFICATION STUDY RESULTS

In order to study the effect of high frequency modes (i.e., greater than 10 Hz) on a structure with a fundamental frequency less than 10 Hz, the horizontal response of a series of fixed-base, uniform cantilever beams was considered. The beams were represented as three types: 1) a flexure beam, in which the deformation is due to bending strain of the cross-section; 2) a shear beam, in which the deformation is due to shearing strain of the cross-section; and 3) a Timoshenko beam, in which the deformation is taken as the sum of bending and shear deformations. Four fundamental frequencies cases of ~ 3 Hz, 5 Hz, 7 Hz, and 9 Hz were chosen for each beam type. An additional frequency case of 6.05 Hz was chosen for the Timoshenko beam to match a representative plant structure. Three base input acceleration time-history motions were selected that are characteristic of motions expected to occur on rock sites similar to those found in the CEUS: 1) Time-History Motion 1, an artificial time-history motion which is compatible with a horizontal design spectrum used in Europe for hard rock sites; 2) Time-History Motion 2, a time-history motion which was developed to match an example design spectrum which is representative of the horizontal spectra for a CEUS rock site; and 3) Time-History Motion 3, an actual earthquake time-history recorded on rock during the 1982 Miramichi, New Brunswick, Ca, aftershock sequence. The response of each beam type and selected fundamental frequency was computed using the modal time history method. Analytic eigenvalue solutions for uniform beams, idealized as continuous elastic bodies, were used to determine the higher mode frequencies, mode shapes, and participation factors. This was done to avoid any numeric discretization error in the idealization of the beams. The solutions are found in the literature as modal frequencies (f_i) and mode shapes (eigenfunctions $\phi_i[x]$), which are determined by the boundary conditions (a vertical cantilever is free at the top and fixed or built-in at the base). Values for modal participation factors for base motion input, Γ_i , are found by suitable normalization and integration of the mode shape functions.

The procedure used to find the spectral amplification functions (ratio of the response of a SDOF oscillator mounted within a structure to the response of the same oscillator mounted on the ground) may be described by the following steps:

1. Given the ground motion acceleration time-history, y_g'' , the relative response acceleration, δ_j'' , is determined for a set of $j = 1, n$ SDOF oscillators with frequency f_j and damping ξ_g . The absolute acceleration of each oscillator is then determined as, $A_{gj} = \delta_j'' + y_g''$, and the spectral acceleration associated with each frequency, f_j , is found as $SA_{gj} = \text{Max}|A_{gj}|$. The plot of SA_{gj} versus f_j is defined as the ground response spectrum for damping ξ_g .
2. Next, also using the ground motion acceleration time-history, y_g'' , the relative response acceleration, δ_i'' , is determined for a set of $i = 1, m$ SDOF oscillators with beam mode frequency f_i and damping ξ_i . The absolute acceleration of each structure mode oscillator is then determined as, $A_i = \delta_i'' + y_g''$.

3. Then, given each mode shape value, $\phi_i(x)$, and participation factor value, Γ_i , the absolute acceleration of each beam position x is found by the linear combination of structure mode response as, $A_x = \sum_1^m \Gamma_i \phi_i(x) A_i + [1 - \sum_1^m \Gamma_i \phi_i(x)] y_g$.
4. Now, given A_x , the relative response acceleration, z_{xj} , is determined for the same set of $j = 1, n$ SDOF oscillators with frequency f_j and damping ξ_g used for determination of the ground response spectrum. The absolute acceleration of each in-structure oscillator is then determined as, $A_{z_{xj}} = z_{xj} + A_x$, and the in-structure spectral acceleration associated with each frequency, f_j , is found as $SA_{z_{xj}} = \text{Max}|A_{z_{xj}}|$. The plot of $SA_{z_{xj}}$ versus f_j is defined as the in-structure response spectrum for position x and for damping ξ_g .
5. The spectral amplification factor for position x is defined as the ratio of the in-structure response spectrum for position x divided by the ground response spectrum, or $AF_x(f_j) = SA_{z_{xj}}/SA_{g_j}$.

For each beam type and selected fundamental frequency, all modes up to 100 Hz were considered. A summary of the fundamental frequencies selected and resulting mode frequencies used for each beam type are provided in Chapter 5. The spectral amplification, as defined by steps 1-5 above, was computed for each beam type and fundamental frequency, for 10 positions ranging from $x/L=0.2$ to $x/L=0.9$. This range of positions should encompass at least 98% of all in-structure equipment locations within a plant. All structure modes, were assumed to have $\xi_i = 7\%$ structural damping with both the ground and in-structure spectra having default damping values of $\xi_g = 5\%$.

This Appendix presents the amplification functions for each selected beam type, fundamental frequency, and input motion. Overall, the study resulted in 39 separate sets of amplification functions (3 beam types, 4 fundamental frequencies, 3 input time histories plus three additional cases). Plots A-1 thru A-39 show the spectral amplification functions for each beam, as a function of both frequency and position, which were determined using each selected time-history input motion.

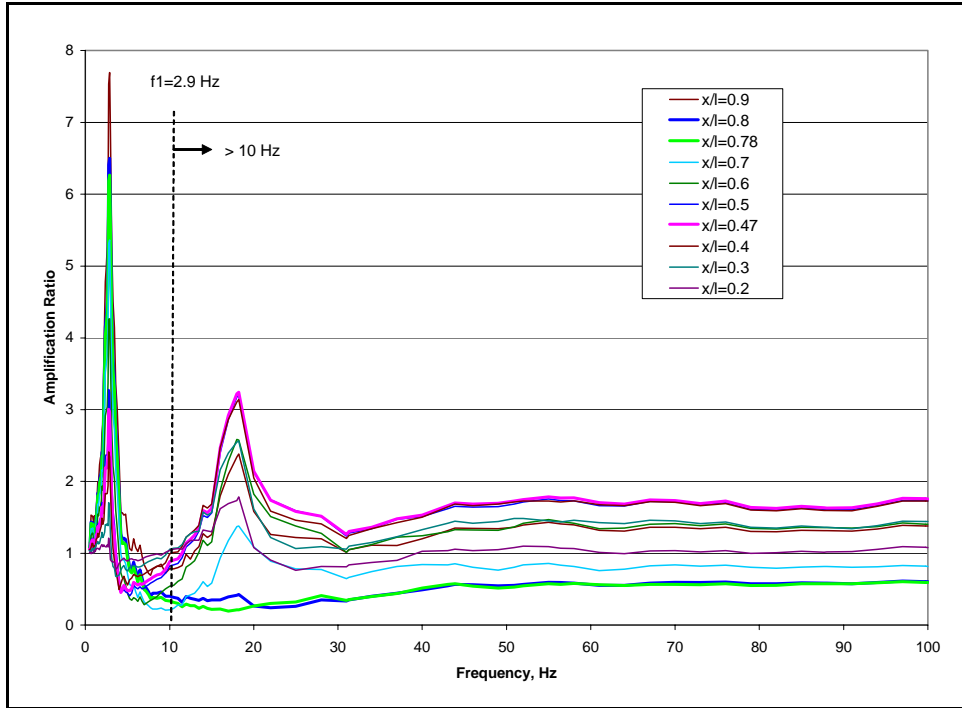


Figure A-1
Comparison of Spectral Amplification for Flexure Beam with $f_1 = 3$ Hz Fundamental Frequency with Time History 1 Input Motion

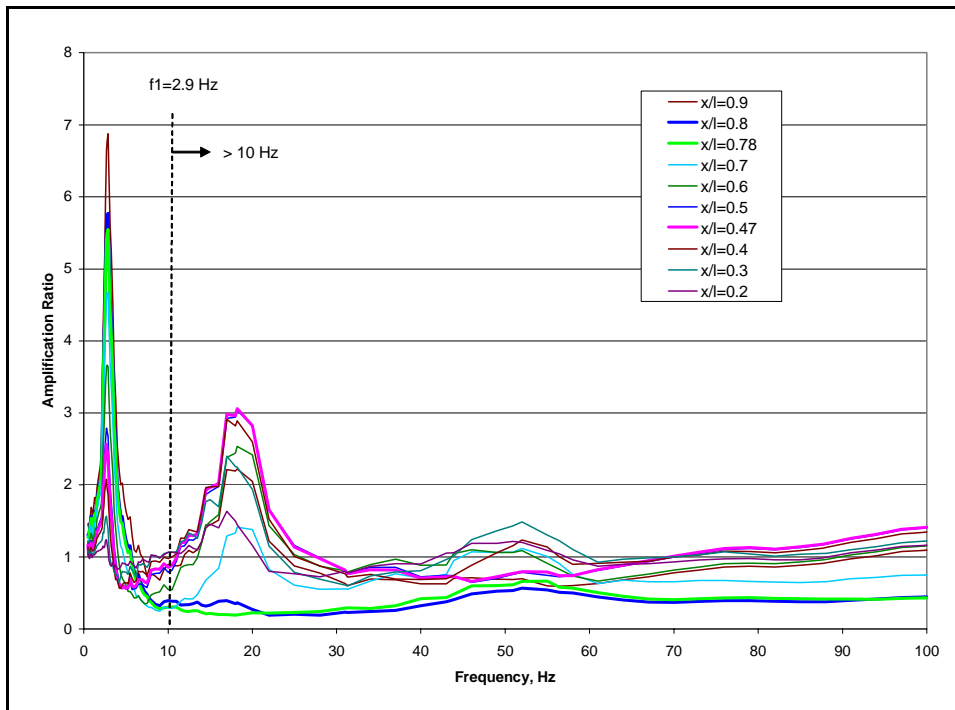


Figure A-2
Comparison of Spectral Amplification for Flexure Beam with $f_1 = 3$ Hz Fundamental Frequency with Time History 2 Input Motion

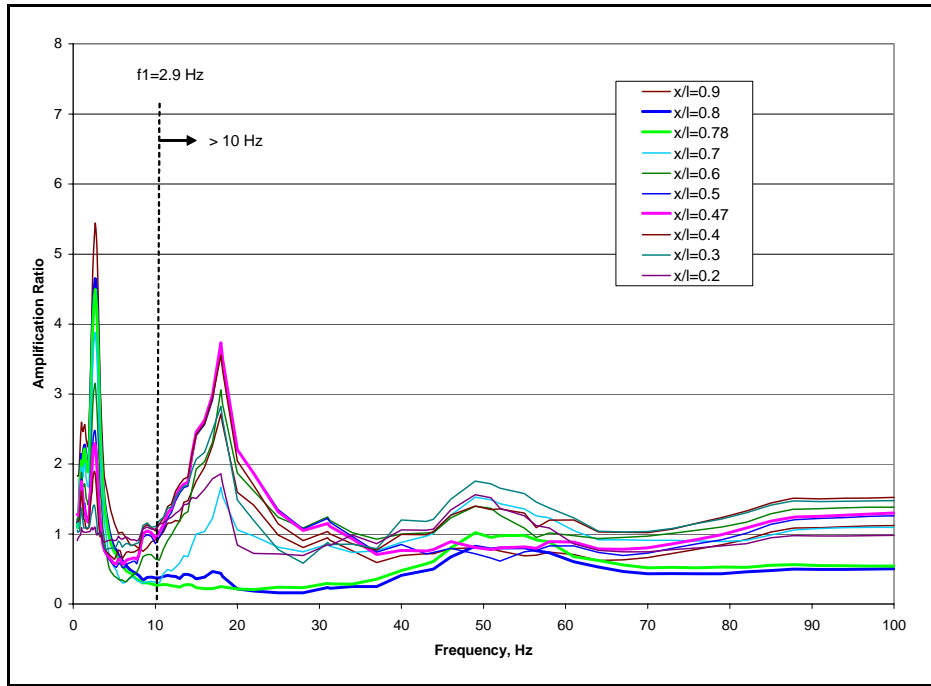


Figure A-3
Comparison of Spectral Amplification for Flexure Beam with $f_1 = 3$ Hz Fundamental Frequency with Time History 3 Input Motion

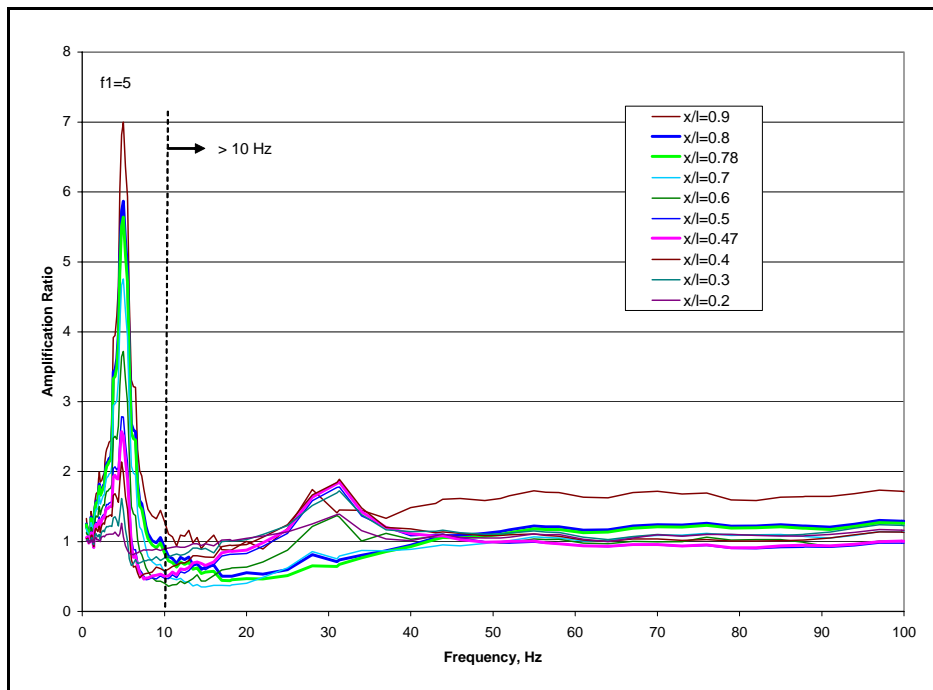


Figure A-4
Comparison of Spectral Amplification for Flexure Beam with $f_1 = 5$ Hz Fundamental Frequency with Time History 1 Input Motion

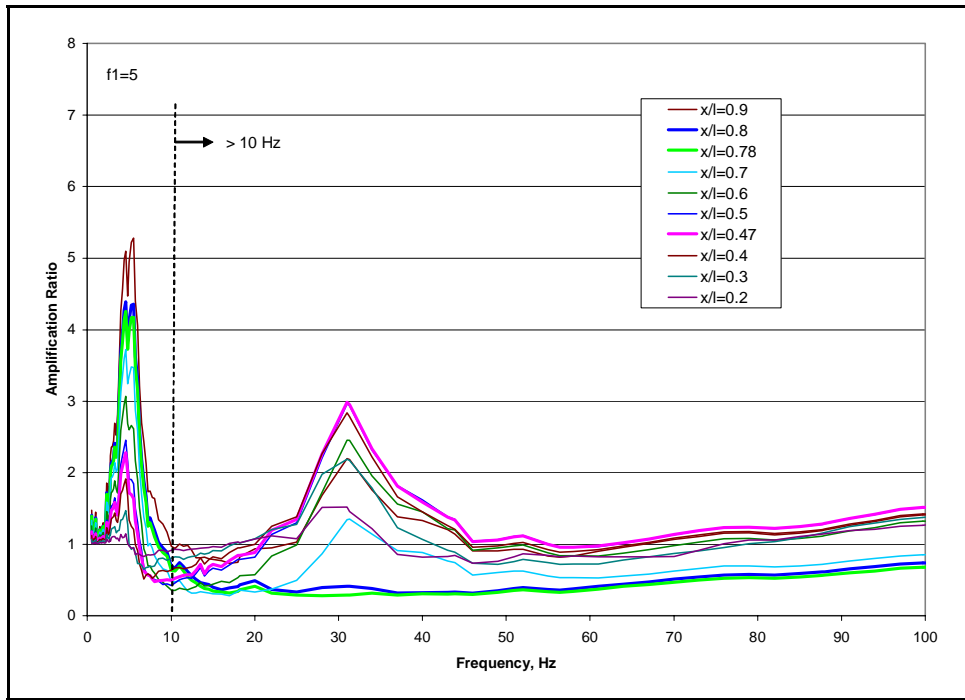


Figure A-5
Comparison of Spectral Amplification for Flexure Beam with $f_1 = 5$ Hz Fundamental Frequency with Time History 2 Input Motion

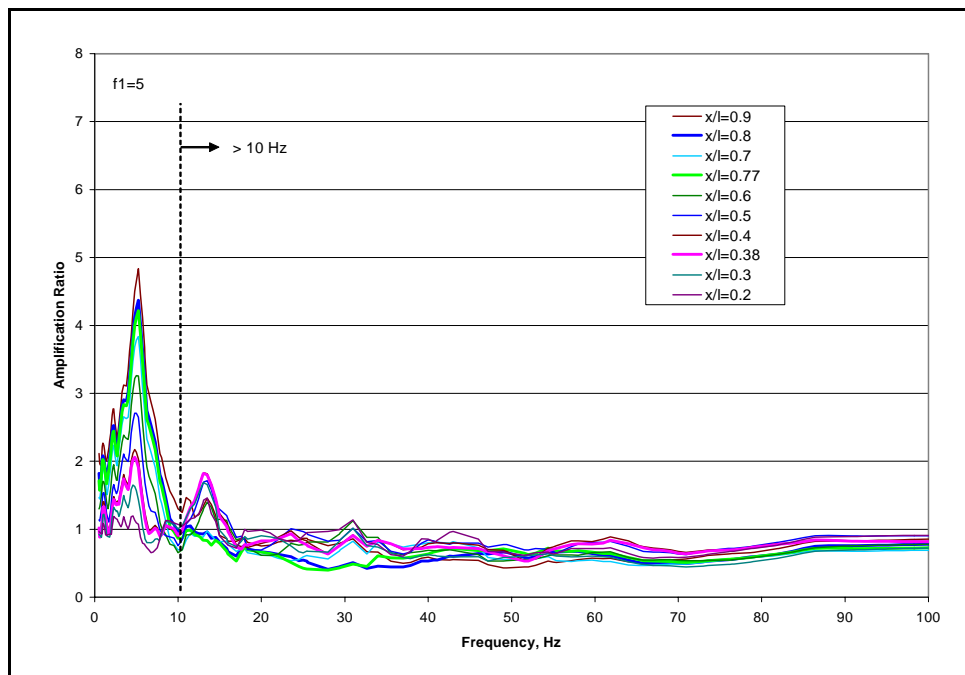


Figure A-6
Comparison of Spectral Amplification for Flexure Beam with $f_1 = 5$ Hz Fundamental Frequency with Time History 3 Input Motion

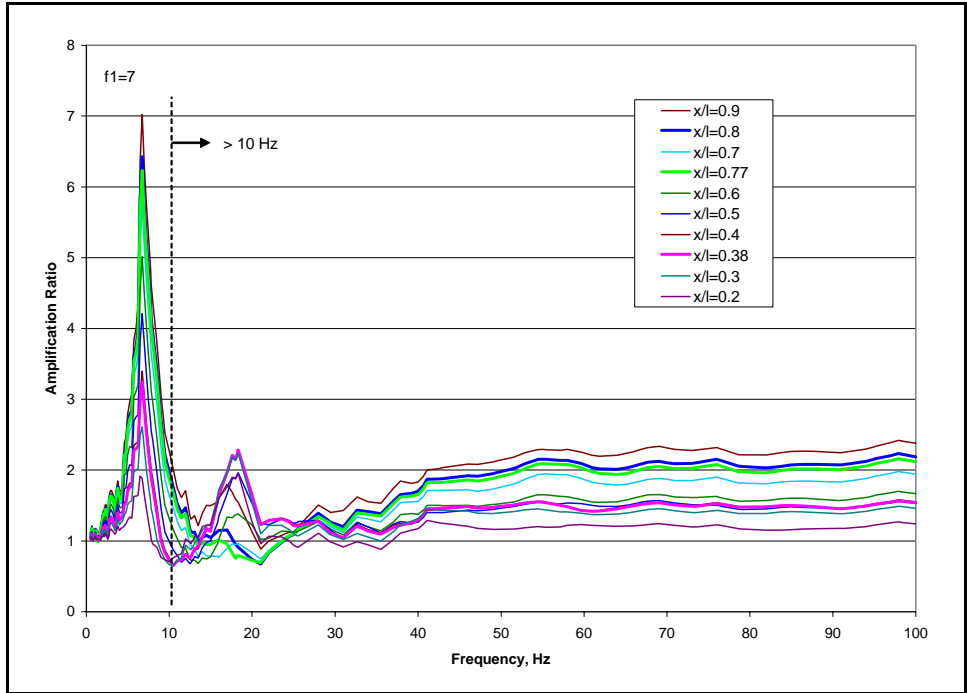


Figure A-7
Comparison of Spectral Amplification for Flexure Beam with $f_1 = 7$ Hz Fundamental Frequency with Time History 1 Input Motion

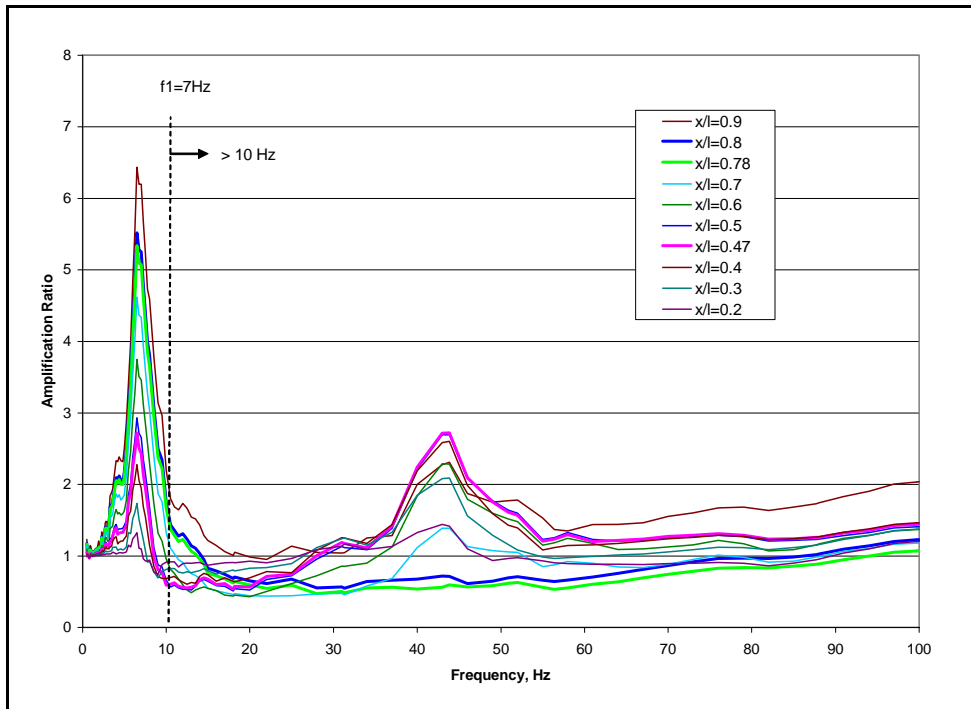


Figure A-8
Comparison of Spectral Amplification for Flexure Beam with $f_1 = 7$ Hz Fundamental Frequency with Time History 2 Input Motion

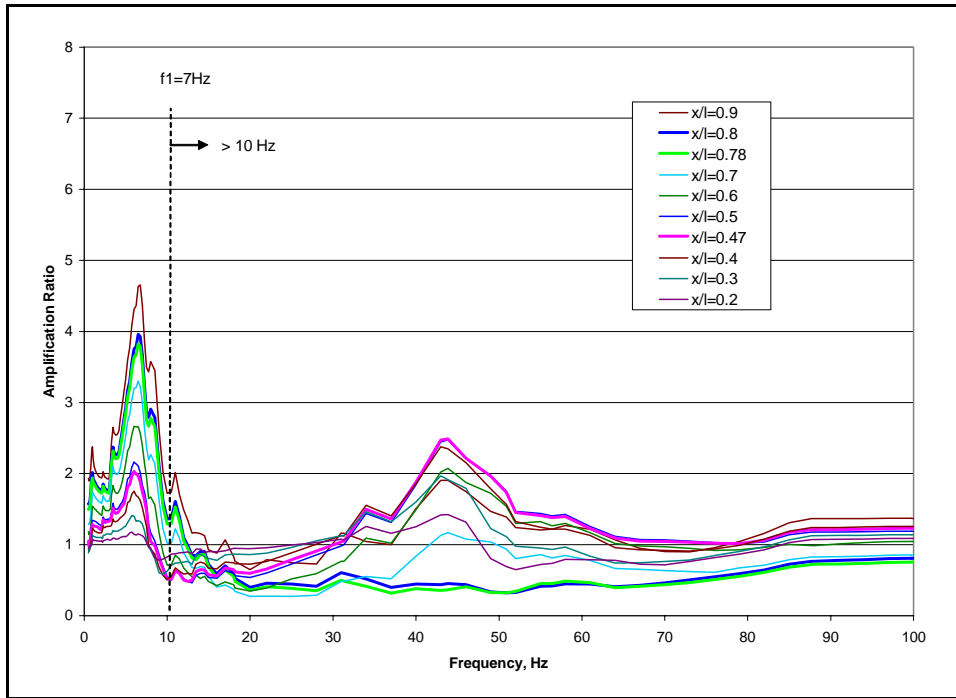


Figure A-9
Comparison of Spectral Amplification for Flexure Beam with $f_1 = 7$ Hz Fundamental Frequency with Time History 3 Input Motion

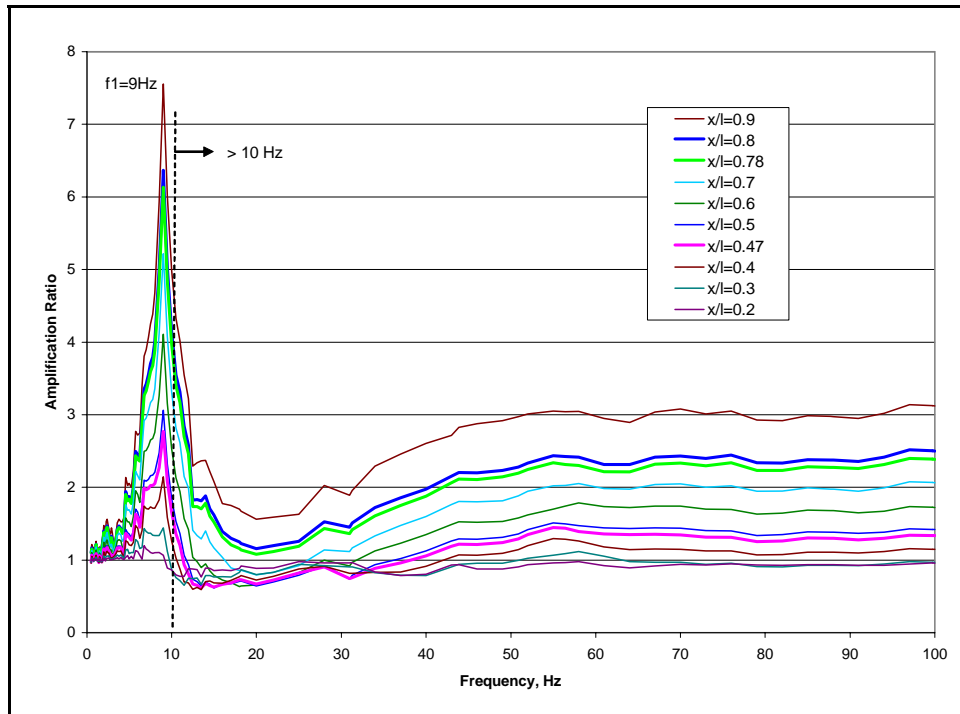


Figure A-10
Comparison of Spectral Amplification for Flexure Beam with $f_1 = 9$ Hz Fundamental Frequency with Time History 1 Input Motion

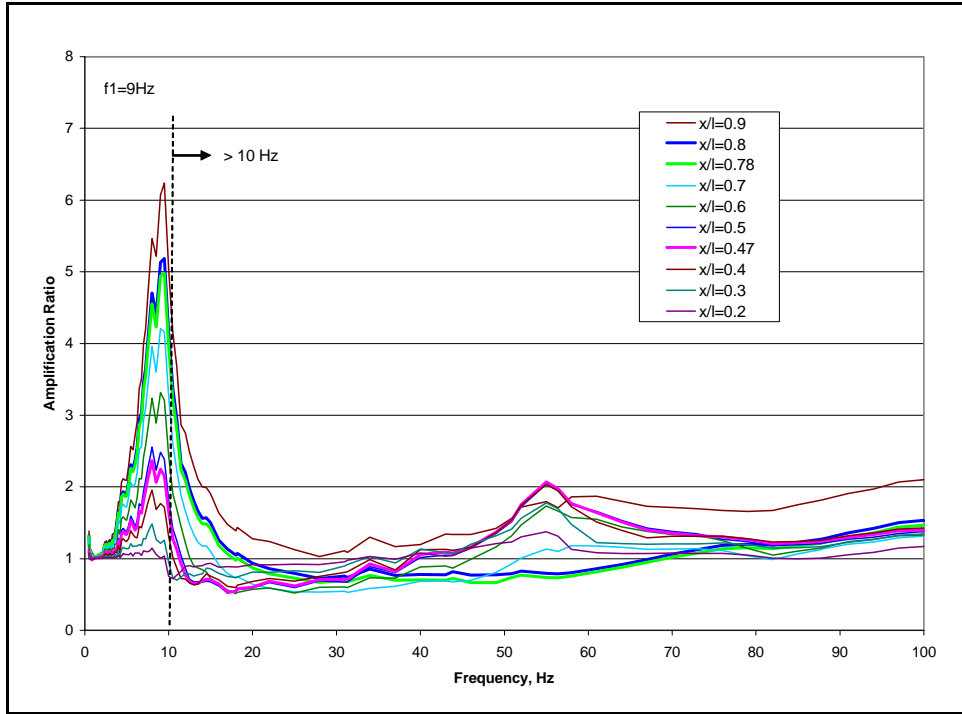


Figure A-11
Comparison of Spectral Amplification for Flexure Beam with $f_1 = 9$ Hz Fundamental Frequency with Time History 2 Input Motion

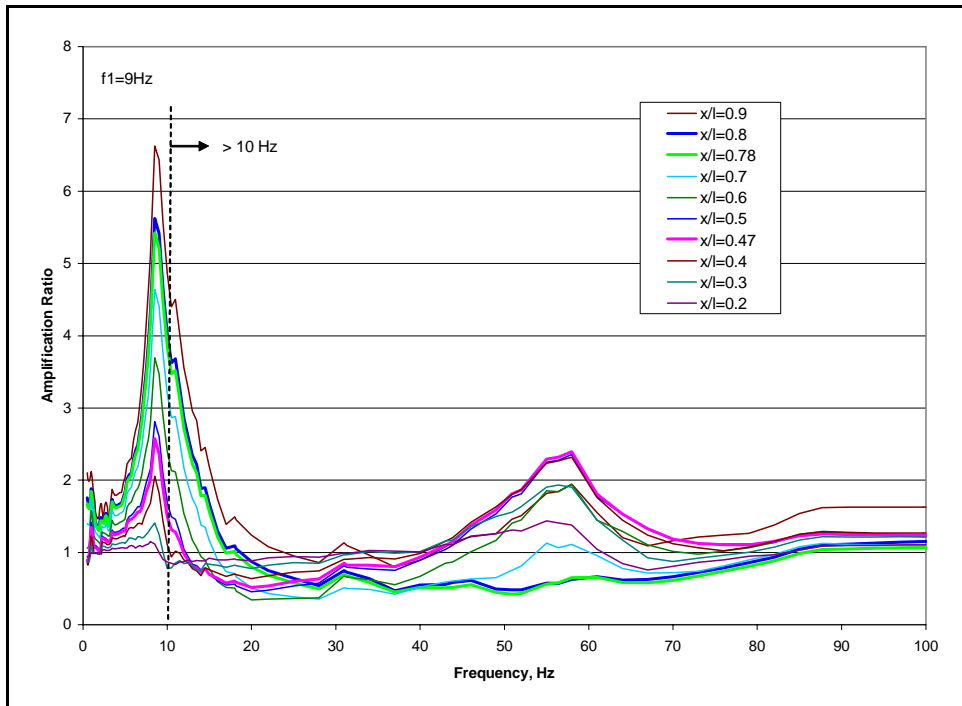


Figure A-12
Comparison of Spectral Amplification for Flexure Beam with $f_1 = 9$ Hz Fundamental Frequency with Time History 3 Input Motion

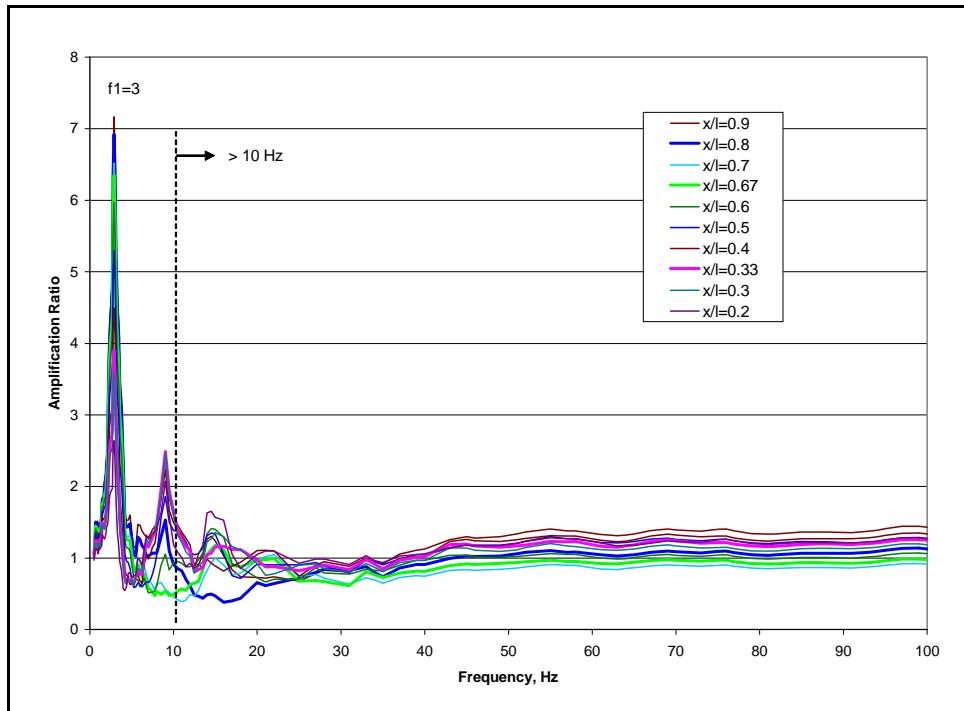


Figure A-13
Comparison of Spectral Amplification for Shear Beam with $f_1 = 3$ Hz Fundamental Frequency with Time History 1 Input Motion

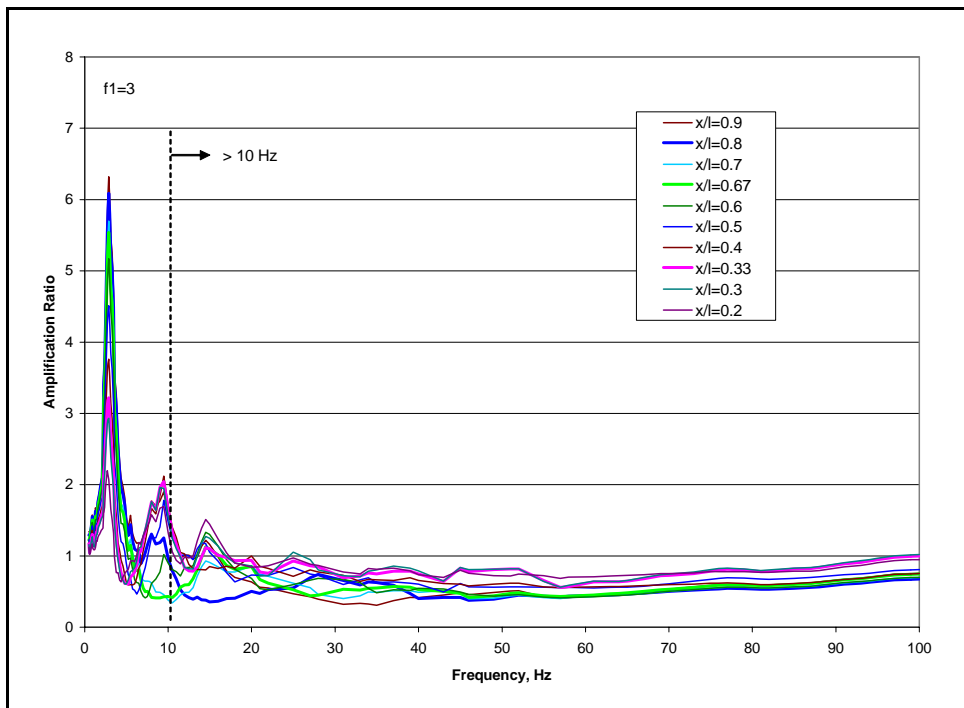


Figure A-14
Comparison of Spectral Amplification for Shear Beam with $f_1 = 3$ Hz Fundamental Frequency with Time History 2 Input Motion

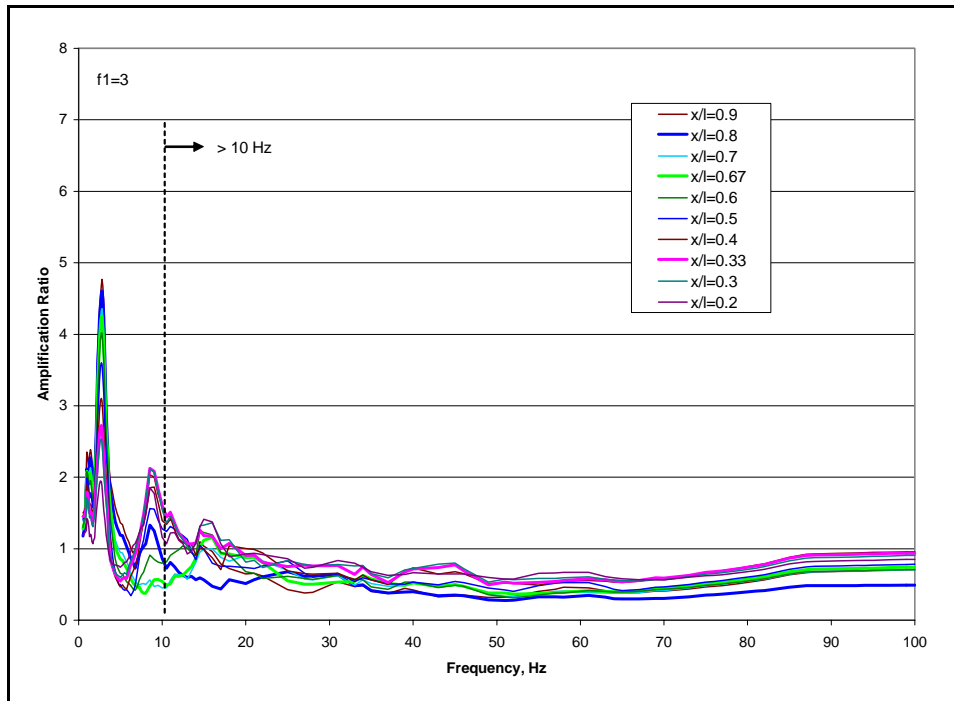


Figure A-15
Comparison of Spectral Amplification for Shear Beam with $f_1 = 3$ Hz Fundamental Frequency with Time History 3 Input Motion

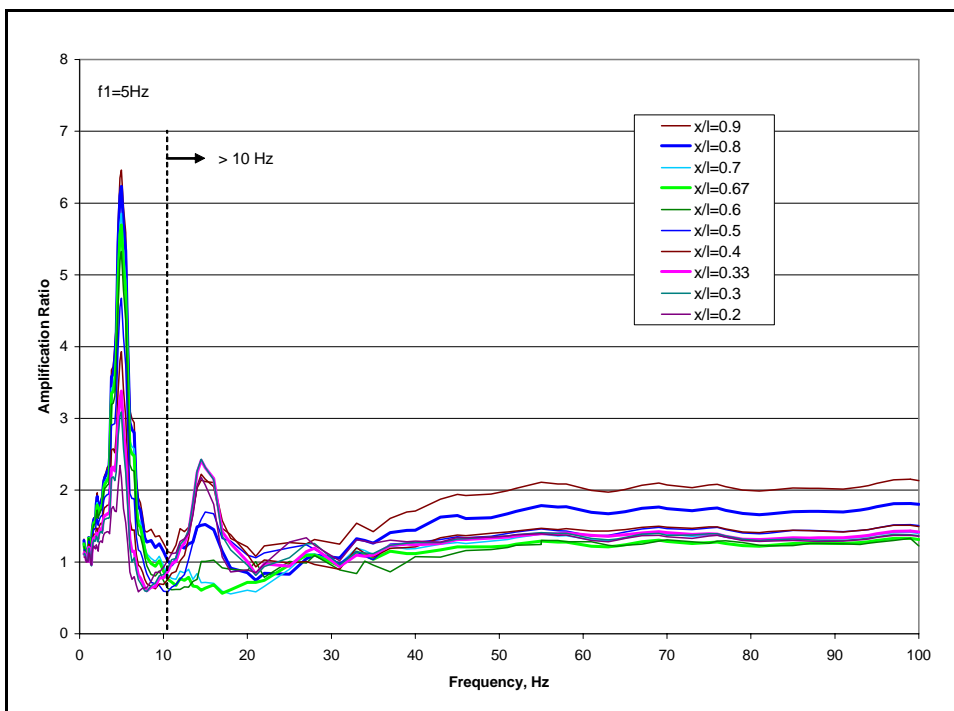


Figure A-16
Comparison of Spectral Amplification for Shear Beam with $f_1 = 5$ Hz Fundamental Frequency with Time History 1 Input Motion

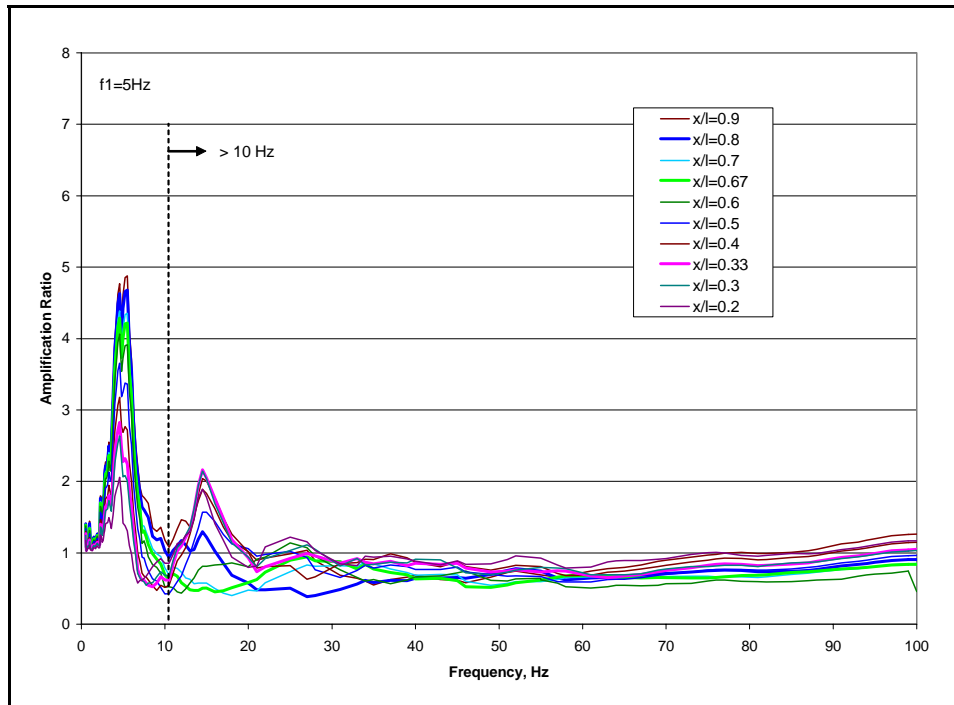


Figure A-17
Comparison of Spectral Amplification for Shear Beam with $f_1 = 5$ Hz Fundamental Frequency with Time History 2 Input Motion

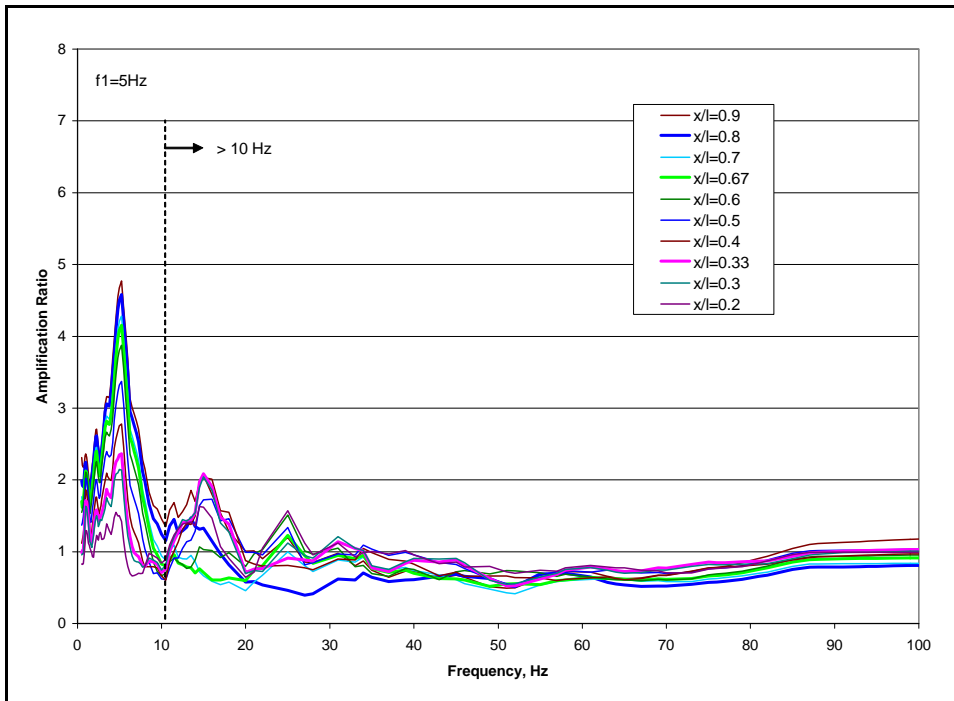


Figure A-18
Comparison of Spectral Amplification for Shear Beam with $f_1 = 5$ Hz Fundamental Frequency with Time History 3 Input Motion

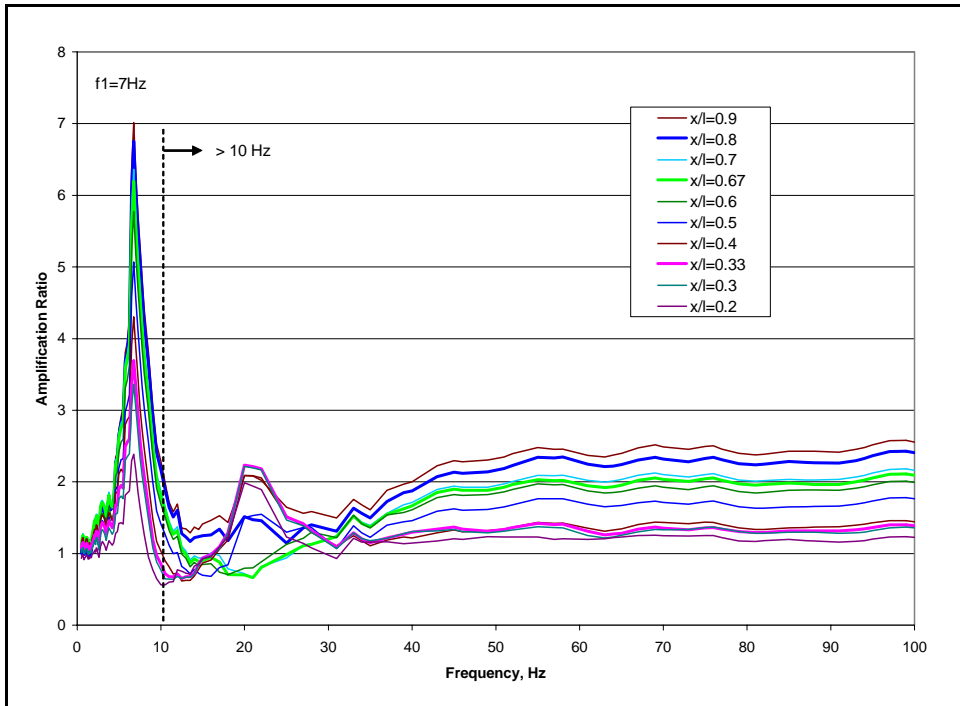


Figure A-19
Comparison of Spectral Amplification for Shear Beam with $f_1 = 7$ Hz Fundamental Frequency with Time History 1 Input Motion

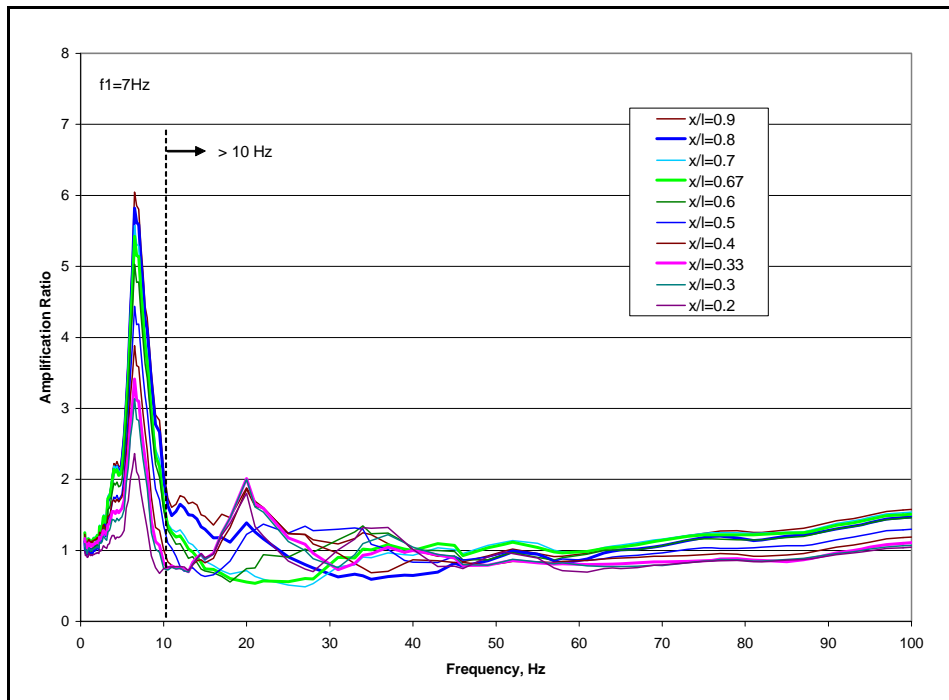


Figure A-20
Comparison of Spectral Amplification for Shear Beam with $f_1 = 7$ Hz Fundamental Frequency with Time History 2 Input Motion

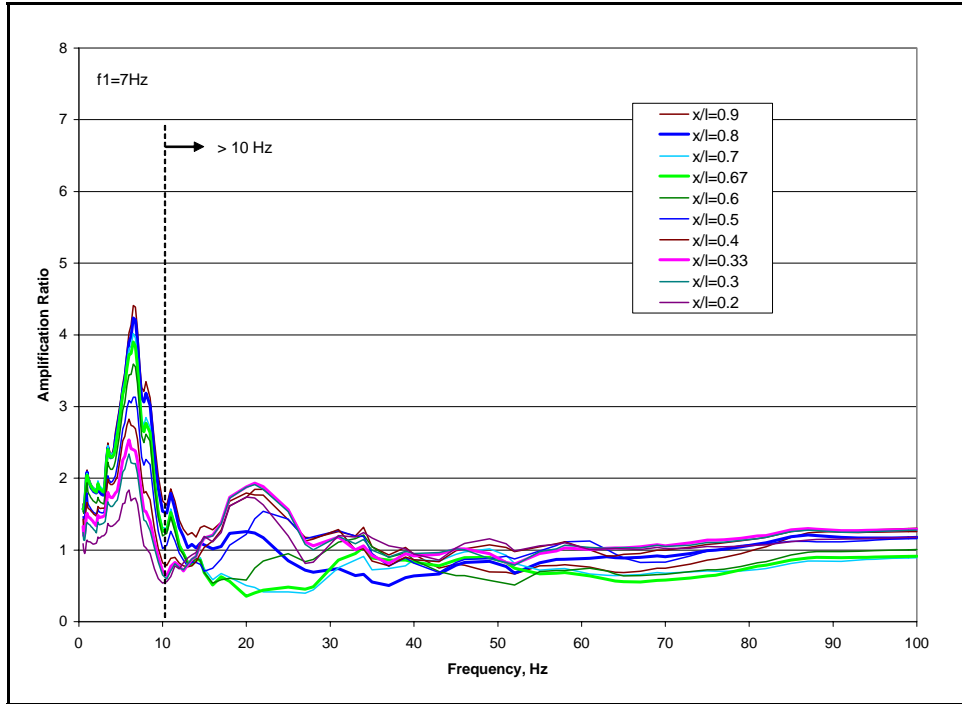


Figure A-21
Comparison of Spectral Amplification for Shear Beam with $f_1 = 7$ Hz Fundamental Frequency with Time History 3 Input Motion

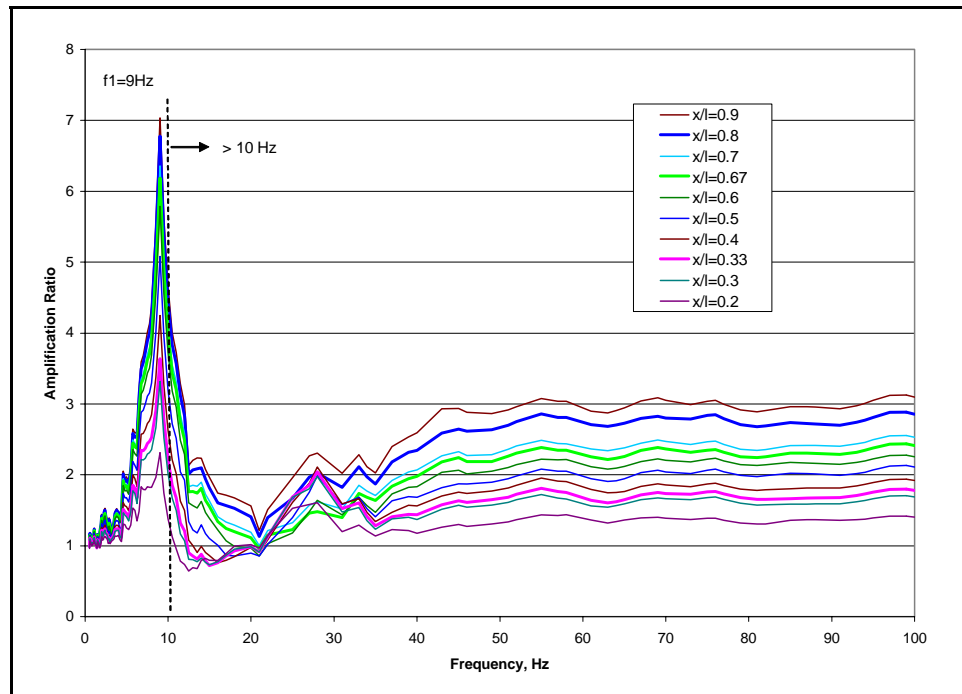


Figure A-22
Comparison of Spectral Amplification for Shear Beam with $f_1 = 9$ Hz Fundamental Frequency with Time History 1 Input Motion

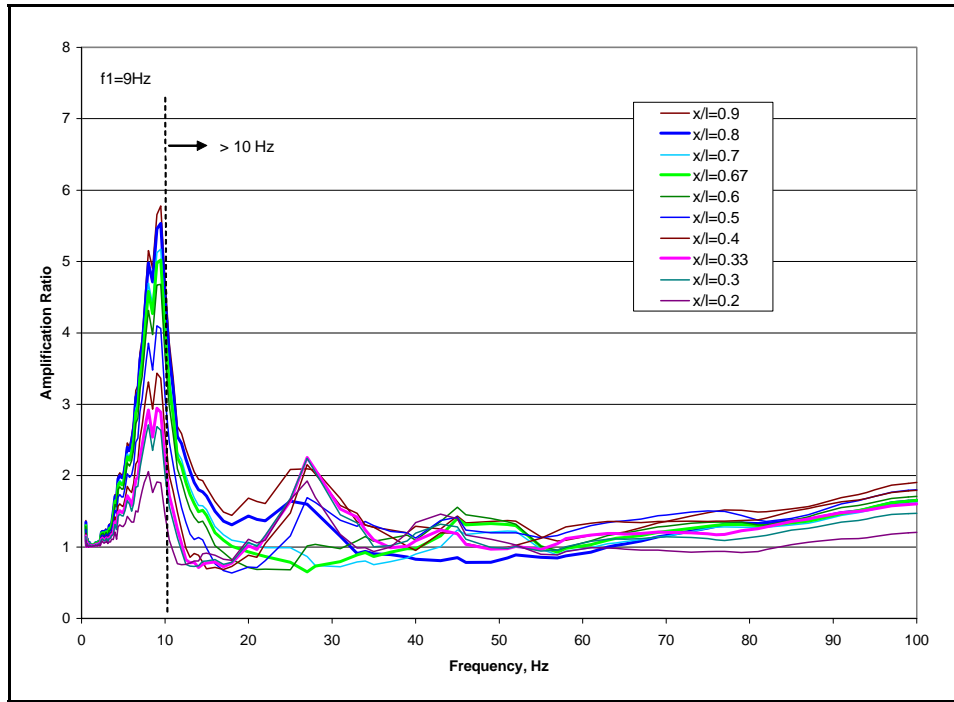


Figure A-23
Comparison of Spectral Amplification for Shear Beam with $f_1 = 9$ Hz Fundamental Frequency with Time History 2 Input Motion

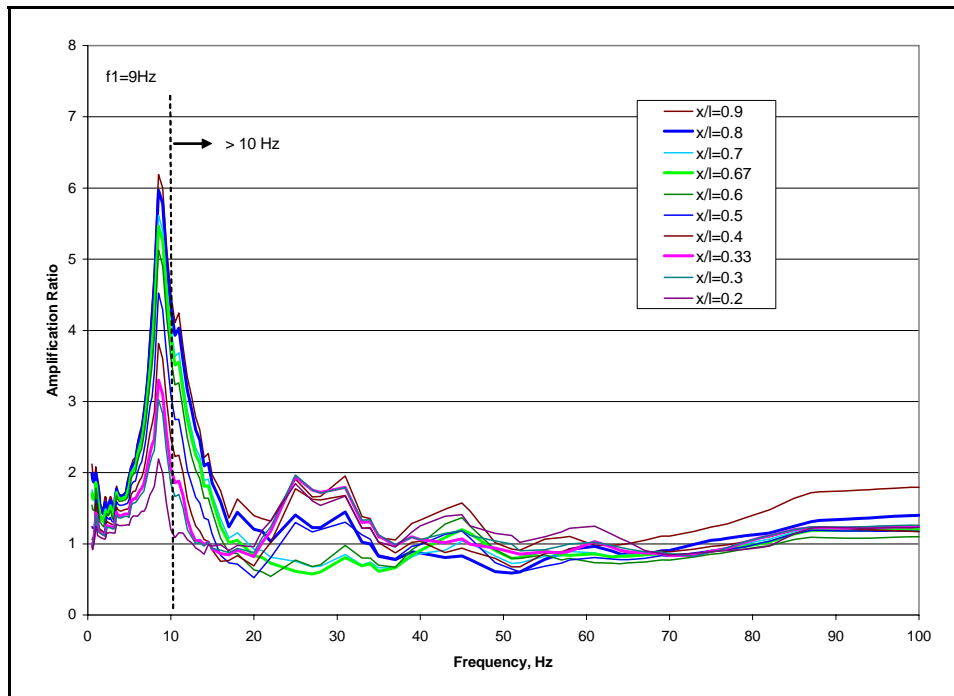


Figure A-24
Comparison of Spectral Amplification for Shear Beam with $f_1 = 9$ Hz Fundamental Frequency with Time History 3 Input Motion

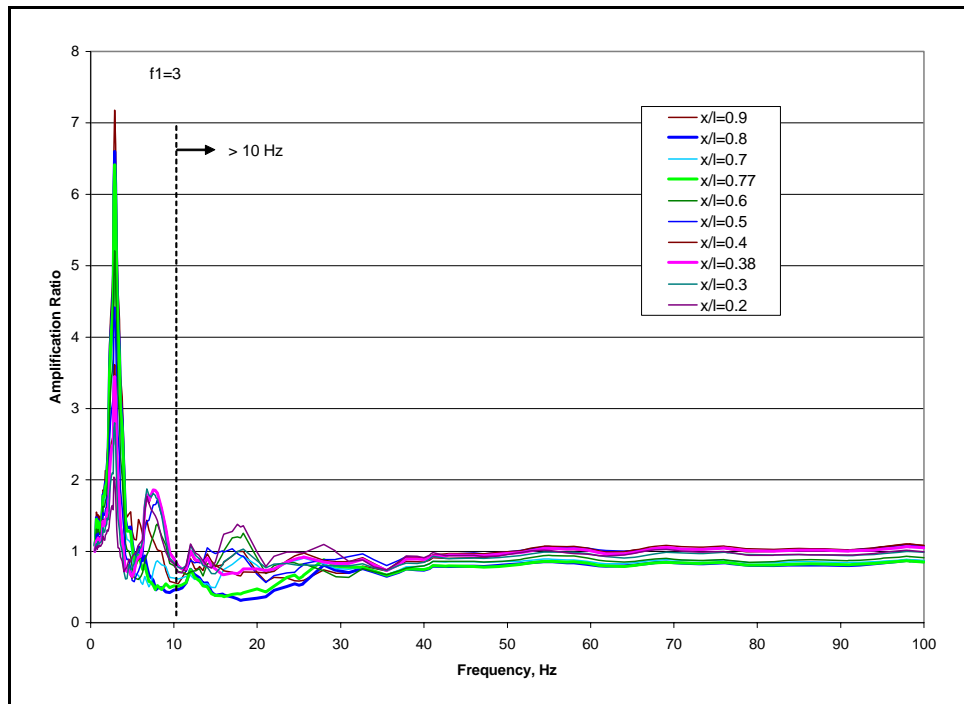


Figure A-25
Comparison of Spectral Amplification for Timoshenko Beam with $f_1 = 3$ Hz Fundamental Frequency with Time History 1 Input Motion

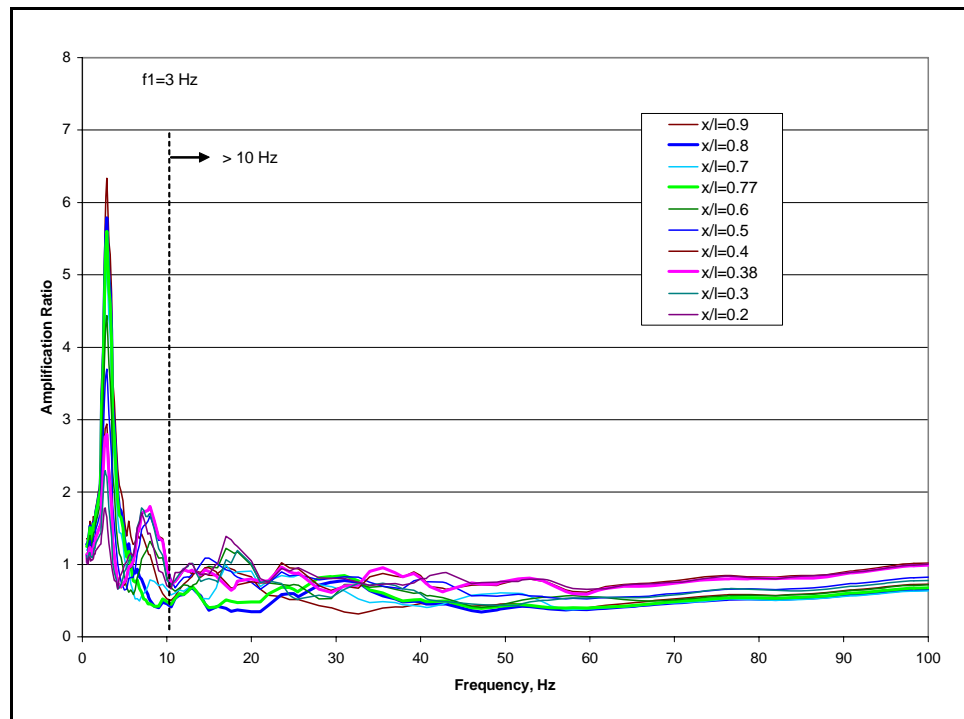


Figure A-26
Comparison of Spectral Amplification for Timoshenko Beam with $f_1 = 3$ Hz Fundamental Frequency with Time History 2 Input Motion

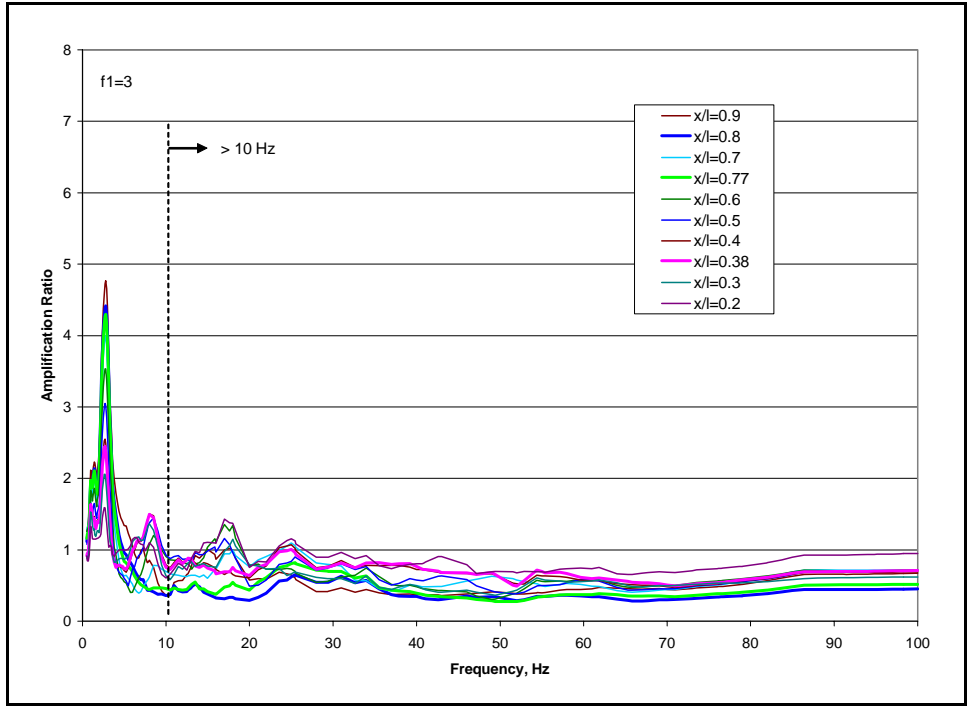


Figure A-27
Comparison of Spectral Amplification for Timoshenko Beam with $f_1 = 3$ Hz Fundamental Frequency with Time History 3 Input Motion

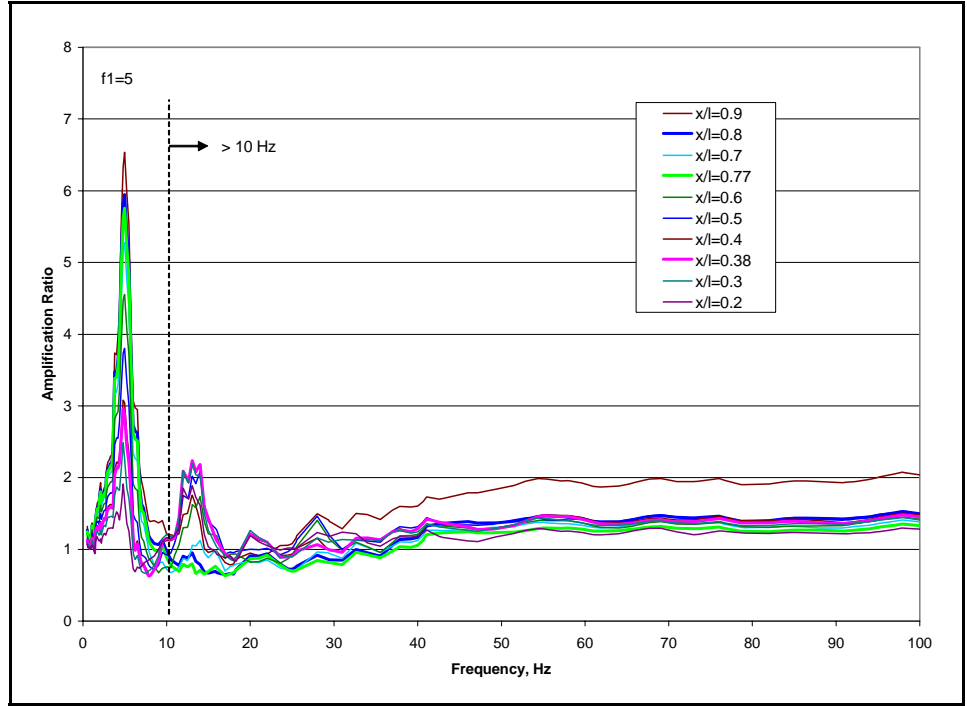


Figure A-28
Comparison of Spectral Amplification for Timoshenko Beam with $f_1 = 5$ Hz Fundamental Frequency with Time History 1 Input Motion

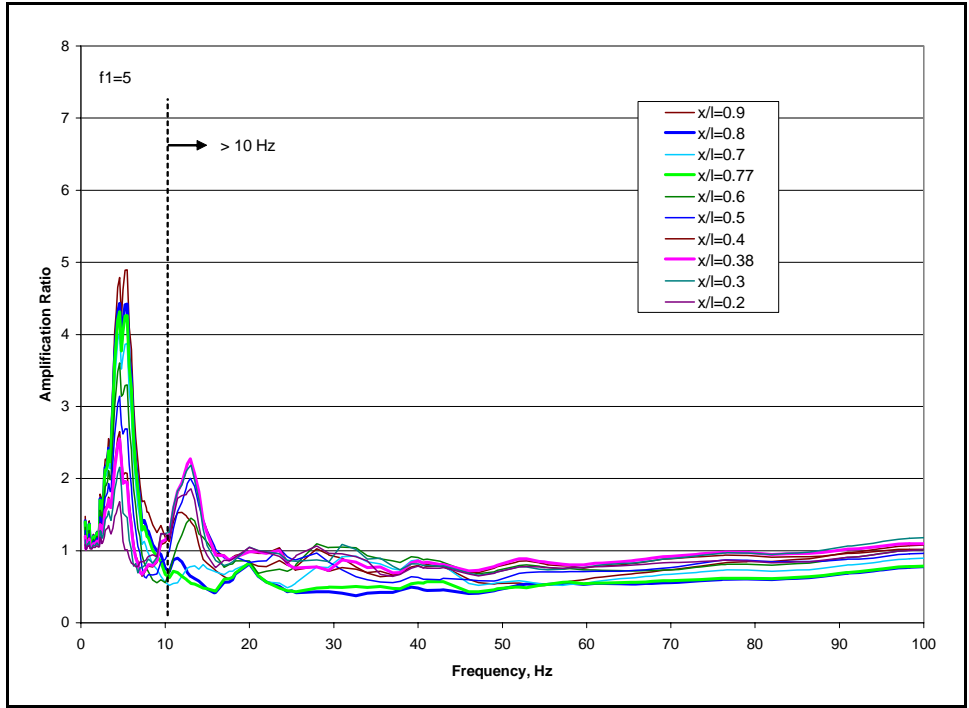


Figure A-29
Comparison of Spectral Amplification for Timoshenko Beam with $f_1 = 5$ Hz Fundamental Frequency with Time History 2 Input Motion

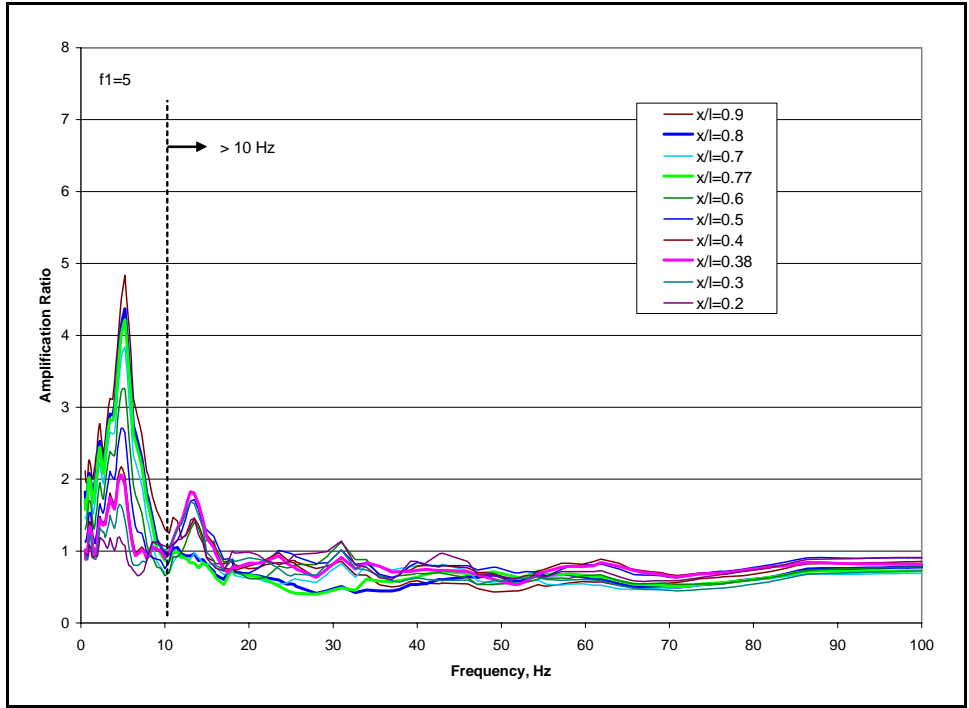


Figure A-30
Comparison of Spectral Amplification for Timoshenko Beam with $f_1 = 5$ Hz Fundamental Frequency with Time History 3 Input Motion

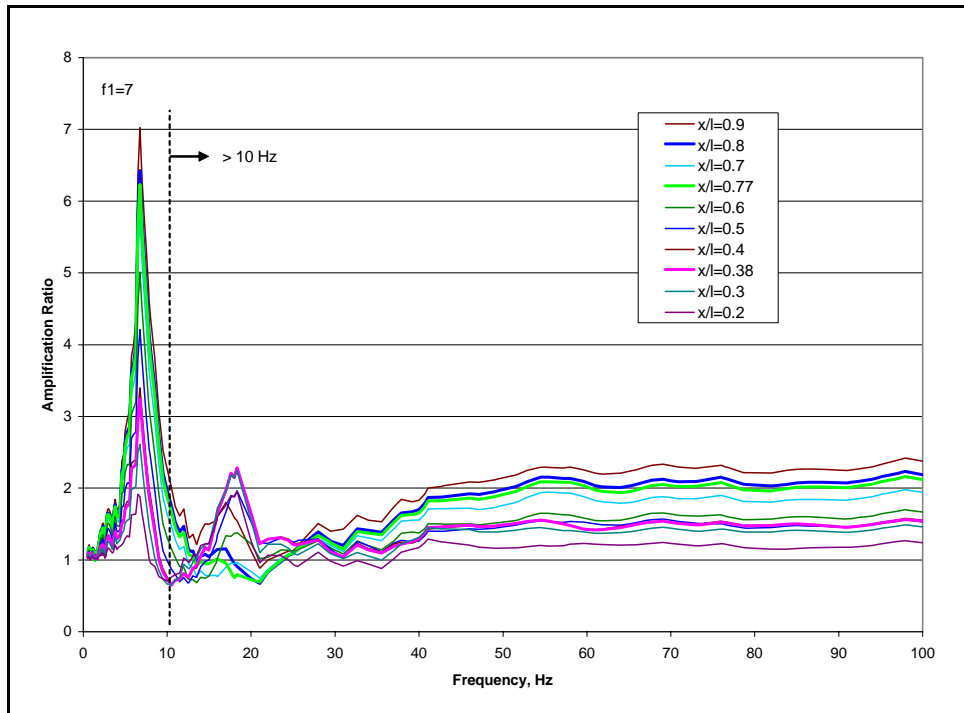


Figure A-31
Comparison of Spectral Amplification for Timoshenko Beam with $f_1 = 7$ Hz Fundamental Frequency with Time History 1 Input Motion

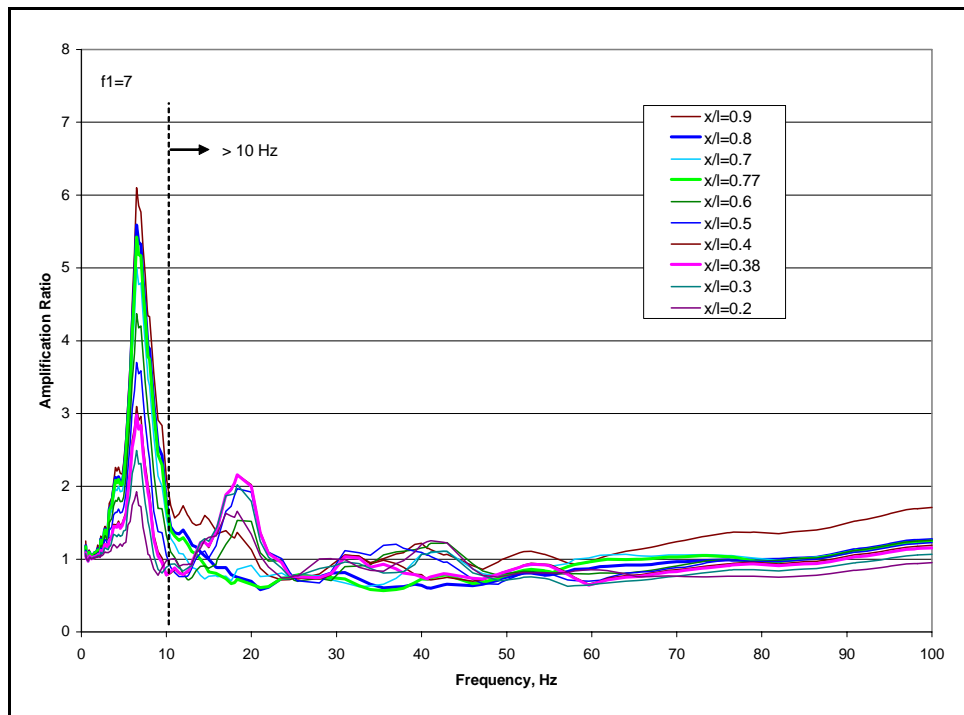


Figure A-32
Comparison of Spectral Amplification for Timoshenko Beam with $f_1 = 7$ Hz Fundamental Frequency with Time History 2 Input Motion

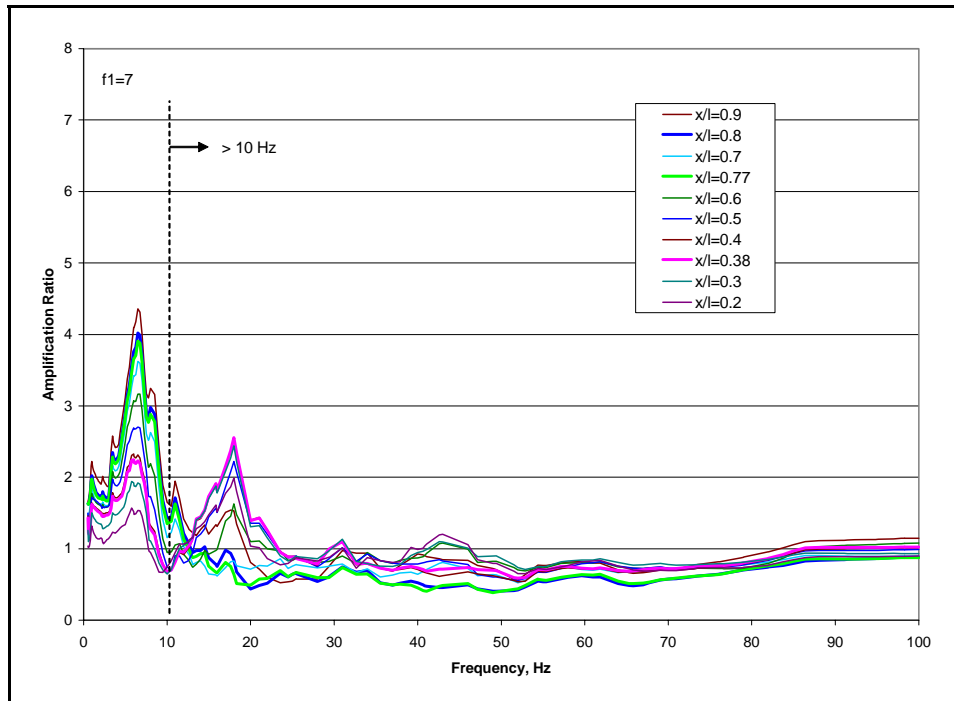


Figure A-33
Comparison of Spectral Amplification for Timoshenko Beam with $f_1 = 7$ Hz Fundamental Frequency with Time History 3 Input Motion

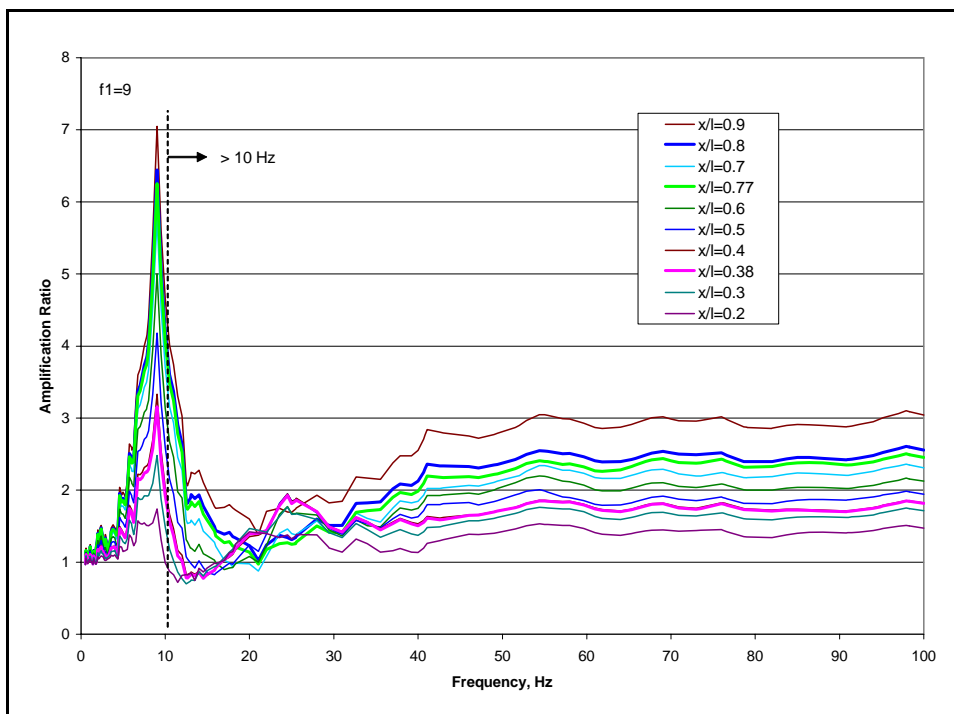


Figure A-34
Comparison of Spectral Amplification for Timoshenko Beam with $f_1 = 9$ Hz Fundamental Frequency with Time History 1 Input Motion

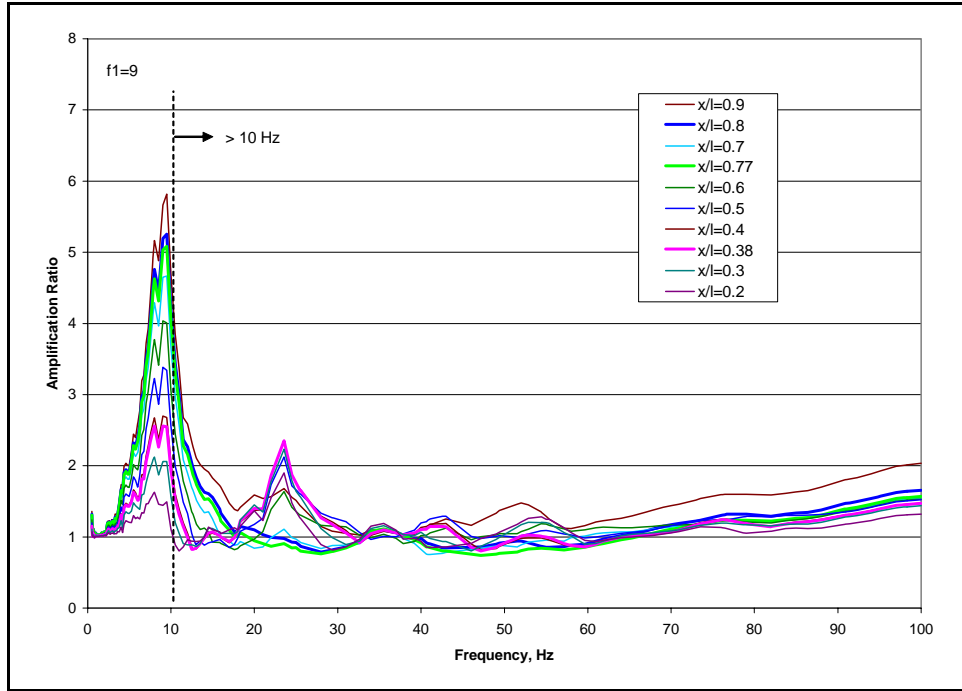


Figure A-35
Comparison of Spectral Amplification for Timoshenko Beam with $f_1 = 9$ Hz Fundamental Frequency with Time History 2 Input Motion

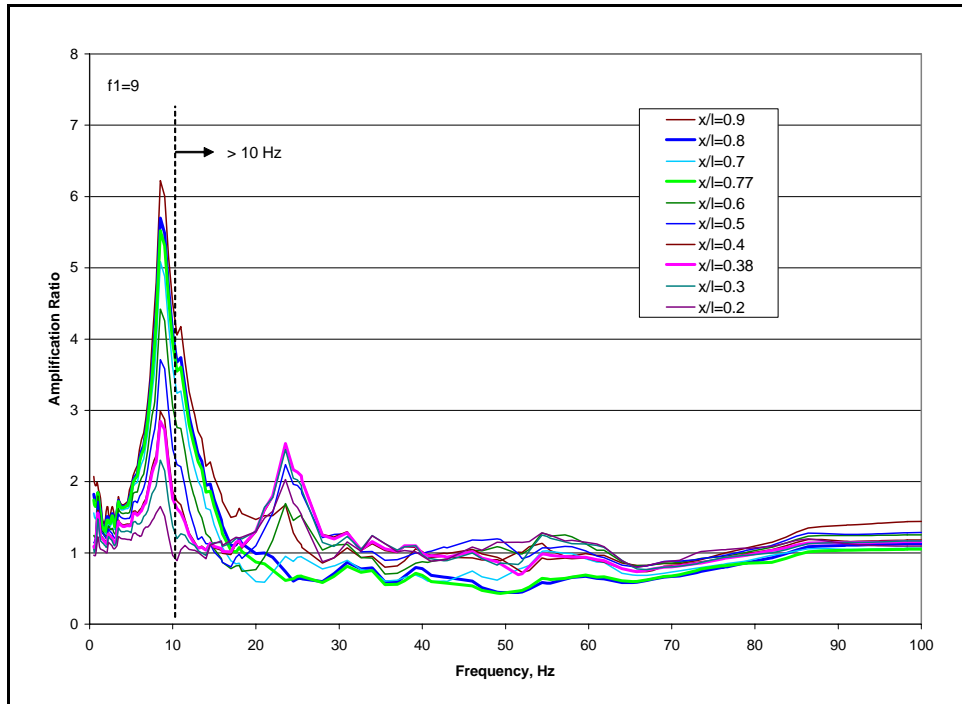


Figure A-36
Comparison of Spectral Amplification for Timoshenko Beam with $f_1 = 9$ Hz Fundamental Frequency with Time History 3 Input Motion

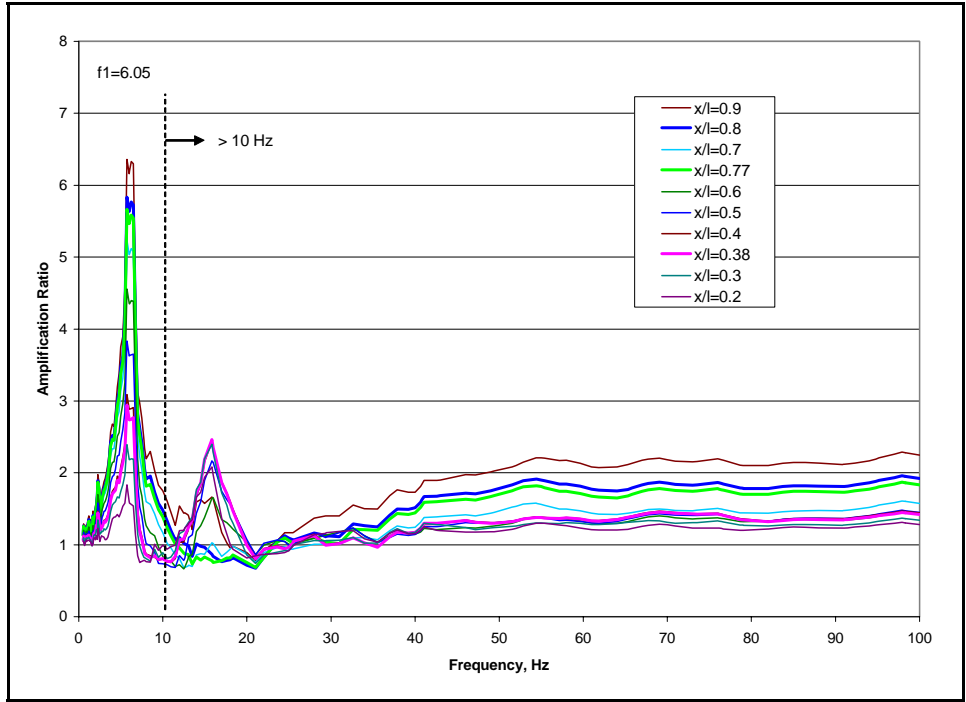


Figure A-37
Comparison of Spectral Amplification for Timoshenko Beam with $f_1 = 6.05$ Hz Fundamental Frequency with Time History 1 Input Motion

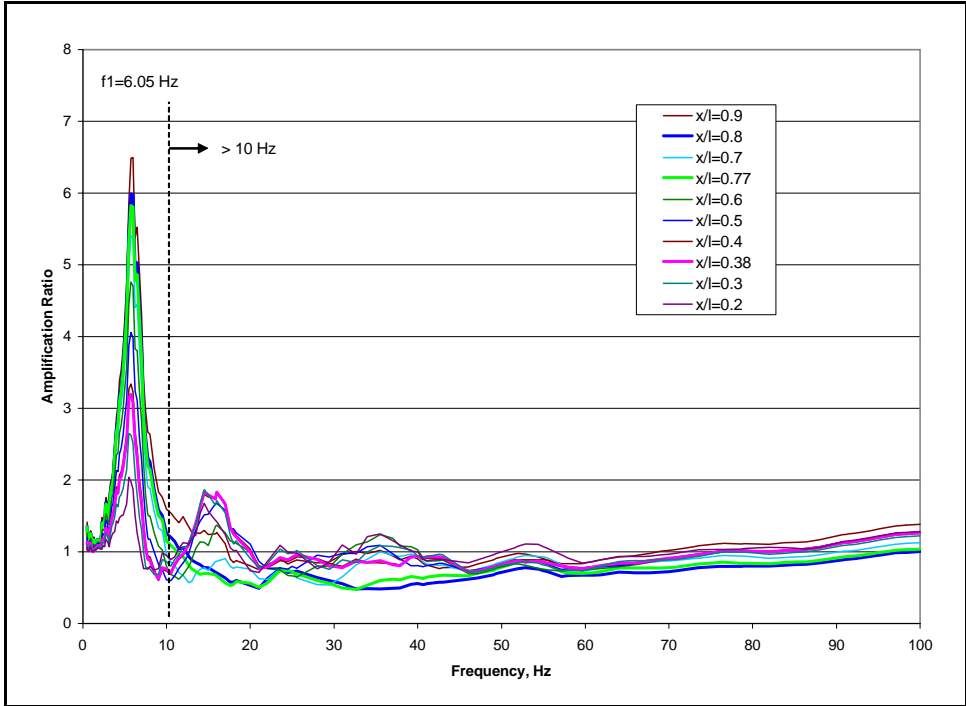


Figure A-38
Comparison of Spectral Amplification for Timoshenko Beam with $f_1 = 6.05$ Hz Fundamental Frequency with Time History 2 Input Motion

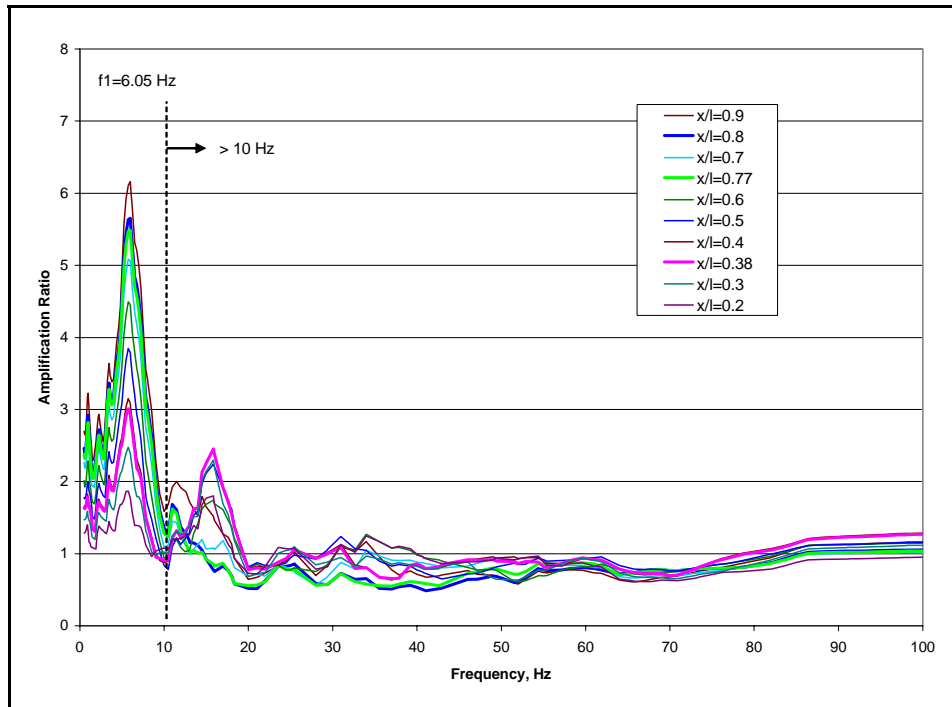


Figure A-39
Comparison of Spectral Amplification for Timoshenko Beam with $f_1 = 6.05$ Hz Fundamental Frequency with Time History 3 Input Motion

Export Control Restrictions

Access to and use of EPRI Intellectual Property is granted with the specific understanding and requirement that responsibility for ensuring full compliance with all applicable U.S. and foreign export laws and regulations is being undertaken by you and your company. This includes an obligation to ensure that any individual receiving access hereunder who is not a U.S. citizen or permanent U.S. resident is permitted access under applicable U.S. and foreign export laws and regulations. In the event you are uncertain whether you or your company may lawfully obtain access to this EPRI Intellectual Property, you acknowledge that it is your obligation to consult with your company's legal counsel to determine whether this access is lawful. Although EPRI may make available on a case-by-case basis an informal assessment of the applicable U.S. export classification for specific EPRI Intellectual Property, you and your company acknowledge that this assessment is solely for informational purposes and not for reliance purposes. You and your company acknowledge that it is still the obligation of you and your company to make your own assessment of the applicable U.S. export classification and ensure compliance accordingly. You and your company understand and acknowledge your obligations to make a prompt report to EPRI and the appropriate authorities regarding any access to or use of EPRI Intellectual Property hereunder that may be in violation of applicable U.S. or foreign export laws or regulations.

The Electric Power Research Institute (EPRI)

The Electric Power Research Institute (EPRI), with major locations in Palo Alto, California, and Charlotte, North Carolina, was established in 1973 as an independent, nonprofit center for public interest energy and environmental research. EPRI brings together members, participants, the Institute's scientists and engineers, and other leading experts to work collaboratively on solutions to the challenges of electric power. These solutions span nearly every area of electricity generation, delivery, and use, including health, safety, and environment. EPRI's members represent over 90% of the electricity generated in the United States. International participation represents nearly 15% of EPRI's total research, development, and demonstration program.

Together...Shaping the Future of Electricity

© 2005 Electric Power Research Institute (EPRI), Inc. All rights reserved. Electric Power Research Institute and EPRI are registered service marks of the Electric Power Research Institute, Inc.

 Printed on recycled paper in the United States of America

1012967

ELECTRIC POWER RESEARCH INSTITUTE

3420 Hillview Avenue, Palo Alto, California 94304-1395 • PO Box 10412, Palo Alto, California 94303-0813 • USA
800.313.3774 • 650.855.2121 • askepri@epri.com • www.epri.com